Molybdenum isotope behaviour in aqueous systems

Rebecca Anna Neely

Faculty of Earth Science
University of Iceland
2017

Molybdenum isotope behaviour in aqueous systems

Rebecca Anna Neely

Dissertation submitted in partial fulfilment of a
Philosophiae Doctor degree in Geology (Geochemistry)

Advisor
Sigurður R. Gíslason
Kevin W. Burton

PhD Committee
Sigurður R. Gíslason
Kevin W. Burton
Eric H. Oelkers

Opponents
Thomas Nägler
Caroline Peacock

Faculty of Earth Science
School of Engineering and Natural Sciences
University of Iceland
Reykjavik, August 2017

Molybdenum isotope behaviour in aqueous systems
Dissertation submitted in partial fulfilment of a *Philosophiae Doctor* degree in Geology (Geochemistry)

Faculty of Earth Science
School of Engineering and Natural Sciences
University of Iceland
Sturlugata 7
101, Reykjavik
Iceland

Telephone: 525 4000

Bibliographic information:
Rebecca Anna Neely, 2017, Molybdenum isotope behaviour in aqueous systems, PhD dissertation, Faculty of Earth Science, University of Iceland, 130 pp.

ISBN 978-9935-9383-0-5

Printing: Háskólaprent
Reykjavik, Iceland, August 2017

Abstract

Molybdenum isotopes are used to quantify changes in Earth's paleoredox conditions but their application relies upon a simplified model in which rivers dominate the ocean input with minor contributions from hydrothermal fluids. The effect of groundwater discharge is rarely considered. This study finds that cold groundwaters ($\delta^{98}Mo_{GROUNDWATER}$ -0.1‰) are compositionally similar to their host rocks ($\delta^{98}Mo_{BASALT}$ -0.15‰) whilst hydrothermal waters are enriched in heavy isotopes ($\delta^{98}Mo_{HYDROTHERMAL}$ +0.2‰ to +1.8‰). Using flux estimates from the literature, the inclusion of these data results in the revaluation of the Mo ocean input from +0.5‰ (just rivers) to +0.35‰ (combined), in the modern day.

As a bioessential element, Mo is important in many biogeochemical cycles: especially, as a cofactor in nitrogenase, the most common nitrogen fixing enzyme. Biological fractionations of some 1.5‰ are observed, with light Mo removed from Lake Mývatn by cyanobacterial uptake during an algal bloom. If preserved, these biological fractionations may need to be considered in the interpretation of the sedimentary record.

Despite the growing evidence that the vapour-phase - formed through magma degassing and fluid boiling - can selectively concentrate and transport metals, the effects on metal stable isotopes remain poorly understood. For example, Mo isotopes show great variability in ore deposits, some of which is attributed to vapour-phase transport. Here we examine the vapour-phase in four geothermal systems in Iceland; the vapour-phase is always lighter than the brine with enrichment factors of some $\varepsilon_{V\text{-}L}$ -2.9‰. This is an important first step towards understanding the mechanisms behind vapour transport and isotopic effects.

Útdráttur

Mólýbden (Mo) samsætur eru oft notaðar til að meta oxunarstig við yfirborð jarðar á ýmsum skeiðum jarðsögunnar. Aðferðin, sem beitt er, byggist á einföldu sjávarlíkani, þar sem styrkur og samsætur Mo í sjó stjórnast fyrst og fremst af árvatni, en jarðhiti á úthafshryggjum hefur til þessa verið talinn hafa lítil áhrif. Þessi rannsókn sýnir að kalt grunnvatn ($\delta^{98}Mo_{GROUNDWATER}$ -0,1‰) er með svipaða samsætusamsetningu og berggrunnurinn sem það flæðir um ($\delta^{98}Mo_{BASALT}$ -0,15‰), en jarðhitavatn inniheldur þyngri samsætur ($\delta^{98}Mo_{HYDROTHERMAL}$ +0,2‰ til +1,8‰). Þessi gögn voru notuð, ásamt áður birtu mati á efnaflutningum til sjávar, til að endurreikna Mo-samsætuhlutföll innflæðis til sjávar við núverandi aðstæður, frá +0,5‰ (árvatn) í +0,35‰ (blanda árvatns og jarðhitavatns).

Mólýbden er nauðsynlegt lífverum og hefur því áhrif á næringarefnahringrásina, sér í lagi sem þáttur í nítrógenasa sem er algengasta niturbindandi ensímið. Aðgreining Mo samsæta vegna ljóstillífunar bláþörunga („cyanobacteria") í Mývatni mældist vera -1,5‰. Þetta er í fyrsta sinn sem þessi aðgreining er mæld í vatnaumhverfi þar sem létta samsætan binst í þörungunum og þunga samsætan verður eftir í vatninu. Nauðsynlegt er að hafa líffræðileg ferli í huga við túlkun og greiningu setlaga, því þessi samsætuaðgreining kann að varðveitast í lögunum.

Í jarðhitakerfum myndast gufufasi vegna afgösunar kviku og suðu jarðhitavökva. Þrátt fyrir vísbendingar um að gufufasinn geti safnað í sig málmum og flutt þá, er lítið vitað um áhrif þessa flutnings á stöðugar samsætur málmanna. Til dæmis eru Mo samsætur í málmgrýti mjög breytilegar, en orsökina má að einhverju leyti rekja til þessa flutnings. Samsætuhlutföll mólýbdens í vatns- og gufufasa fjögurra íslenskra jarðhitakerfa voru rannsökuð í þessu verkefni. Samsætur gufufasans (V) reyndust ávallt léttari en jarðhitavökvans (L), og er auðgunin (ε_{V-L}) -2,9‰. Þetta er mikilvægt fyrsta skref í átt að skilningi á ferlum þeim sem stjórna gufuflutningum og túlkun á áhrifum flutninganna á samsætur.

“The great book, always open and which we should make an effort to read, is that of nature”
-Antoni Gaudí

Table of Contents

List of Figures

List of Tables

Acknowledgements

This work was funded by Initial Training Network grant number 290336, MetTrans, from the European Union (so my first heartfelt thanks are to Europe). I would like to thank all of the senior MetTrans researchers for their guidance during these years, Don Porcelli for his leadership, and Hákon Aðalsteinsson, Landsvirkjun for the opportunity and support. In particular Maria Petrunova, University of Oxford and all of the administration staff at Háskóli Íslands and Durham University are also thanked for keeping the show on the road!

Kevin, you opened the door to Iceland many years ago and I don't think either of us could have known, at the time, where it would lead. And Siggi, when that door was open, you welcomed me in. Thank you both for supporting me through project changes and challenges and for always reminding me that there is a bigger picture.

I know that you will both share in my thanks to ÍSOR who made so much of this work possible. Without their generosity, knowledge, and enthusiasm this work would be a lot colder and a lot less interesting.

> "...the nature and capabilities of colleagues are crucial to the evolution of a career. They provide stimulation and advice on discovering and evaluating opportunities at each juncture in life." (Hubert L. Barnes)

I have been fortunate to be a part of some incredible research communities: colleagues who quickly became friends. There's Bambi and Geysir, understanding every up and every down of this process; MetTrans, filled with creativity, support, and laughter no matter where in the world we are; Durham, allowing me to love the details, the joy, and the occasional heartbreak of data; and Folda, reminding me that no matter what the situation, there is a life outside.

You have all inspired me far beyond the limits of this work.

With nearly 10 addresses during this time I want to thank each and every housemate for making me feel like I had a home despite living out of a suitcase. In particular, Hannah -- for holding down the Icelandic fort -- I am sorry that for so many of the months we lived together we actually lived apart.

And, for the most consistent home -- the one I have always known I could return to, no questions asked, no judgements made -- I thank my Mum and Dad. If you batted an eyelid at mine and Jemma's departures to odd islands at the extremities of Europe, you never let me feel it. Without you this work never could have started, let alone be finished. Failure has never been, but will always remain, an option.

Finally, to my very own circle of niceness -- Sandra and Cat -- your support has known no limits. I hope that everyone has the fortune to find such incredible companions for their adventures into the unknown.

1 Introduction to molybdenum

With the rapid expansion of analytical capabilities the analysis and use of molybdenum isotopes, whilst still not routine, has become more widely applied in every area of the Earth Sciences. The most traditional application of this system is perhaps as a proxy for the oxidation state of the oceans (e.g. Anbar & Rouxel 2007; Archer & Vance 2008; Arnold et al., 2004; Asael et al., 2013; Barling & Anbar 2004; Cheng et al., 2016; Dickson & Cohen 2012; Dickson et al., 2014; Goldberg et al., 2016; Kursweil et al., 2015; Noordmann et al., 2015; Pearce et al., 2008; Siebert et al., 2003; Voegelin et al., 2010; Zhou et al., 2009) and atmosphere (e.g. Anbar et al., 2007; Duan et al., 2010; Voegelin et al., 2010): investigating the details of periods of dramatic changes in the Earth's climate and conditions. Molybdenum is also a bioessential element and with the greatest isotope fractionation expected in low temperature environments, the study of Mo isotopes in biology (e.g. Lierman et al., 2005; Nägler et al., 2004; Wasylenki et al., 2007; Zerkle et al., 2011) and anthropogenic contamination (e.g. Rahaman et al., 2014) have also proved informative. Initially, the characterisation of crustal rocks was for the purposes of constraining the terrestrial input to the oceans (e.g. Anbar & Rouxel 2007; Arnald et al., 2004; Siebert et al., 2003). However, it soon became clear that despite the high temperature, the crustal reservoir was far from being homogenous and so, magmatic and crustal processes have become a focus for study in their own rights (e.g. Greber et al., 2014; Freymouth et al., 2015; König et al., 2016; Willbold et al., 2015, 2017; Yang et al., 2015, 2017). Particular interest has been paid to molybdenites, the most significant ore deposits for Mo (e.g. Weiser & De Laeter 2003; Greber et al., 2011; Hannah et al., 2007; Song et al., 2011; Breillat et al., 2016; Shafiei et al., 2015; Wang et al., 2016; Yao et al., 2016) and the most recent application is that of planetary chemistry and formation (e.g. Burkhardt et al., 2011; Burkhardt et al., 2014).

It is clear that Mo isotopes have been applied to a particularly diverse range of problems in the Earth Sciences however; many assumptions are still made due to a paucity of primary observational constraints and the diversity of fractionation pathways. This thesis provides some insight into a few rarely explored areas of Mo isotope geochemistry.

1) Groundwater chemistry

2) Hydrothermal (geothermal) processes

3) Biological fractionation in the natural environment

4) Vapour phase transport

This introduction gives a brief overview of Mo chemistry and geochemistry whilst also noting the two recent Reviews in Mineralogy and Geochemistry: Anbar 2004 and Kendall et al., 2016.

1.1 Molybdenum chemistry

Molybdenum (Mo) is a transition metal: a group six element with an atomic number of 42. The electron configuration of Mo, $1s^2\ 2s^2\ 2p^6\ 3s^2\ 3p^6\ 4s^2\ 3d^{10}\ 4p^6\ 5s^1\ 4d^5$, means that it can exist in a variety of oxidation states. The most stable oxidation sates are +4 (e.g. molybdate ion, MoO_4^{2-}) and +6 (e.g. molybdenum disulfide, MoS_2). There are 7 naturally occurring isotopes, ^{92}Mo (14.84%), ^{94}Mo (9.25%), ^{95}Mo (15.92%), ^{96}Mo (16.68%), ^{97}Mo (9.55%), ^{98}Mo (24.13%) and ^{100}Mo (9.63%) (Anbar and Rouxel, 2007). All naturally occurring isotopes of Mo are stable save for ^{100}Mo which is still considered stable due to its long half-life ($t_{1/2} = 8.6 \times 10^{18}$ y).

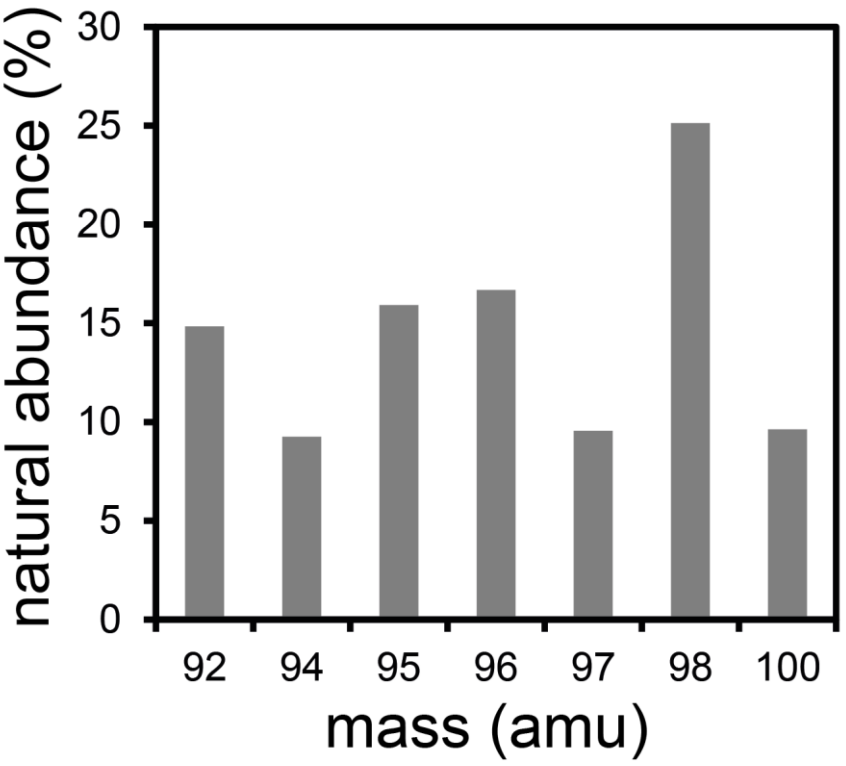

Figure 1: The abundance of the 7 naturally occurring isotopes of molybdenum. The double spike (see Chapter 2.3) is made up of ^{97}Mo and ^{100}Mo.

Molybdenum is readily oxidised – as demonstrated by the space occupied by Mo^{6+} on the Eh-pH diagram (Fig. 2) – and is most commonly found in oxygenated aqueous environments as the MoO_4^{2-}, molybdate anion. The similarities between the MoO_4^{2-} anion and SO_4^{2-}, sulfate – including charge, ionic radii, coordination, and redox behaviour – underpin why sulfur and molybdenum are so often associated and similar in their environmental chemistry. As such, the behaviour of these two anions is often discussed together in this thesis. This association with sulfur is of significance in the study of Mo in the Earth's environment. The behaviour of Mo in the oceans changes dramatically in the presence of free sulfur (as discussed below) and molybdenite (MoS_2) is its most significant ore mineral and host.

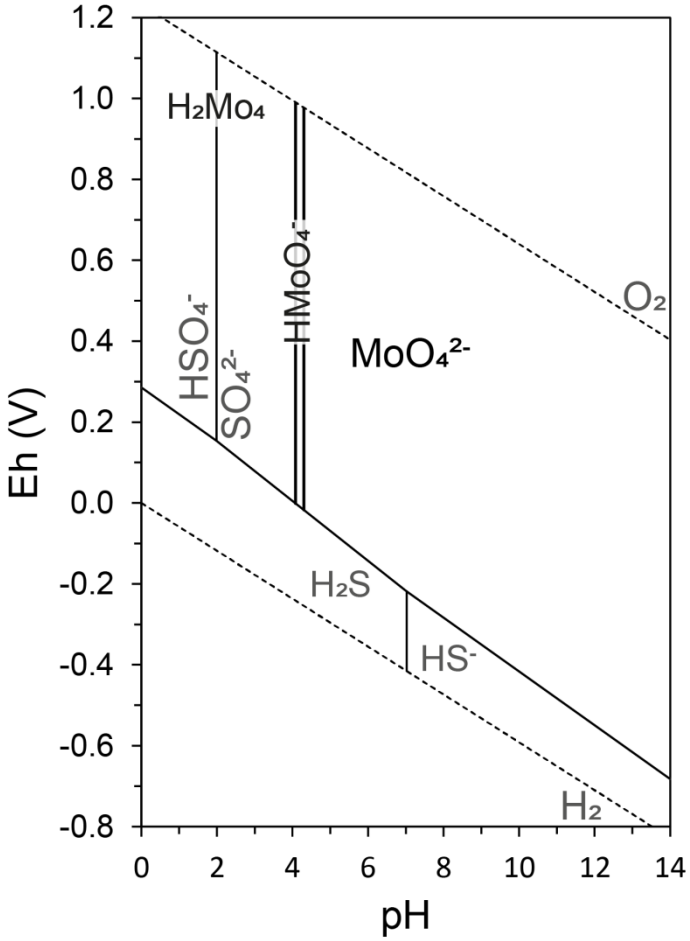

Figure 2: Aqueous speciation of dissolved molybdenum. pH-Eh diagram at 25°C and 105 Pa for the S-O-H system with available, oxidised, Mo data superimposed. Mo speciation below the SO_4^{2-} - H_2S transition is not well characterised although it is thought to be dominated by oxythiomolybdate species ($MoO_{4-x}S_x^{2-}$). Calculations are based on the minteq.v4 database within PHREEQC (Parkhurst & Appelo 2013). The stability field for water lies between the two dashed lines.

1.2 Molybdenum geochemistry

1.2.1 Mineral hosts of molybdenum

Molybdenum is found in relatively low concentrations, of 1 to 2 ppm, in the Earth's crust (Taylor and McLennan, 1985). However, it is unevenly distributed with higher concentrations associated with sulfur in both sedimentary and igneous (porphyry) settings.

Molybdenum is preferentially incorporated into minerals containing Ti^{4+} and Fe^{3+}, thus in basaltic and silicic igneous rocks Mo is often concentrated in ilmenite, titano-magnetite (~10 ppm), and sphene and relatively high Mo concentrations are also found in olivine (~10 ppm), but are lower in pyroxenes (~0.4 ppm) and plagioclase (~0.2 ppm) (see

Arnórsson & Óskarsson, 2007). In sulfides, concentrations can vary by orders of magnitude, from 0.15 ppm in mid-ocean ridge basalt sulfides (Patten et al., 2013) to up to 60% by weight Mo in MoS_2 (the most significant ore-type and host of Mo). In sediments, Mo is often found in high concentrations in association with organic rich black shales (e.g. from 50 to 200 ppm in black shales from the Czech Republic; Kurzeil et al., 2015) whilst carbonates have very low Mo concentrations, typically less than 0.05 ppm (Voegelin et al., 2009).

The high concentration of Mo in black shales is the starting point for the use of Mo as a proxy for oceanic anoxic and atmospheric oxidation reconstructions.

1.2.2 Weathering of molybdenum: from continents to oceans

Although particulates are known to dominate the flux from the continents to the oceans for many elements, the degree to which they contribute to ocean chemistry depends on subsequent dissolution (Oelkers et al., 2011). Molybdenum is highly soluble, and is largely transported to the oceans in the dissolved phase as MoO_4^{2-}. In early leaching studies (e.g Siebert et al., 2003) the large amount of Mo available from rocks upon dissolution lead to released Mo isotope compositions being identical to the source rocks, resulting in the assumption that fractionation as a result of erosion, chemical weathering, and transport were minimal (close to 0‰). However, since that early work, a large amount of data for rivers at every scale has been obtained, and this demonstrates that a considerable fractionation can occurs during the transfer of Mo from the terrestrial to oceanic reservoir.

Whilst the continental crust has a bulk composition of between δ^{98}Mo +0.1‰ and +0.35‰ with a maximum value for the upper continental crust of +0.15‰ (Willbold et al., 2017), global rivers range between +0.35‰ to +2.05‰ (Archer & Vance 2008). This global enrichment of heavy Mo isotopes in the dissolved phase of rivers is also observed in local catchment studies such as, Pearce et al., 2010 ($\delta^{98}Mo_{ICELAND\ RIVERS}$ of 0‰ to +1‰ in a basaltic (<0‰) catchment). The preferential incorporation of heavy Mo isotopes in the dissolved phase has been attributed to a number of different processes: i) catchment lithology (Neubert et al., 2011) and incongruent dissolution during weathering (e.g. Voegelin et al., 2012); ii) absorption of isotopically light Mo to organic phases in soils (e.g. Siebert et al., 2015; King et al., 2016); iii) addition of isotopically heavy groundwaters (Pearce et a., 2010); and iv) adsorption of light Mo to riverine particles (e.g. Archer & Vance 2008; Pearce et al., 2010).

Whilst there is a large spread in riverine data for Mo, the global average yields a mean Mo concentration of 0.8 ppb (Miller et al., 2011) and a Mo isotope composition of δ^{98}Mo +0.5‰ (Archer & Vance et al., 2008). In the modern setting, this riverine Mo flux is considered the dominant Mo input to the oceans: accounting for some 90% of the total flux with the remaining 10% from hydrothermal circulation (e.g. Wheat et al., 2002).

1.2.3 Molybdenum as a proxy for ocean anoxia

In oxygenated seawater Mo exists as the conservative anion MoO_4^{2-} and is very slowly removed into sediments by ferromanganese oxides. This slow removal results in strong isotopic fractionations of ~3‰ with the lighter isotopes being adsorbed onto the ferromanganese oxides resulting in isotopically light oxic sediments and isotopically heavy seawater (e.g Barling et al., 2001; Siebert et al., 2003; Barling & Anbar 2004; Wasylenki et al., 2008). In contrast, at times of euxinia and free sulfur in the waters, the oxothiomolybdate complexes, $MoO_{4-x}S_x^{2-}$, are highly particle reactive and are readily removed from the water column with very little isotope fractionation due to this quantitative removal. Erikson & Helz (2000) calculated that the "geochemical switch" between these two behaviours exists when the H_2S concentration is 0.4±0.1 ppm. In between these two extremes there lies an intermediate sink which is neither fully oxic nor euxinic. Under such circumstances Mo is also removed from solution but to a much lesser extent than under true euxinia.

It is this strongly contrasting behaviour under these conditions that enables Mo to be a useful proxy of redox in the geologic past. Molybdenum concentrations and isotopes, in a variety of sedimentary rocks, in conjunction with other tracers have been used to quantify the varying contribution of these sinks through time (e.g. Anbar & Rouxel 2007; Archer & Vance 2008; Arnold et al., 2004; Asael et al., 2013; Barling & Anbar 2004; Cheng et al., 2016; Dickson & Cohen 2012; Dickson et al., 2014; Goldberg et al., 2016; Kursweil et al., 2015; Noordmann et al., 2015; Pearce et al., 2008; Siebert et al., 2003; Voegelin et al., 2010; Zhou et al., 2009). Whilst initial studies simplified the mass balance using only two sinks (oxic and euxinic; Arnold et al., 2004) more recent reconstructions account for the complexity of the Mo sinks, including the anoxic intermediary. However, it remains common to assume that rivers are the only source of Mo to the oceans and it is this assumption that the first data chapter of this thesis is concerned with.

In chapter 3 – *"Molybdenum isotope behaviour in groundwaters and terrestrial hydrothermal systems, Iceland"* - the potential contribution of groundwaters to the oceanic Mo budget is discussed. Whilst data remain limited, groundwaters in Iceland are shown to be isotopically light, similar in composition to the host basalts and certainly lighter than the compositions of comparable rivers reported in the literature. This suggests that if the groundwater flux of Mo to the oceans is comparable to the riverine flux (as suggested by Moore (1996)) then this contribution to the ocean mass balance may need to be revaluated to take the groundwater flux and composition into account.

In addition, this study makes use of well characterised hydrothermal systems to investigate the potential for Mo isotope fractionation associated with hydrothermal circulation. Substantially adding to the current literature data on Mo isotopes in hydrothermal settings, these data show a large isotopic range with isotopically heavy hydrothermal compositions, in contrast to the only direct studies in the literature (McManus et al., 2002; Pearce et al., 2010). Although a minor contributor to today's ocean mass balance it is likely that in the geologic past hydrothermal circulation was a more significant input to the oceans.

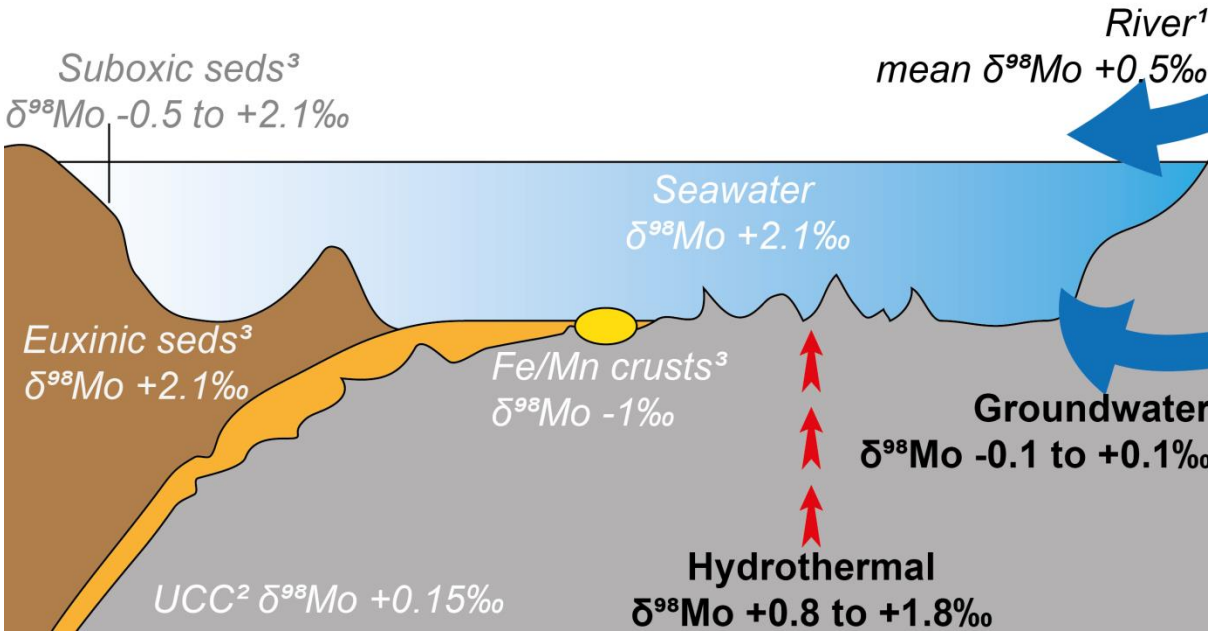

Figure 3: A schematic of the Mo isotope ocean budget (adapted from Anbar & Rouxel 2007). In black text are the three inputs to the ocean, the riverine input (1) – dominant in the modern ocean - from Archer & Vance (2008) and in bold are the new hydrothermal and groundwater data, found in chapter 3. In grey and white text are the upper continental crust (2) after Willbold et al. (2017) and the ocean output, sediment values (3) from Anbar & Rouxel (2007) and Kendall et al. (2016).

1.3 Molybdenum biogeochemistry

The scarcity of Mo in the Earth's crust belies its importance for the metabolism of living organisms and for the global biogeochemical cycles of major elements such as nitrogen, sulfur, and carbon through its participation in the active sites in of metalloenzymes (Pau and Lawson 2002). Many elements that are not biologically essential are far more abundant than Mo. However, it is Mo that is required by most organisms including bacteria, archea, fungi, plants, and animals (including humans). Molybdenum has been known to be of biological importance since the early 1900s when Bortels (1930) first reported that Mo could have a stimulatory effect on the biological fixation of nitrogen. However, it took until the 1970s for recognition of the presence of Mo in the nitrogenase enzyme. To date, Mo has been discovered in roughly 30 different enzymes and it is thought that virtually the entire global biosphere cycling of N depends upon Mo (Williams and Fraústo da Silva, 2002).

In the N-cycle, where both nitrogenase and nitrate reductase are key operatives the predominance of Mo is notable. Nitrogen fixation, the process of making the chemically inert N_2 gas into biologically available nitrogen compounds is at the base of almost every ecosystem. All known N_2-fixing organisms use a dinitrogenase enzyme with an Fe-Mo cofactor (Howard and Rees, 1996, Fig. 4; Macleod & Holland 2013). When Mo is scarce there are known homologous alternative dinitrogenases. Some archea bacteria are able to

use tungsten (W) in place of Mo in Moco while other prokaryotes use either Fe or V in FeMoco (Williams and Fraústo da Silva, 2002). These alternate enzymes have only been found secondarily to the Mo-containing centres and are significantly less efficient than the primary enzymes (Joerger et al., 1988).

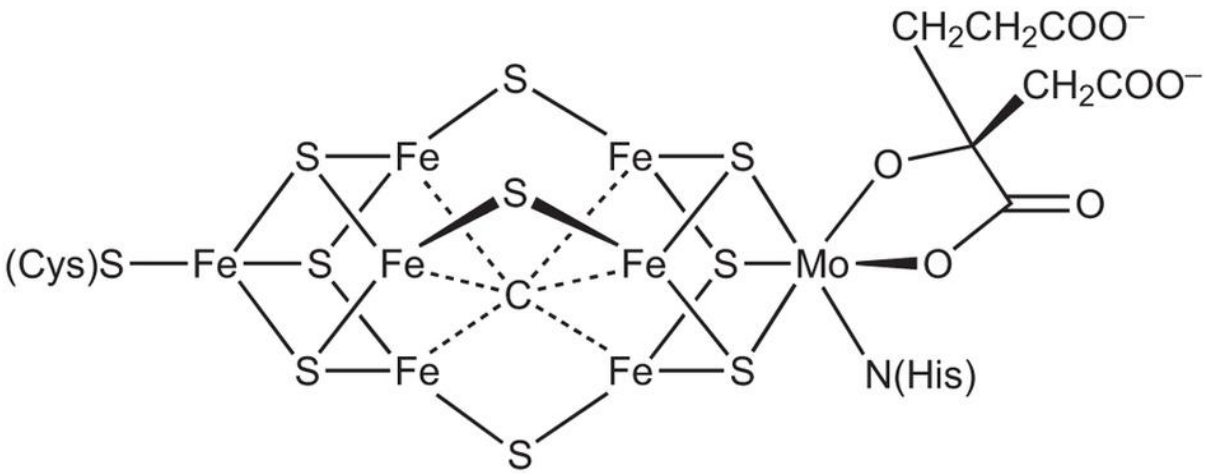

Figure 4: Atomic structure of the FeMoco of molybdenum-dependent nitrogenase from Macleod & Holland (2013).

The role played by Mo in biochemistry is disproportionately significant when its relative scarcity is taken into account. As may be expected, studies have shown that the biological uptake of Mo favours isotopically light Mo leaving a residually heavy growing media (e.g. e.g. Lierman et al., 2005; Nägler et al., 2004; Wasylenki et al., 2007; Zerkle et al., 2011). However, these studies are few and have not focussed on the aqueous environment save for the experimental study by Zerkle et al., 2011).

In chapter 4 - *"Quantifying the effect of primary productivity on molybdenum isotopes in a natural environment: Lake Mývatn, Iceland"* - a year of monthly spot samples are used to investigate the seasonal variation of Mo isotopes in a lake affected by cyanobacterial blooms. Using both Mo and S isotopes, and a simple numerical model of the lake, fractionations of some 1.5‰ between the cyanobacteria and the lake waters are inferred. The cyanobacteria are preferentially enriched in the light isotopes and the lake waters are left residually heavy.

1.4 Molybdenum ore deposits

Whilst Mo isotopes in molybdenites (MoS_2) have been analysed for some time, their application as a tracer for ore formation is only in its infancy (c.f. Kendall et al., 2016).

Multiple studies have shown that molybdenites have large variations in Mo isotope composition (e.g. Wieser et al., 2003; Hannah et al., 2007; Mathur et al 2010; Greber et al., 2011, 2014: Shafiei et al., 2015; Wang et al., 2016; Yao et al., 2016), from δ^{98}Mo -1.6‰ to +2.3‰ with a mean of 0.04±1.04‰ as summarised in Breillat et al. (2016). These large variations occur at every scale. The cause of these variations has been attributed to a number of potential controls and processes, including: temperature (see Breillat et al., 2016), fractional crystallisation (Hannah et al., 2007; Greber et al., 2014), variations in source magma and redox conditions (Greber et al., 2014; Greber et al., 2011; Mathur et al., 2010; Wang et al., 2016); and vapour phase formation and transport (Shafiei et al., 2015; Yao et al., 2016).

It is with the vapour transport that chapter 5 – *"Molybdenum isotope fractionation in hydrothermal systems: phase segregation and subsequent vapour transport"* – is concerned. With the vapour phase now viewed as a fluid capable of transporting important quantities of ore components in its own right (Heinrich et al., 1999) the vapour transport of Mo is of interest not only for the interpretation of ore deposits but also for the fundamental understanding of Mo isotope behaviour. Despite the growing evidence that the vapour phase - formed through magma degassing and ore fluid boiling - can selectively concentrate and transport metals, the effects of vapour phase transport on metal stable isotopes remain poorly understood with Shafiei et al. (2015) arguing for a preference for the accumulation of light isotopes in the vapour phase and Yao et al. (2016) the exact opposite with heavy isotopes enriched in the vapour phase.

Making use of the easily accessible geothermal fields in Iceland chapter 5 examines the liquid and vapour phases of four geothermal fields and finds that the vapour phase is always enriched in light isotopes and, conversely, the residual brine is isotopically heavy.

As described in the introduction, this thesis comprises three self-contained data chapters:

- Molybdenum isotope behaviour in groundwaters and terrestrial hydrothermal systems, Iceland *(Pending minor revisions at Earth and Planetary Science Letters)*
- Quantifying the effect of primary productivity on molybdenum isotopes in a natural environment: Lake Mývatn, Iceland *(Pending major revision and resubmission at Earth and Planetary Science Letters)*
- Molybdenum isotope fractionation in hydrothermal systems: phase segregation and subsequent vapour transport

At the close of each chapter is a specific acknowledgement and author contribution summary.

References

ANBAR, A. D. 2004. Molybdenum stable isotopes: observations, interpretations and directions. Reviews in Mineralogy and Geochemistry, 55, 429-454.

ANBAR, A. D., DUAN, Y., LYONS, T. W., ARNOLD, G. L., KENDALL, B., CREASER, R. A., KAUFMAN, A. J., GORDON, G. W., SCOTT, C., GARVIN, J. & BUICK, R. 2007. A Whiff of Oxygen Before the Great Oxidation Event? Science, 317, 1903-1906.

ANBAR, A. D. & ROUXEL, O. 2007. Metal stable isotopes in paleoceanography. Annu. Rev. Earth Planet. Sci., 35, 717-746.

ARCHER, C. & VANCE, D. 2008. The isotopic signature of the global riverine molybdenum flux and anoxia in the ancient oceans. Nature Geoscience, 1, 597-600.

ARNOLD, G. L., ANBAR, A., BARLING, J. & LYONS, T. 2004. Molybdenum isotope evidence for widespread anoxia in mid-Proterozoic oceans. Science, 304, 87-90.

ARNÓRSSON, S. & ÓSKARSSON, N. 2007. Molybdenum and tungsten in volcanic rocks and in surface and< 100 C ground waters in Iceland. Geochimica et Cosmochimica Acta, 71, 284-304.

ASAEL, D., TISSOT, F. L. H., REINHARD, C. T., ROUXEL, O., DAUPHAS, N., LYONS, T. W., PONZEVERA, E., LIORZOU, C. & CHÉRON, S. 2013. Coupled molybdenum, iron and uranium stable isotopes as oceanic paleoredox proxies during the Paleoproterozoic Shunga Event. Chemical Geology, 362, 193-210.

BARLING, J., ARNOLD, G. L. & ANBAR, A. D. 2001. Natural mass-dependent variations in the isotopic composition of molybdenum. Earth and Planetary Science Letters, 193, 447-457.

BARLING, J. & ANBAR, A. D. 2004. Molybdenum isotope fractionation during adsorption by manganese oxides. Earth and Planetary Science Letters, 217, 315-329.

BORTELS, H. 1930. Molybdän als Katalysator bei der biologischen Stickstoffbindung. Archiv für Mikrobiologie, 1, 333-342.

BREILLAT, N., GUERROT, C., MARCOUX, E. & NÉGREL, P. 2016. A new global database of δ98Mo in molybdenites: A literature review and new data. Journal of Geochemical Exploration, 161, 1-15.

BURKHARDT, C., KLEINE, T., OBERLI, F., PACK, A., BOURDON, B. & WIELER, R. 2011. Molybdenum isotope anomalies in meteorites: constraints on solar nebula evolution and origin of the Earth. Earth and Planetary Science Letters, 312, 390-400

BURKHARDT, C., HIN, R. C., KLEINE, T. & BOURDON, B. 2014. Evidence for Mo isotope fractionation in the solar nebula and during planetary differentiation. Earth and Planetary Science Letters, 391, 201-211

CHENG, M., LI, C., ZHOU, L., ALGEO, T. J., ZHANG, F., ROMANIELLO, S., JIN, C.-S., LEI, L.-D., FENG, L.-J. & JIANG, S.-Y. 2016. Marine Mo biogeochemistry in the context of dynamically euxinic mid-depth waters: A case study of the lower Cambrian Niutitang shales, South China. Geochimica et Cosmochimica Acta, 183, 79-93.

DICKSON, A. J. & COHEN, A. S. 2012. A molybdenum isotope record of Eocene Thermal Maximum 2: Implications for global ocean redox during the early Eocene. Paleoceanography, 27.

DICKSON, A. J., COHEN, A. S. & COE, A. L. 2014. Continental margin molybdenum isotope signatures from the early Eocene. Earth and Planetary Science Letters, 404, 389-395.

DUAN, Y., ANBAR, A. D., ARNOLD, G. L., LYONS, T. W., GORDON, G. W. & KENDALL, B. 2010. Molybdenum isotope evidence for mild environmental oxygenation before the Great Oxidation Event. Geochimica et Cosmochimica Acta, 74, 6655-6668.

ERICKSON, B. E. & HELZ, G. R. 2000. Molybdenum(VI) speciation in sulfidic waters:: Stability and lability of thiomolybdates. Geochimica et Cosmochimica Acta, 64, 1149-1158.

FREYMUTH, H., VILS, F., WILLBOLD, M., TAYLOR, R. N. & ELLIOTT, T. 2015. Molybdenum mobility and isotopic fractionation during subduction at the Mariana arc. Earth and Planetary Science Letters, 432, 176-186.

GOLDBERG, T., POULTON, S. W., WAGNER, T., KOLONIC, S. F. & REHKÄMPER, M. 2016. Molybdenum drawdown during Cretaceous Oceanic Anoxic Event 2. Earth and Planetary Science Letters, 440, 81-91.

GREBER, N. D., HOFMANN, B. A., VOEGELIN, A. R., VILLA, I. M. & NÄGLER, T. F. 2011. Mo isotope composition in Mo-rich high- and low-T hydrothermal systems from the Swiss Alps. Geochimica et Cosmochimica Acta, 75, 6600-6609.

GREBER, N. D., PETTKE, T. & NÄGLER, T. F. 2014. Magmatic–hydrothermal molybdenum isotope fractionation and its relevance to the igneous crustal signature. Lithos, 190–191, 104-110.

HOWARD, J. B. & REES, D. C. 1996. Structural basis of biological nitrogen fixation. Chemical reviews, 96, 2965-2982.

JOERGER, R. D., BISHOP, P. E. & EVANS, H. J. 1988. Bacterial alternative nitrogen fixation systems. Critical reviews in microbiology, 16, 1-14.

KENDALL, B., DAHL, T., ANABAR, A. 2016. Good Golly, Why Moly? The Stable Isotope Geochemistry of Molybdenum, Reviews in Mineralogy and Geochemistry, 82, 683-732.

KING, E. K., THOMPSON, A., CHADWICK, O. A. & PETT-RIDGE, J. C., 2016. Molybdenum sources and isotopic composition during early stages of pedogenesis along a basaltic climate transect. Chemical Geology.

KÖNIG, S., WILLE, M., VOEGELIN, A. & SCHOENBERG, R. 2016. Molybdenum isotope systematics in subduction zones. Earth and Planetary Science Letters, 447, 95-102.

KURZWEIL, F., DROST, K., PAŠAVA, J., WILLE, M., TAUBALD, H., SCHOECKLE, D. & SCHOENBERG, R. 2015. Coupled sulfur, iron and molybdenum isotope data from black shales of the Teplá-Barrandian unit argue against deep ocean oxygenation during the Ediacaran. Geochimica et Cosmochimica Acta, 171, 121-142.

LIERMANN, L. J., GUYNN, R. L., ANBAR, A. & BRANTLEY, S. L. 2005. Production of a molybdophore during metal-targeted dissolution of silicates by soil bacteria. Chemical Geology, 220, 285-302.

MACLEOD, K. C. & HOLLAND, P. L. 2013. Recent developments in the homogeneous reduction of dinitrogen by molybdenum and iron. Nat Chem, 5, 559-565.

MCMANUS, J., NÄGLER, T. F., SIEBERT, C., WHEAT, C. G. & HAMMOND, D. E. 2002. Oceanic molybdenum isotope fractionation: Diagenesis and hydrothermal ridge-flank alteration. Geochemistry, Geophysics, Geosystems, 3, 1-9.

MILLER, C. A., PEUCKER-EHRENBRINK, B., WALKER, B. D. & MARCANTONIO, F. 2011. Re-assessing the surface cycling of molybdenum and rhenium. Geochimica et Cosmochimica Acta, 75, 7146-7179.

NÄGLER, T.F., MILLS M.M., SIEBERT, C. 2004 Biological fractionation of Mo isotopes duringN2 fixation by Trichodesmium sp. IMS 101. Geochimica et Cosmochimica Acta, 68, A364.

NEUBERT, N., HERI, A., VOEGELIN, A., NÄGLER, T., SCHLUNEGGER, F. & VILLA, I. 2011. The molybdenum isotopic composition in river water: constraints from small catchments. Earth and planetary science letters, 304, 180-190.

NOORDMANN, J., WEYER, S., MONTOYA-PINO, C., DELLWIG, O., NEUBERT, N., ECKERT, S., PAETZEL, M. & BÖTTCHER, M. E. 2015. Uranium and molybdenum isotope systematics in modern euxinic basins: Case studies from the central Baltic Sea and the Kyllaren fjord (Norway). Chemical Geology, 396, 182-195.

OELKERS, E. H., GISLASON, S. R., EIRIKSDOTTIR, E. S., JONES, M., PEARCE, C. R. & JEANDEL, C. 2011. The role of riverine particulate material on the global cycles of the elements. Applied Geochemistry, 26, Supplement, S365-S369.

PATTEN, C., BARNES, S.-J., MATHEZ, E. A. & JENNER, F. E. 2013. Partition coefficients of chalcophile elements between sulfide and silicate melts and the early crystallization history of sulfide liquid: LA-ICP-MS analysis of MORB sulfide droplets. Chemical Geology, 358, 170-188.

PAU, R. N. & LAWSON, D. M. 2002. Transport, Homeostasis, Regulation, and Binding of Molybdate and Tungstate to. Metals Ions in Biological System: Volume 39: Molybdenum and Tungsten: Their Roles in Biological Processes, 31.

PEARCE, C. R., COHEN, A. S., COE, A. L. & BURTON, K. W. 2008. Molybdenum isotope evidence for global ocean anoxia coupled with perturbations to the carbon cycle during the Early Jurassic. Geology, 36, 231-234.

PEARCE, C. R., BURTON, K. W., VON STRANDMANN, P. A., JAMES, R. H. & GÍSLASON, S. R. 2010. Molybdenum isotope behaviour accompanying weathering and riverine transport in a basaltic terrain. Earth and Planetary Science Letters, 295, 104-114.

RAHAMAN, W., GOSWAMI, V., SINGH, S. K. & RAI, V. K. 2014. Molybdenum isotopes in two Indian estuaries: Mixing characteristics and input to oceans. Geochimica et Cosmochimica Acta, 141, 407-422.

SHAFIEI, B., SHAMANIAN, G., MATHUR, R. & MIRNEJAD, H. 2015. Mo isotope fractionation during hydrothermal evolution of porphyry Cu systems. Mineralium Deposita, 50, 281-291.

SIEBERT, C., NÄGLER, T. F., VON BLANCKENBURG, F. & KRAMERS, J. D. 2003. Molybdenum isotope records as a potential new proxy for paleoceanography. Earth and Planetary Science Letters, 211, 159-171.

SIEBERT, C., PETT-RIDGE, J. C., OPFERGELT, S., GUICHARNAUD, R. A., HALLIDAY, A. N. & BURTON, K. W. 2015. Molybdenum isotope fractionation in soils: Influence of redox conditions, organic matter, and atmospheric inputs. Geochimica et Cosmochimica Acta, 162, 1-24.

SONG, S., HU, K., WEN, H., ZHANG, Y., LI, K. & FAN, H. 2011. Molybdenum isotopic composition as a tracer for low-medium temperature hydrothermal ore-forming systems: A case study on the Dajiangping pyrite deposit, western Guangdong Province, China. Chinese Science Bulletin, 56, 2221-2228.

TAYLOR S. R. and MCLENNAN, S. M. (1985) The Continental Crust: Its Composition and Evolution. Blackwell Scientific Public.

VOEGELIN, A. R., NÄGLER, T. F., SAMANKASSOU, E. & VILLA, I. M. 2009. Molybdenum isotopic composition of modern and Carboniferous carbonates. Chemical geology, 265, 488-498.

VOEGELIN, A. R., NÄGLER, T. F., BEUKES, N. J. & LACASSIE, J. P. 2010. Molybdenum isotopes in late Archean carbonate rocks: implications for early Earth oxygenation. Precambrian Research, 182, 70-82.

VOEGELIN, A. R., NÄGLER, T. F., PETTKE, T., NEUBERT, N., STEINMANN, M., POURRET, O. & VILLA, I. M. 2012. The impact of igneous bedrock weathering on the Mo isotopic composition of stream waters: Natural samples and laboratory experiments. Geochimica et Cosmochimica Acta, 86, 150-165.

WANG, Y., ZHOU, L., GAO, S., LI, J.-W., HU, Z.-F., YANG, L. & HU, Z.-C. 2016. Variation of molybdenum isotopes in molybdenite from porphyry and vein Mo deposits in the Gangdese metallogenic belt, Tibetan plateau and its implications. Mineralium Deposita, 51, 201-210.

WASYLENKI, L., ANBAR, A., LIERMANN, L., MATHUR, R., GORDON, G. & BRANTLEY, S. 2007. Isotope fractionation during microbial metal uptake measured by MC-ICP-MS. Journal of Analytical Atomic Spectrometry, 22, 905-910.

WASYLENKI, L. E., ROLFE, B. A., WEEKS, C. L., SPIRO, T. G. & ANBAR, A. D. 2008. Experimental investigation of the effects of temperature and ionic strength on Mo isotope fractionation during adsorption to manganese oxides. Geochimica et Cosmochimica Acta, 72, 5997-6005.

WHEAT, C. G., MOTTL, M. J. & RUDNICKI, M. 2002. Trace element and REE composition of a low-temperature ridge-flank hydrothermal spring. Geochimica et Cosmochimica Acta, 66, 3693-3705.

WIESER, M. E. & DE LAETER, J. R. 2003. A preliminary study of isotope fractionation in molybdenites. International Journal of Mass Spectrometry, 225, 177-183.

WILLIAMS, R. & FRAUSTO DA SILVA, J. 2002. The involvement of molybdenum in life. Biochemical and biophysical research communications, 292, 293-299.

WILLBOLD, M., HIBBERT, K., LAI, Y. J., FREYMUTH, H., HIN, R. C., COATH, C., VILS, F. & ELLIOTT, T. 2015. High-Precision Mass-Dependent Molybdenum Isotope Variations in Magmatic Rocks Determined by Double-Spike MC-ICP-MS. Geostandards and Geoanalytical Research.

WILLBOLD, M. & ELLIOTT, T. 2017. Molybdenum isotope variations in magmatic rocks. Chemical Geology, 449, 253-268.

YANG, S., PAN, W., FRIESEN, G. D., BURGESS, B., CORBIN, J. L., STIEFEL, E. & NEWTON, W. 1982. Iron-molybdenum cofactor from nitrogenase. Modified extraction methods as probes for composition. Journal of Biological Chemistry, 257, 8042-8048.

YANG, J., SIEBERT, C., BARLING, J., SAVAGE, P., LIANG, Y.-H. & HALLIDAY, A. N. 2015. Absence of molybdenum isotope fractionation during magmatic differentiation at Hekla volcano, Iceland. Geochimica et Cosmochimica Acta, 162, 126-136.

YANG, J., BARLING, J., SIEBERT, C., FIETZKE, J., STEPHENS, E. & HALLIDAY, A. N. 2017. The molybdenum isotopic compositions of I-, S- and A-type granitic suites. Geochimica et Cosmochimica Acta, 205, 168-186.

YAO, J., MATHUR, R., SUN, W., SONG, W., CHEN, H., MUTTI, L., XIANG, X. & LUO, X. 2016. Fractionation of Cu and Mo isotopes caused by vapor-liquid partitioning, evidence from the Dahutang W-Cu-Mo ore field. Geochemistry, Geophysics, Geosystems.

ZERKLE, A., SCHEIDERICH, K., MARESCA, J., LIERMANN, L. & BRANTLEY, S. 2011. Molybdenum isotope fractionation by cyanobacterial assimilation during nitrate utilization and N2fixation. Geobiology, 9, 94-106.

ZHOU, L., GAO, S., CHRIS, H., COREY, A. & XIE, S. 2009. Preliminary Mo isotope data of Phanerozoic clastic sediments from the northern margin of the Yangtze block and its implication for paleoenvironmental conditions. Chinese Science Bulletin, 54, 822-829.

2 Molybdenum isotope analysis

Molybdenum (Mo), atomic number 42, is a group six transition metal. The electron configuration of Mo, $1s^2\ 2s^2\ 2p^6\ 3s^2\ 3p^6\ 4s^2\ 3d^{10}\ 4p^6\ 5s^1\ 4d^5$, means that it can exist in a variety of oxidation states; the most stable are +4 (e.g. molybdate ion, MoO_4^{2-}) and +6 (e.g. molybdenum disulfide, MoS_2). There are thirty-five known isotopes of Mo, ranging from atomic mass 83 to 117. Only 7 of these isotopes occur naturally: ^{92}Mo (14.84%), ^{94}Mo (9.25%), ^{95}Mo (15.92%), ^{96}Mo (16.68%), ^{97}Mo (9.55%), ^{98}Mo (24.13%), and ^{100}Mo (9.63%) (Anbar & Rouxel, 2007). These 7 natural isotopes are all stable, save for ^{100}Mo which, due to its long half-life (t1/2 = 8.6 x 1018 y), is also treated as stable.

With advances in mass spectrometer instrumentation, the number and mass spread of isotopes and their application to a range of topics in Earth Science make Mo a prime target for isotopic study. At its most simplistic, a mass spectrometer measures mass and charge (m/q). Therefore, the analytical set-up and prior chemical separation of the analyte from the sample matrix are designed to ensure that only singly charged analyte ions make it through to detection. It is essential to ensure that the entire procedure is interference free. There are two main types of interference: matrix effects, in which the analyte sensitivity is influenced by other sample constituents, and spectral interferences, in which overlapping peaks add to and mask the analyte signal.

In analytical chemistry, the matrix effect is defined by the IUPAC as "the combined effect of all components of the sample other than the analyte on the measurement of the quantity. If a specific component can be identified as causing an effect then this is referred to as interference" (in Gosetti et al., 2010). Spectral interferences include: isobaric overlap, in which another element's isotope has the same mass as the analyte, doubly charged ions (M^{2+}) of twice the mass, polyatomic ions which form from the most abundant ions present (often Ar, O, N, and H), and a sub-set of polyatomic interferences which are the refractory oxide ions (MO^+, MO_2^+, and MO_3^+).

The first step in ensuring that interferences are kept to a minimum is to separate the element of interest (the analyte, in this case Mo) from the sample matrix. This is done via a chemical purification process known as column chromatography.

2.1 Chemical separation

There are a number of different methods in the literature for the chemical separation of Mo. Some of them are matrix specific (e.g. Nakagawa et al. (2008) for seawater analysis) and all have their advantages and disadvantages. They range from two stage (anion followed by cation exchange) procedures (e.g. Anbar et al., 2001; Barling et al., 2001; Arnold et al., 2004; Pietruszka et al., 2006) to single pass anion exchange columns (e.g. Siebert et al., 2001; Pearce et al., 2009; Willbold et al., 2015), and chelating resins (e.g.

Malinovsky et al., 2005) whilst others (e.g Burkhardt et al., 2011, 2014) have increased the complexity to three stages, utilising both anion and cation exchange resins, in order to be able to deal with low Mo concentrations and the inevitably larger sample sizes. Other groups (e.g. Qi & Masuda 1994; Dauphas et al., 2001) have exploited the affinity of Mo for organic complexes such as $C_{16}H_{35}O_4P_3$ and employ solvent extraction procedures prior to a more typical anion exchange column.

In this study we followed the Mo separation procedure outlined in Pearce et al. (2009) with the addition of a third matrix elution step of 12 ml of 0.5 M HF, before the collection of Mo, to ensure complete removal of Zn (Fig. 1). In concurrent Mo isotope literature Pearce et al. (2009) has emerged as a method of choice, used in Pearce et al. (2010a, b); Dickson et al. (2012; 2014); Rahaman et al. (2014); and King et al. (2016). King et al. (2016) found it necessary to reduce the total procedural blanks with the addition of a 200 ml 1 M HCl resin wash step and Mo elution in 30 ml of 1 M HCl. However, total procedural blank was still 5 ng. Without such modifications, the total procedural blanks in this study were maintained below 1 ng (<1% of the total Mo processed per sample).

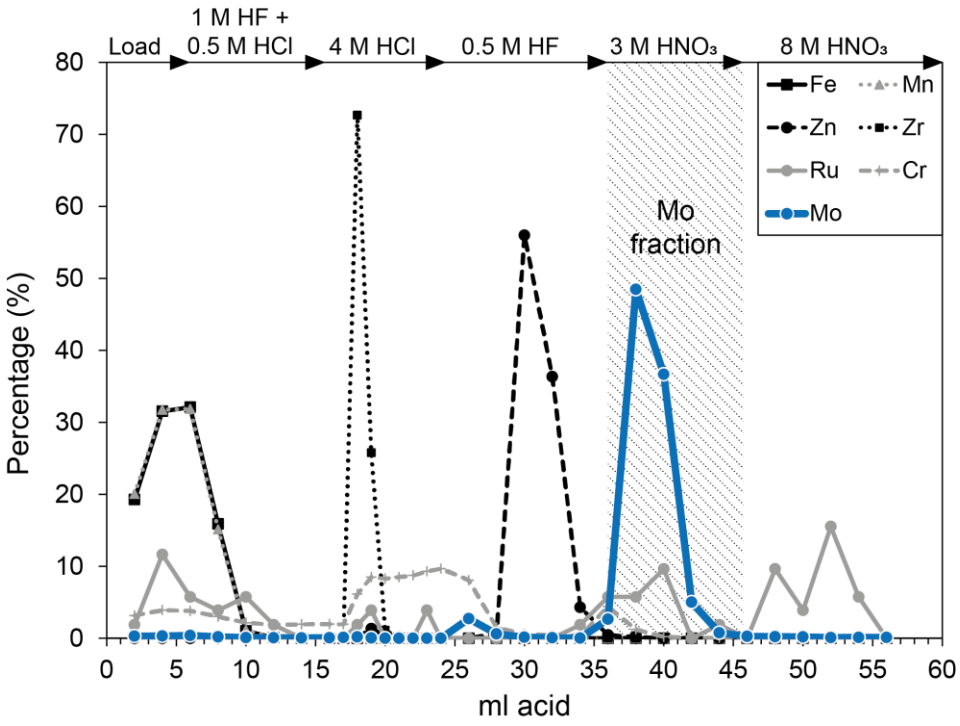

Figure 1: Elution curve for selected elements in the column calibration. The complete procedure is described in detail in the text and is adapted from Pearce et al., 2009. The calibration is for 180 mg dissolution of BCR-1 (a more complex matrix than most of the samples analysed in this study).

Willbold et al. (2015) published a further Mo purification method towards the end of this study. It is developed specifically for low Mo, high matrix samples and allows quantitative isolation of Mo from a range of silicate (up to 200 mg) and metal matrices. A selection of

the more complex matrix samples (basalts and hydrothermal vent fluids) were duplicated through this chemistry; no resolvable differences are found between the data from the Willbold et al. (2015) or Pearce et al. (2009) methods.

After Mo isolation, all samples are evaporated to dryness before being oxidised with concentrated (16 M) HNO_3 and dried down a final time. Samples are taken up in 0.5 M HNO_3 to generate concentrations of 150 to 200 ppb for isotopic analysis. In this study, all Mo isotope analyses were carried out using a Thermo Scientific Neptune instrument at the Earth Science Department, Durham University, UK.

2.2 Analytical set-up

Molybdenum isotopes are typically measured via multi collector inductively coupled plasma mass spectrometry (MC ICP-MS). Some early Mo isotope analyses were carried out by thermal ionisation mass spectrometry (TIMS) (e.g. Becker and Walker, 2003; Crouch and Tuplin, 1964; Murthy, 1962; 1963; Qi and Masuda, 1994; Wetherill, 1964). However, analysis is limited by the relatively high ionisation potential of Mo, the loss of Mo compounds by evaporation, and the potential contamination from the filament material (Anbar, 2004; Wieser and de Laeter , 2000). Significant advantages of MC ICP-MS over TIMS are the relatively high ionisation efficiency and speed of sample analysis. In addition, instrumental mass bias varies smoothly during analytical sessions and can therefore be easily accounted for (Albarède& Beard 2004).

2.2.1 Sample introduction system

The most common sample introduction system, and the one used throughout this work, is the aspiration of a liquid sample, as an aerosol, into the argon (Ar) plasma. The addition of an Aridus II desolvating nebuliser is made, in place of a more typical cyclonic spray chamber, in order to increase sensitivity.

The sample is introduced via a Cetac-35 nebuliser, with a measured uptake rate 30-40 µl min^{-1}, and is subsequently aspirated into a heated (110 °C) PFA spray chamber: vapourising the sample. The sample then enters a fluoropolymer membrane desolvator module, heated to 160 °C; this maintains the sample as a vapour, allowing the volatile solvent to permeate the porous wall of the membrane, reducing the potential for oxide formation. A counter current flow of Ar sweep gas is used to remove these solvent vapours whilst allowing the targeted, non-volatile analyte (the Mo in this case) to continue through to the torch and on to ionisation.

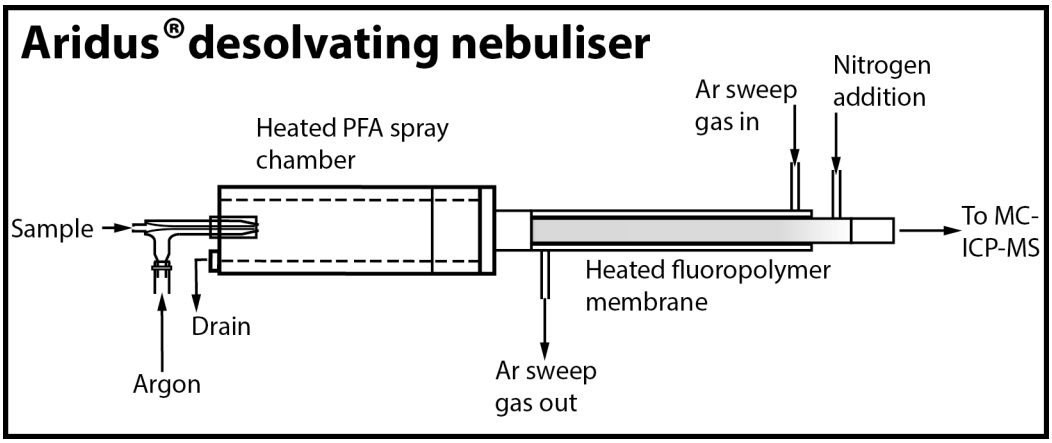

Figure 2: Schematic diagram of the Aridus desolvating nebuliser. Details are found within the following text.

With a 'traditional' cyclonic spray chamber sample loss is ~90% (Jarvis, 1997) whilst with an Aridus this is reduced to ~40%. Analyte sensitivity typically increases by a factor of 4 to 10 times when using the Aridus; in this study early tests (with a PFA 50 nebuliser) showed that sensitivity increased from 45 v ppm^{-1} to 370 v ppm^{-1} when moving from wet to dry plasma. Typical total Mo sensitivity was 300 v ppm^{-1} during analytical runs with a maximum of 450 v ppm^{-1}. This sensitivity compares favourably with recent data from Willbold et al., 2015 who, using a similar analytical set-up, report a sensitivity of 250 v ppm^{-1}.

The Aridus also allows the addition of nitrogen (N_2) gas into the sample gas flow which, being thermally more conductive than Ar, increases the plasma temperature and therefore the ionisation efficiency. These additional gas flows are adjusted daily to achieve maximum sensitivity and signal stability: additional Ar at 4.5 to 5 l min^{-1} and N_2 at ~4 ml min^{-1}.

Ionisation of the sample occurs in the Ar plasma (an electrically neutral volume of gas made of positively and negatively ionised atoms and molecules). The analyte is introduced into the plasma through a torch made up of three concentric quartz tubes: the outer carries the Ar cooling gas to prevent melting, the sample is injected through the innermost, and the intermediate tube carries the 'auxiliary' gas supply (which is used to shape, lift, and stabilise the plasma). The plasma is generated by coupling the load coil to a radio frequency power source. The torch is seeded with free electrons that go on to ionise the Ar gas through collisions, generating a self-sustaining plasma

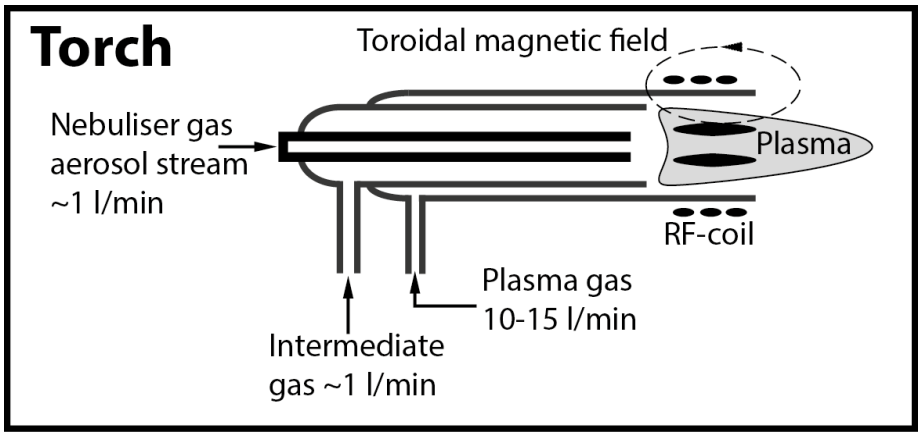

Figure 3: Plasma torch (Fassel type) schematic. Approximate gas flows are indicated. The torch consists of three concentric quartz tubes, fully describe in the preceding text.

2.2.2 Mass spectrometer interface

A critical design feature of the ICP-MS is the differentially pumped interface region. The sample introduction system runs at atmospheric pressure whilst the mass spectrometer must operate under high vacuum (to avoid collisions and loss of kinetic energy). As such, the interface between the two is crucial.

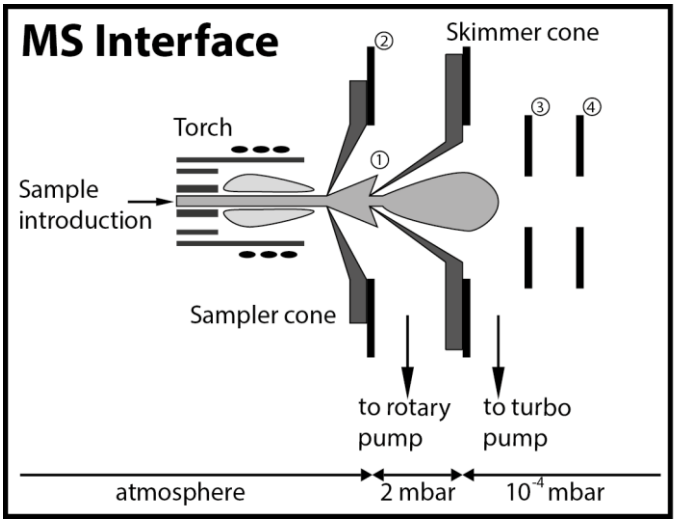

1: Expansion chamber 2: Water-cooled plates 3: Extraction lens 4: Ground plate

Figure 4: Mass spectrometer interface schematic. The differentially pumped interface region, as indicated at the bottom of this figure, is a critical design feature to allow for the extraction of the ions from the plasma.

The sample aerosol emerges from the torch as a mixture of atoms, ions, and undissociated molecular fragments. The ions are extracted due to a decrease in pressure from the torch to

the mass spectrometer. This interface consists of two nickel apertures: the sampler cone (aperture ~0.8 to 1.2 mm) and the skimmer cone (aperture ~0.4 to 0.8 mm). In this study an x-type skimmer cone is used (with its tendency to generate oxides mitigated by the use of the Aridus introduction system). These cones allow ions to pass through but deflect the majority of uncharged molecules and atoms. The space between them is known as the expansion chamber and is evacuated by a rotary pump to a pressure of ~0.5 kPa.

2.2.3 Analyser

A stack of ion lenses focus the ion beam beyond the skimmer cone; they extract, shape, and steer the ion beam through the flight tube. This lens stack contributes a second pressure drop to ~10^{-9} kPa after the final lens. Maintaining this high vacuum in the flight tube is essential for achieving high abundance sensitivity.

The use of the Ar plasma results in a range of analyte energies due to the thermal energy spread of the ions. In order to control this kinetic ion energy range, the MC ICP-MS makes use of double-focusing instrumentation: a first stage electrostatic field and second stage magnetic sector. The electrostatic analyser consists of two curved plates of equal and opposite potential which deflect the ions as they travel through the electric field. The force on the ion due to the electric field is equal to the centripetal force and therefore ions of the same kinetic energy are focused. The magnetic sector separates ions by charge to mass ratios (m/q). As a charged particle enters the magnetic field, the charge is deflected in a circular motion of unique radius. Those ions not selected by the voltage difference and the magnetic field will either collide with the side of the flight tube or not pass through the slit to the detector.

Ions of equal m/q are therefore all focused to the exit slit even if they start out from the plasma source with slightly different energies and direction vectors. The larger the slit, the higher the transmission but this must be balanced with decreasing the aperture size improving the energy resolution. Therefore, a compromise between high resolution and high transmission must be reached. All Mo analyses were carried out in low resolution mode.

2.2.4 Ion current detectors

The ion beam detection system must be designed so that the masses of interest are resolved and their ion currents amplified to an extent that useful precision is attained. The detector used in the Neptune (and in most instances) is the Faraday Cup. The Faraday Cup detects ions as positive electric charges when the ions enter the carbon-coated metal box through a narrow slit before interacting with an inclined metal electrode that collects incoming ions. The positive ions striking this electrode cause the accumulation of a positive charge which is neutralised by an electric current flowing from earth through a large (10^{11} Ω) resistor. According to Ohm's law, the potential difference across the resistor is proportional to the ion current.

As a multi collector, the Neptune has the ability to measure up to nine isotopes simultaneously, making use of its eight moveable cups and additional, fixed axial cup. All measurements were made in static mode, monitoring masses 91 to 100 with the following cup configuration: L4-^{91}Zr, L3-^{92}Mo, L2-^{94}Mo, L1-^{95}Mo, C-^{96}Mo, H1-^{97}Mo, H2-^{98}Mo, H3-^{99}Ru, H4-^{100}Mo. This cup configuration allows for monitoring of the Zr and Ru direct isobaric interferences as well as all of the Mo isotopes necessary for data deconvolution. A gain calibration was, at a minimum, carried out at the beginning of every analytical session. Each analysis represents the average of 1 block of 50 cycles with an integration time of 4 s. Machine blank measurements were made, using the same method, before every sample and standard; typical signal:background ratios were ca. 600. A 3 minute wash in 0.5 M HNO^3 preceded all blank-sample pair measurements.

2.3 Data reduction

The determination of natural isotope fractionation necessitates its resolution from fractionation that occurs during the processes outlined above: chemical purification and isotope analysis (Siebert et al., 2001). Whilst in early studies single element spiking was successful (e.g. Anbar et al., 2001; Barling et al., 2001, 2004) measurement uncertainties can be reduced through the use of an isotopic double spike. Double spike is a powerful method to correct for instrumental mass fractionation with the major advantages of: accounting for fractionation during chemical separation (if sample-spike equilibration occurs before chemistry then quantitative yields are not necessary); resolving instrumental mass bias from natural fractionation in a single run; and providing Mo concentration data to a precision hard to obtain by any other method. Other data reduction methods, such as single element spiking and standard bracketing, rely on fractionation-free chemical separation and 100% yield as Mo has been shown to fractionate during column chromatography (Anbar et al., 2001; Siebert et al., 2001). When doping with a different element to the analyte it is also necessary to assume that instrumental mass fractionation is the same for both elements and the analysed mass range must be increased, reducing the number of isotopes of the target element that can be monitored.

The double-spike design follows that outlined in Siebert et al. (2001) and makes use of the Rudge et al. (2009) "cocktail list" for finding optimal double-spike compositions. The double-spike consists of an almost 1:1 ratio of ^{97}Mo:^{100}Mo. Both of these Mo isotopes are in relatively low abundance in natural samples (9.55% and 9.63% respectively), there are no elemental isobaric interferences on ^{97}Mo (and the potential ^{100}Ru interference can be easily reduced and accounted for), highly enriched single spikes are commercially available, and the mass difference between ^{97}Mo and ^{100}Mo is the same as between ^{98}Mo and ^{95}Mo (the most commonly reported Mo isotopes). The double-spike and in-house reference solution (NIST 3134, lot number 891 307) were calibrated with guidance from Dr. Christopher Pearce by doping with Pd as described by Siebert et al. (2001) and Skierszkan et al. (2015).

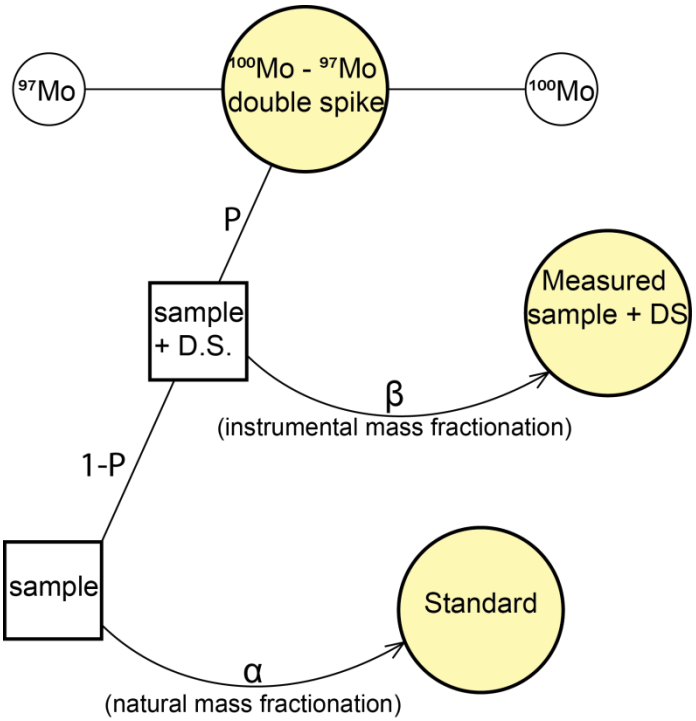

Figure 5: A schematic diagram of the double spike technique. Lines with arrows represent mass fractionation, lines without arrows represent mixing. The single spikes, ^{97}Mo and ^{100}Mo, are mixed to form the double spike (D.S.). The sample is then mixed with the double spike to form the sample double spike mixture. The mixture consists of a proportion p (per mole of element) of double spike to 1−p of natural sample. In the mass spectrometer, this mixture undergoes instrumental mass fractionation with a fractionation factor of β so that a different composition is measured. Similarly α represents the natural fractionation factor between the sample and the defined standard. The double spike inversion takes the yellow circled compositions (double spike composition, the measured value of the sample-D.S. mixture, and the standard composition) as inputs to determine the unknown fractionation factors (α and β), the proportion of double spike (p), and the values of the sample-D.S. mixture and natural sample. Adapted from Rudge et al., 2009.

Knowing the precise spike composition allows for inversion of the measurements to obtain the true sample value, corrected for mass fractionation. This method measures the relative amounts of four isotopes (^{97}Mo/^{95}Mo, ^{98}Mo/^{95}Mo, and ^{100}Mo/^{95}Mo), two of which (^{97}Mo and ^{100}Mo) are enriched. A schematic diagram, based on Rudge et al. (2009) can be seen in figure. The double-spike (DS) is a mix of the two single spikes, in this case ^{97}Mo and ^{100}Mo. When the double-spike is added to the natural sample they form a mixture in the proportions denoted by p and 1-p. This mixture is measured on the MC ICP-MS and due to the instrumental mass fractionation factor β varies from the 'true' value. For stable isotopes that undergo mass-dependent fractionation, n is the composition of a standard. The mass fractionation, both natural and instrumental, is assumed to follow a single, exponential law. The double spike inversion takes the measured compositions of DS, n, and m as inputs to determine α, β, p, N, and M.

Data reduction in this study was carried out offline using a spreadsheet deconvolution routine (Pearce et al. 2009; Dickson et al., 2014) based on the Newton-Raphson deconvolution procedure from Albarède & Beard 2004. All data are normalised to the daily mean of SRM NIST 3134. All Mo isotope variations are reported as parts-per-thousand relative to a reference solution with errors, unless otherwise stated, of 2 standard deviations from the mean. In this case the reference solution is SRM NIST 3134, as proposed to be the international reference material by Greber et al. (2012) and Goldberg et al. (2013).

$$\delta^{98}Mo_{NIST} = [(^{98}Mo/^{95}Mo_{SAMPLE}/(^{8}Mo/^{95}Mo_{NIST})-1] \times 1000$$

Standard reproducibility was determined by measurement of an in-house standard, Romil $\delta^{98}Mo_{NIST}$ = 0.05±0.05‰, n=183 (Fig. 6). IAPSO seawater (Fig. 7) was run as an "unknown standard" yielding $\delta^{98}Mo_{NIST}$ = 2.09±0.08‰ (n=43, n_{chem}=17), which is comparable to the mean of published literature values $\delta^{98}Mo_{NIST}$ = 2.08±0.10‰ (Gerber et al., 2012; Pearce et al., ;2009; Skierszka et al., 2015; Siebert et al., 2003). An additional Open University external standard (Ou-Mo) was also run: $\delta^{98}Mo_{NIST}$ = -0.35±0.03‰, n=11, comparable with the mean, from Imperial College London and the Open University, of $\delta^{98}Mo_{NIST}$ = -0.37±0.04‰ reported in Goldberg et al., 2013 (Fig. 7). Therefore, the long term reproducibility is, at worst, ±0.08‰ which makes isotopic variations in natural samples easily resolvable from analytical error. The standard data for the analytical and full procedural standards are given in table appendix A.

Table 1: Molybdenum isotope standard data for the analytical (NIST, RoMil, OU-Mo) and full procedure (IAPSO) standards reported relative to SRM NIST 3134.

Standard	$\delta^{98}Mo_{NIST}$ (‰)	2 S.D.	n	95% conf.
NIST3134	0.00	0.03	300	0.003
Romil	+0.05	0.05	183	0.007
OU-Mo	-0.35	0.03	13	0.015
IAPSO	+2.09	0.08	43	0.024

Comparisons with published values are made in the text and figures 6 and 7.

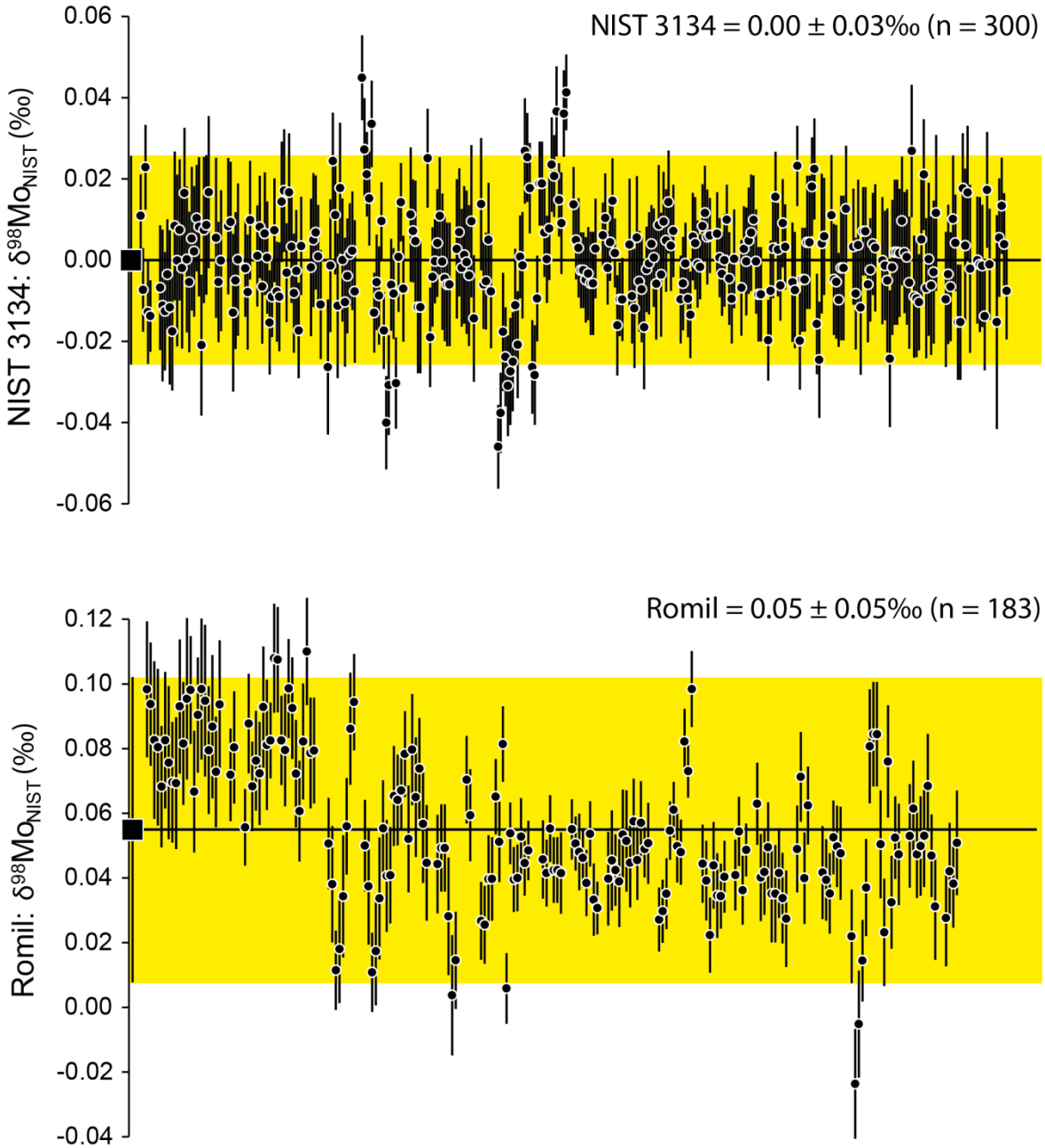

Figure 6: Analysis of analytical standards, NIST 3134 and Romil, over a two year period. Black circles denote individual analyses, normalised to NIST 3134 = 0; error bars on individual analyses are 2 se. The normalised mean with 2 sd error bars is shown as the black square and yellow shading.

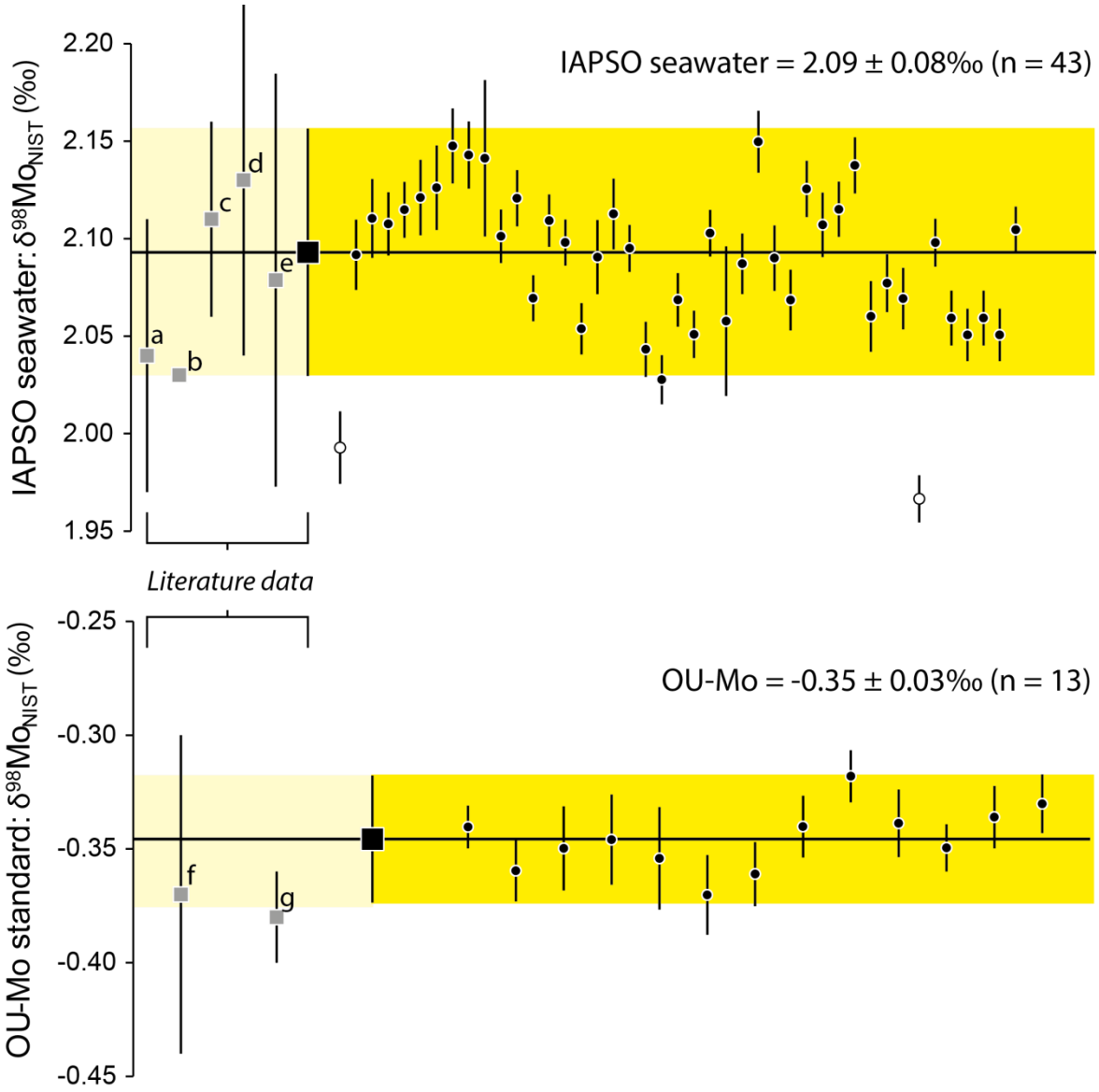

Figure 7: Analysis of the chemistry and analytical standard, IAPSO seawater, over a two year period and the inter laboratory analytical standard, OU-Mo. Black circles denote individual analyses, normalised to NIST 3134 = 0; error bars on individual analyses are 2 se. The normalised mean with 2 sd error bars is shown as the black square and yellow shading. In each case, the preceding grey squares are literature data.

a: Pearce et al., 2010 (as normalised to NIST 3134 = 0 ‰ in Goldberg et al., 2013)
b: Siebert et al., 2003 (as normalised to NIST 3134 = 0 ‰ in Goldberg et al., 2013)
c&d: Greber et al., 2012
e: Analysed at Oxford Earth Sciences (mean of data in Greber et al., 2012 and this thesis)
f: Analysed at Imperial College, London, Goldberg et al., 2013
g: Analysed at The Open University, Goldberg et al., 2013

References

ALBARÈDE, F. & BEARD, B. 2004. Analytical methods for non-traditional isotopes. Reviews in mineralogy and geochemistry, 55, 113-152.

ANBAR, A. D., KNAB, K. A. & BARLING, J. 2001. Precise Determination of Mass-Dependent Variations in the Isotopic Composition of Molybdenum Using MC-ICPMS. Analytical Chemistry, 73, 1425-1431.

ANBAR, A. D. 2004. Molybdenum stable isotopes: observations, interpretations and directions. Reviews in Mineralogy and Geochemistry, 55, 429-454.

ANBAR, A. D. & ROUXEL, O. 2007. Metal stable isotopes in paleoceanography. Annu. Rev. Earth Planet. Sci., 35, 717-746.

ARNOLD, G. L., ANBAR, A., BARLING, J. & LYONS, T. 2004. Molybdenum isotope evidence for widespread anoxia in mid-Proterozoic oceans. Science, 304, 87-90.

BARLING, J., ARNOLD, G. L. & ANBAR, A. D. 2001. Natural mass-dependent variations in the isotopic composition of molybdenum. Earth and Planetary Science Letters, 193, 447-457.

BARLING, J. & ANBAR, A. D. 2004. Molybdenum isotope fractionation during adsorption by manganese oxides. Earth and Planetary Science Letters, 217, 315-329.

BECKER , H., & WALKKER, R. J., 2003. Efficient mixing of the solar nebula from uniform Mo isotopic composition of meteorites. Nature, 425, p. 152-155.

BURKHARDT, C., KLEINE, T., OBERLI, F., PACK, A., BOURDON, B. & WIELER, R. 2011. Molybdenum isotope anomalies in meteorites: constraints on solar nebula evolution and origin of the Earth. Earth and Planetary Science Letters, 312, 390-400.

BURKHARDT, C., HIN, R. C., KLEINE, T. & BOURDON, B. 2014. Evidence for Mo isotope fractionation in the solar nebula and during planetary differentiation. Earth and Planetary Science Letters, 391, 201-211.

CROUCH, E. A. C., & TUPLIN, T. A., 1964. Isotopic Composition + Atomic Weight of Naturally Occurring Molybdenum - Possible Reflexion of Creation Process. Nature, 202, p. 1282-1284.

DAUPHAS, N., REISBERG, L., & MARTY, B., 2001. Solvent extraction, ion chromatography, and mass spectrometry of molybdenum isotopes. Analytical Chemistry, 73, p. 2613- 2616.

DICKSON, A. J. & COHEN, A. S. 2012. A molybdenum isotope record of Eocene Thermal Maximum 2: Implications for global ocean redox during the early Eocene. Paleoceanography, 27.

DICKSON, A. J., COHEN, A. S. & COE, A. L. 2014. Continental margin molybdenum isotope signatures from the early Eocene. Earth and Planetary Science Letters, 404, 389-395.

GOLDBERG, T., GORDON, G., IZON, G., ARCHER, C., PEARCE, C. R., MCMANUS, J., ANBAR, A. D. & REHKÄMPER, M. 2013. Resolution of inter-laboratory discrepancies in Mo isotope data: an intercalibration. Journal of Analytical Atomic Spectrometry, 28, 724-735.

GOSETTI, F., MAZZUCCO, E., ZAMPIERI, D. & GENNARO, M. C. 2010. Signal suppression/enhancement in high-performance liquid chromatography tandem mass spectrometry. Journal of Chromatography A, 1217, 3929-3937.

GREBER, N. D., SIEBERT, C., NÄGLER, T. F. & PETTKE, T. 2012. δ98/95Mo values and Molybdenum Concentration Data for NIST SRM 610, 612 and 3134: Towards a Common Protocol for Reporting Mo Data. Geostandards and Geoanalytical Research, 36, 291-300.

JARVIS, K. E. 1997. Inductively coupled plasma-mass spectrometry. In: GILL, R. (ed.) Modern analytical geochemistry. An introduction to quantitative chemical analysis for Earth, Environmental and Materials Scientissts. Pearson Education

KING, E. K., THOMPSON, A., CHADWICK, O. A. & PETT-RIDGE, J. C. 2016. Molybdenum sources and isotopic composition during early stages of pedogenesis along a basaltic climate transect. Chemical Geology.

MALINOVSKY, D., HAMMARLUND, D., ILYASHUK, B., MARTINSSON, O. & GELTING, J. 2007. Variations in the isotopic composition of molybdenum in freshwater lake systems. Chemical Geology, 236, 181-198.

MURTHY, V. R., 1962. Isotopic Anomalies of Molybdenum in Some Iron Meteorites. Journal of Geophysical Research, 67, p. 905-907.

MURTHY, V. R., 1963. Elemental and Isotopic Abundances of Molybdenum in Some Meteorites. Geochimica et Cosmochimica Acta, 27, p. 1171-1178.

NAKAGAWA, Y., FIRDAUS, M. L., NORISUYE, K., SOHRIN, Y., IRISAWA, K. & HIRATA, T. 2008. Precise isotopic analysis of mo in seawater using multiple collector-inductively coupled mass spectrometry coupled with a chelating resin column preconcentration method. Analytical chemistry, 80, 9213-9219.

PEARCE, C. R., COHEN, A. S. & PARKINSON, I. J. 2009. Quantitative Separation of Molybdenum and Rhenium from Geological Materials for Isotopic Determination by MC-ICP-MS. Geostandards and Geoanalytical Research, 33, 219-229.

PEARCE, C. R., BURTON, K. W., VON STRANDMANN, P. A., JAMES, R. H. & GÍSLASON, S. R. 2010. Molybdenum isotope behaviour accompanying weathering and riverine transport in a basaltic terrain. Earth and Planetary Science Letters, 295, 104-114.

PIETRUSZKA, A. J., WALKER, R. J. & CANDELA, P. A. 2006. Determination of mass-dependent molybdenum isotopic variations by MC-ICP-MS: An evaluation of matrix effects. Chemical Geology, 225, 121-136.

Qi, L., and Masuda, A., 1994. The Isotopic Composition and Atomic-Weight of Molybdenum. International Journal of Mass Spectrometry and Ion Processes, 130, p. 65-72.

RAHAMAN, W., GOSWAMI, V., SINGH, S. K. & RAI, V. K. 2014. Molybdenum isotopes in two Indian estuaries: Mixing characteristics and input to oceans. Geochimica et Cosmochimica Acta, 141, 407-422.

RUDGE, J. F., REYNOLDS, B. C. & BOURDON, B. 2009. The double spike toolbox. Chemical Geology, 265, 420-431.

SIEBERT, C., NÄGLER, T. F. & KRAMERS, J. D. 2001. Determination of molybdenum isotope fractionation by double-spike multicollector inductively coupled plasma mass spectrometry. Geochemistry, Geophysics, Geosystems, 2.

SIEBERT, C., NÄGLER, T. F., VON BLANCKENBURG, F. & KRAMERS, J. D. 2003. Molybdenum isotope records as a potential new proxy for paleoceanography. Earth and Planetary Science Letters, 211, 159-171.

SKIERSZKAN, E. K., AMINI, M. & WEIS, D. 2015. A practical guide for the design and implementation of the double-spike technique for precise determination of molybdenum isotope compositions of environmental samples. Analytical and Bioanalytical Chemistry, 1-11.

WETHERILL, G. W., 1964. Isotopic composition and concentration of molybdenum in iron meteorites. Journal of Geophysical Research, 69, p. 4403-4408.

WIESER, M. E. & DE LAETER, J. R. 2003. A preliminary study of isotope fractionation in molybdenites. International Journal of Mass Spectrometry, 225, 177-183.

WILLBOLD, M., HIBBERT, K., LAI, Y. J., FREYMUTH, H., HIN, R. C., COATH, C., VILS, F. & ELLIOTT, T. 2015. High-Precision Mass-Dependent Molybdenum Isotope Variations in Magmatic Rocks Determined by Double-Spike MC-ICP-MS. Geostandards and Geoanalytical Research.

3 Molybdenum isotope behaviour in groundwaters & terrestrial hydrothermal systems, Iceland

Rebecca A. Neely[1], Sigurdur R. Gislason[1], Magnus Ólafsson[2], Alex J. McCoy-West[3], Christopher R. Pearce[4], Kevin W. Burton3

[1]Institute of Earth Science, University of Iceland, IS-101 Reykjavík, Iceland

[2]ÍSOR, Iceland GeoSurvey, Orkugardur, Grensásvegur 9, IS-109, Reykjavík, Iceland

[3]Department of Earth Science, Durham University, Science Labs, Durham, DH1 3LE, UK

[4]National Oceanography Centre Southampton, University of Southampton Waterfront Campus, European Way, Southampton, SO14 3ZH, UK.

Molybdenum (Mo) isotopes have proved useful in the reconstruction of paleoredox conditions, but their application generally relies upon a simplified model of ocean inputs, in which rivers dominate Mo fluxes to the oceans and hydrothermal fluids are considered to be a minor contribution. To date, however, little attention has been paid to the extent of Mo isotope variation of hydrothermal waters, or to the potential effect of direct groundwater discharge to the oceans. Here we present Mo isotope data for two Icelandic groundwater systems (Mývatn and Þeistareykir) that are both influenced by hydrothermal (geothermal) processes. The cold (<10°C) groundwaters ($\delta^{98/95}Mo_{GROUNDWATER}$ = -0.40‰ to +0.22‰; n = 13) show little, if any, fractionation from the host basalt ($\delta^{98/95}Mo_{BASALT}$ = -0.4‰ to -0.1‰) and are, on average, lighter than both global and Icelandic rivers. In contrast, waters that are hydrothermally influenced (>10°C) possess isotopically heavy $\delta^{98/95}Mo_{HYDROTHERMAL}$ values of +0.22‰ to +1.81‰ (n = 18) with the possibility that the high temperature endmembers are even heavier. Although the mechanisms driving this fractionation remain unresolved, the incongruent dissolution of the host basalts and both the dissolution and precipitation of sulfides are considered. Regardless of the processes driving these variations, the $\delta^{98}Mo$ data presented in this study indicates that groundwater and hydrothermal waters have the potential to alter ocean budget calculations, and may prove useful in the interpretation of molybdenite data in ore genesis studies.

3.1 Introduction

Molybdenum (Mo) is an essential micronutrient and redox sensitive transition metal that provides key information in Earth and environmental studies. Molybdenum stable isotopes have been extensively used as a paleoredox proxy (e.g. Asael et al., 2013; Barling et al., 2001; Barling & Anbar 2004; Archer & Vance 2008; Pearce et al., 2008; Goldberg et al., 2009), as well as in the study of ore formation (e.g. Greber et al., 2014; Breillat et al., 2016), and planetary evolution (e.g. Burkhardt et al., 2014).

Despite having generally low crustal concentrations (~1-2 ppm; Taylor and McLennan, 1985), Mo is the most abundant transition metal in the modern oceans at ~10 ppb (e.g. Nakagawa et al., 2012, Table 1). This relatively high concentration results from the efficient transport of Mo from the continents to the oceans, due to the solubility of Mo phases transported via oxidative weathering, and its subsequent slow removal from the oceans in the presence of dissolved O^{2-}.The resulting residence time of Mo in the oceans of 440 ka (Miller et al., 2011), is more than two orders of magnitude greater than the ocean mixing time of approximately 1.5 ka, consequently the oceans have uniform Mo elemental and isotope compositions (Nakagawa et al., 2012).

Under oxidising conditions Mo is present in solution as the stable molybdate ion, MoO_4^{2-}, (Fig. 2). In this form Mo is slowly removed from the water column through uptake into ferromanganese phases, which preferentially incorporate isotopically light Mo (e.g. Barling et al., 2001; Barling & Andbar 2004; Goldberg et al., 2009; Miller et al., 2011; Wasylenki et al., 2011). As a result of this fractionation the modern oceans are the heaviest Mo reservoir on Earth (Kendall et al., 2016). In contrast, Mo is readily removed from solution in anoxic-sulfidic waters with very little isotopic fractionation. In the presence of reduced sulfur, Mo forms oxothiomolybdate ions, $MoO_{4-x}S_x^{2-}$, which are highly particle-reactive and thus rapidly removed from solution (e.g. Barling et al., 2001). This behaviour underpins the application of Mo isotopes and abundances as a proxy for past ocean anoxia (e.g. Pearce et al., 2008; Asael et al., 2013).

Early paleoredox studies assumed a comparatively straightforward ocean budget in which Mo input was dominated by the dissolved riverine phase that was assumed to be stable through time and to directly reflect the chemical signature of continental rocks. However, many studies have since demonstrated that the average riverine composition is heavier than the catchment bedrock, both globally (e.g. $\delta^{98}Mo_{GLOBAL\ RIVERS}$ = +0.35‰ to +2.05‰; Archer & Vance 2008) and locally (e.g. $\delta^{98}Mo_{ICELAND\ RIVERS}$ = 0‰ to +1‰ in a basaltic (<0‰) catchment; Pearce et al., 2010). This enrichment in heavy isotopes in the dissolved phase is attributed to a number of processes including: incongruent dissolution during weathering (e.g. Neubert et al., 2011; Voegelin et al., 2012); adsorption of isotopically light Mo to organic phases in soils (e.g. Siebert et al., 2015; King et al., 2016); and, although considered small in terms of mass balance, adsorption of light Mo to riverine particles (e.g. Archer & Vance 2008; Pearce et al., 2010).

In contrast to the dissolved riverine Mo flux, little attention has been paid to the potential Mo contributions of groundwater to the oceans. Groundwaters may affect seawater chemistry both directly (through submarine groundwater discharge) and indirectly as a significant source of river base flow (Church 1996). Indeed, Pearce et al. (2010) attributed some of the observed progressive increase in riverine δ^{98}Mo to the addition of isotopically

heavy groundwater, and Rad et al. (2007) have shown that volcanic island weathering rates may have been underestimated by up to a factor of 5 where the subsurface water flow is not accounted for. The significance of groundwater contributions to riverine and seawater Mo signatures is poorly constrained due to the paucity of data. To date only King et al. (2016) have reported groundwater δ^{98}Mo data, and these are characterised by isotopically heavy δ^{98}Mo compositions (0.00‰ to +0.26‰) relative to the catchment bedrock (δ^{98}Mo 0.19‰) in Hawaii, attributed to the retention of light isotopes in soils and the preferential leaching of heavy Mo.

In terms of ocean budgets, groundwater contributions to base flow are accounted for in the global riverine discharge. However, the direct contribution of Mo to seawater from submarine groundwater discharge has rarely been taken into account in marine mass balance. Using 226Ra, Moore (1996) demonstrated that submarine groundwater discharge over 350 km of south-eastern coastline of the United States of America is comparable to the observed river discharge, resulting in groundwater contributions of up to 40% of the river-water flux. Direct groundwater discharge may therefore contribute a significant proportion of the water flux to the oceans.

At the present day, rivers (potentially including substantial groundwater contributions) are thought to contribute some 90% of oceanic Mo inputs, with the remaining 10% accounted for by chemical exchange in oceanic hydrothermal systems (McManus et al., 2002). When applying Mo as a paleoredox proxy to time periods such as the Archean, hydrothermal heat losses were likely much greater than at present (Lowell & Keller 2003). In this case the hydrothermal input of Mo may have been more significant in seawater mass balance. Through detailed study of fluid inclusions from identified hydrothermal vents of mid-Archean age in the Barberton formation, South Africa, De Ronde et al. (1997) found that the vent fluids likely had similar chemical signatures to those of modern day vents. As such, the study and characterisation of modern hydrothermal systems will enable better constraints to be placed on inputs to the oceans through geologic time.

Data for mid-ocean ridge (MOR) hydrothermal waters are currently limited to a low-temperature (sampling at 25°C, formation fluids ~63°C) flank system at Juan de Fuca, with endmember fluids of δ^{98}Mo +0.6‰ (McManus et al., 2002). However, it is unclear if this signal represents basalt-seawater interaction or if it was inherited from the overlying sediments. Whilst high-temperature hydrothermal systems are not thought to be significant sources of Mo to the oceans (Miller et al., 2011) the only value currently available for a terrestrial hydrothermal system is δ^{98}Mo -3.7‰ (Pearce et al., 2010) and this exceptionally light value remains difficult to explain.

This study presents Mo isotope and elemental data for two groundwater systems, in northeast Iceland both of which have been influenced by hydrothermal activity. These results allow us to assess the processes controlling Mo behaviour in these systems, and to quantify the input of these sources to the oceans.

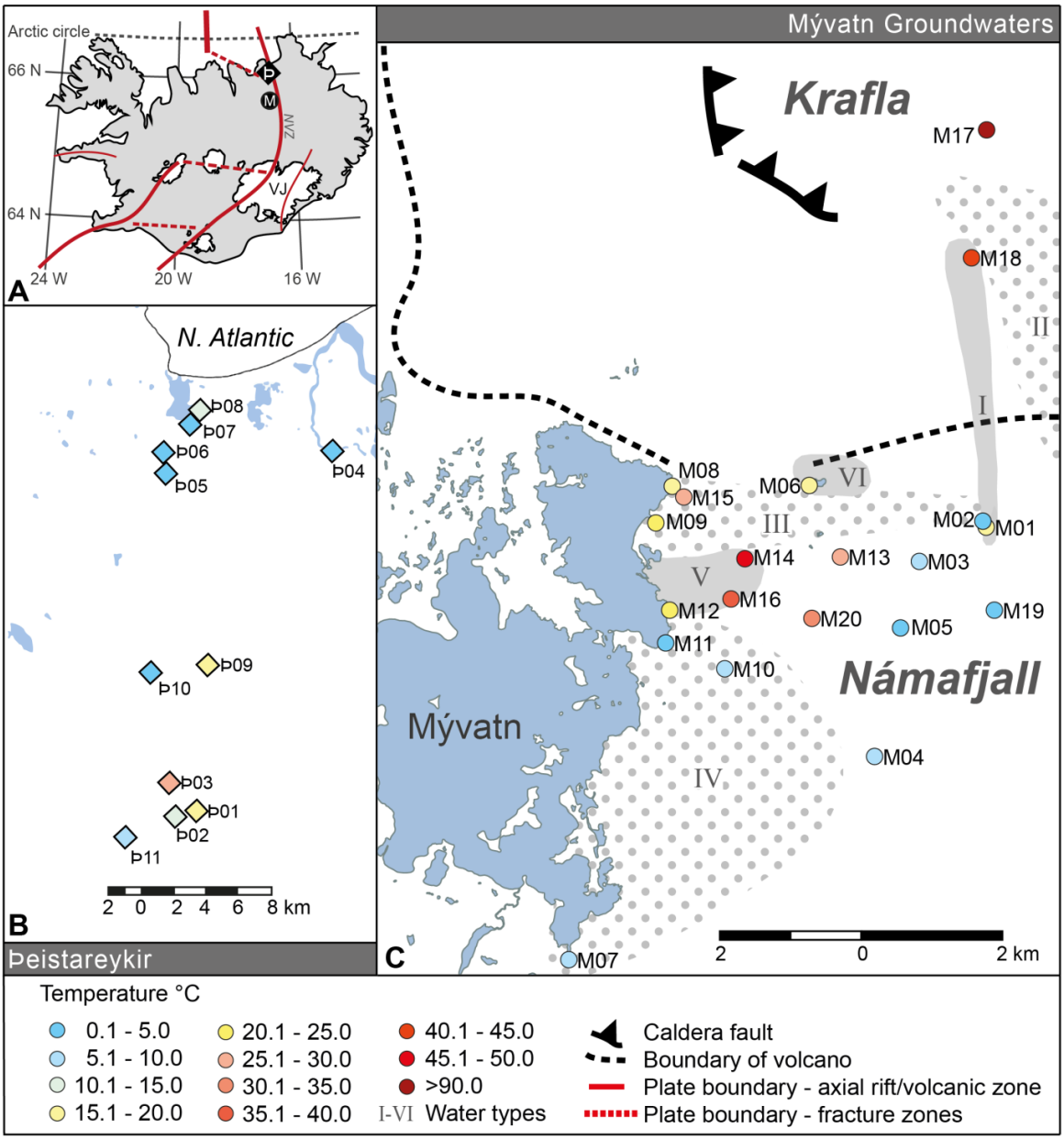

Figure 1: Map showing the location and sampling temperatures of the Mývatn (M) and Þeistareykir (Þ) groundwater samles in the northern volcanic zone (NVZ) of Iceland. Inset A shows the two groundwater systems in relation to the major geographical features of Iceland; the main volcanic and fracture zones are shown in red and major icecaps and glaciers in white. Inset B depicts the Þesitaryekir sampling locations (diamonds) and inset C the Mývatn groundwater samples (circles). As the main study area, the Mývatn samples are overlying a simple base map including the Krafla caldear features (Gudmundsson & Arnorsson 2002) and the groundwater types (I-VI) defined based on their chemistry by Ármannsson et al. (2000). The cold growdwaters for both systems are sourced from as far south as Vatnajöjull (VJ) glacier.

3.2 Geological setting and methods

3.2.1 Geological setting

Hydrothermal (geothermal) activity in Iceland is widespread and associated with both active volcanic centres and off-axis fracture systems. The studied groundwater systems (Fig.1) are both meteoric in origin and located in the northern volcanic zone (NVZ), which extends from the centre of Iceland into the North Atlantic Ocean.

The first groundwater system is located in the Mývatn area of northeast Iceland (Fig. 1c). It is associated with the volcanic centre of Krafla, an 8 km caldera with a fissure swarm extending 50 km to the north and 40 km to the south. The Krafla geothermal fields are located within the caldera whilst the Námafjall geothermal field lies outside within the southern fissure swarm (Fig. 1) (Gudmundsson & Arnórsson 2005). The fluids are dilute (900 ppm to 1500 ppm total dissolved solids; Gudmundsson & Arnórsson 2002, 2005; Kaasalainen & Stefánsson 2012) and are of meteoric origin (based upon δD and $\delta^{18}O$ content; Darling & Ármannsson, 1989 in Gudmundsson & Arnórsson 2002). Groundwaters in this region have been divided into six distinct groups by Ármannsson et al. (2000) based upon their geographic location, δD, $\delta^{18}O$, and Cl and B concentrations. These classifications are shown in figure 1. There is some debate as to whether the dominant geothermal source is from Krafla or Námafjall (e.g. Armannsson et al., 2000; Ólafsson et al., 2015). Most recently Ólafsson et al. (2015) used Cl/B ratios to demonstrate that the, warm, Mývatn groundwaters may be dominated by fluids from the Krafla geothermal system. Due to the utilisation of these fields for geothermal energy these systems are well characterised; this study makes use of these waters to examine Mo behaviour in both cold groundwaters and hydrothermally influenced systems.

The second groundwater system, Þeistareykir, is located in the westernmost fissure swarm in the NVZ, characterised by large normal faults and rift fissures (Sveinbjornsdottir et al., 2013). The high temperature geothermal activity is linked to magma intrusions associated with the most recent volcanic activity ~2500 years ago (Sveinbjornsdottir et al., 2013). Like the Mývatn groundwater system, the fluids are dilute meteoric waters (~750 ppm to 1100 ppm dissolved solids; Óskarsson et al., 2013) that originate from south of the area (Sveinbjornsdottir et al., 2013).

3.2.2 Methods

Groundwater samples (Mývatn: M01 – M20 and Þeistareykir: Þ01 – Þ11) were collected during routine sampling carried out by the Icelandic GeoSurvey (ÍSOR) in conjunction with Landsvirkjun (National Power Company of Iceland) (ÍSOR report for Landsvirkjun; Kristinsson et al., 2014). Samples for Mo isotope analysis were filtered (0.2 μm) into 1 L, pre-cleaned, high density polyethylene bottles, acidified and stored in the dark before analysis. Physical properties, sampling conditions, and major- and trace-element concentrations, from Kristinsson et al. (2014), are reproduced in the electronic supplements (Table ES1). All Mo isotope data measured in this study are reported in Table 1.

In situ pH and Eh (redox potential) values, at the measured sampling temperature of the waters, were calculated by PHREEQC version 3.0.6 (Parkhurst & Appelo 2013) using the

minteq.v4 database. Redox was determined using the measured iron and sulfur speciation and by assuming atmospheric oxygen saturation at the measured water temperature. The results from each approach were compared, and although the absolute values vary depending on the defined redox couple, the relative trends do not. The best approximation of redox shows that oxidised MoO42- dominates the groundwaters (Fig. 2), as is known to be the case for most Icelandic waters below 200°C (Arnórsson and Ívarsson 1985).

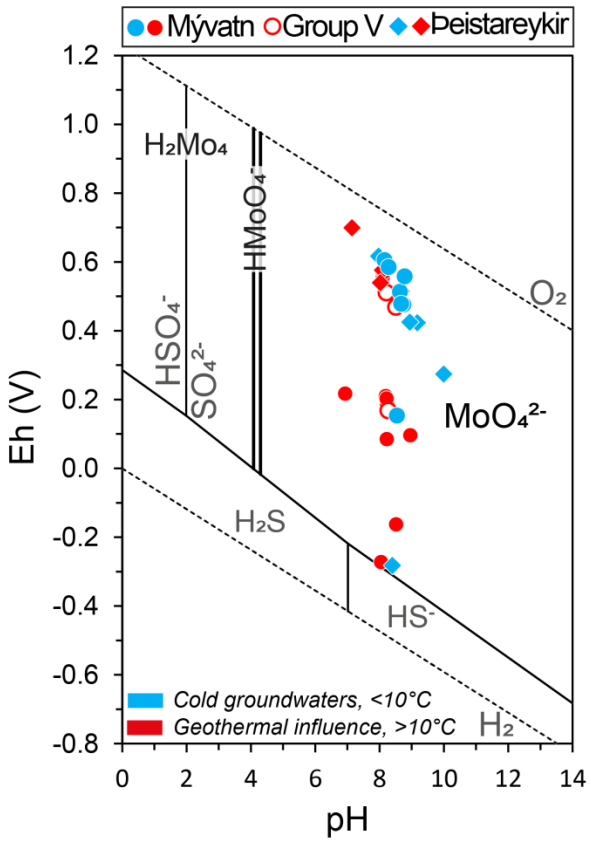

Figure 2: pH-Eh diagram at 25°C and 105 Pa for the S-O-H system with available, oxidised, Mo data superimposed. Mo speciation below the SO42- - H2S transition is not well characterised although it is thought to be dominated by oxythiomolybdate species (MoO4 xSx2-). Calculated in situ pH and Eh for the groundwater samples are plotted and, despite a range in Eh values, all are dominated by MoO42-. Calculations are based on the minteq.v4 database within PHREEQC (Parkhurst & Appelo 2013). The stability field for water lies between the two dashed lines.

In addition to the water samples, 8 rock and sulfide samples were analysed (Table 2). The rock samples are basalts from depth within the Reykjanes geothermal system, Iceland. These were powdered in an agate mill before total dissolution of ~50 mg in a concentrated HF HNO_3 mix (1:2). The sulfides; chalcopyrite (0.2 g), pyrrhotite (0.6 g) and pyrite (0.7 g) are from peridotite and serpentinite hosted ores in the Outokumpu district, Finland, thought to be fragments of ophiolitic ultramafic-mafic rocks. The sulfides were dissolved using a combination of HNO_3 and HCl acids. After complete dissolution the basalts were dried

down before re-dissolution in HCl and treated in the same manner as the groundwater samples; the sulfides were purified using different purification chemistry, as detailed in section 2.3.

3.2.3 Molybdenum isotope chemistry and analysis

Sample preparation and δ^{98}Mo measurements were undertaken in the Department of Earth Sciences at Durham University. Preliminary Mo concentrations were determined by inductively coupled plasma mass spectrometry (ICP-MS). A volume of each sample was then weighed and spiked with a ^{97}Mo-^{100}Mo double-spike to yield a ~1:1 ratio of spike to natural Mo with 50 100 ng of natural Mo (basalt samples were spiked during digestion). Chemical separation of Mo was achieved using a single pass anion exchange procedure detailed in Pearce et al. (2009), with an additional 12 ml 0.5 M HF matrix elution step to ensure complete removal of Zn before final Mo elution in 3 M HNO_3. Sulfide separates were purified using a double pass through anion exchange columns following the protocol described in Willbold et al. (2017), where dilute ascorbic acid is used during sample loading for optimal Fe removal.

Molybdenum isotope compositions were measured using a multi-collector ICP-MS (Thermo-Finnigan Neptune, Durham University) equipped with an Aridus II desolvating nebuliser. Samples were aspirated at ~35 µl min 1 and the maximum sensitivity was ~400 V ppm^{-1}. Measurements were made in low resolution mode using X-cones and static collectors. Analyses consisted of 50 cycles of 4s integrations. Total procedural blanks were <1 ng Mo and data processing was conducted offline using a deconvolution routine (Pearce et al. 2009) based on the Newton-Raphson method.

All Mo isotope compositions are reported in conventional delta notation in parts-per-thousand relative to a reference solution (Eq. 1) with errors given as 2 standard deviations from the mean. Given the inconsistent reporting of Mo isotope data in the literature it is important to note that all data, including literature data, are reported referenced to SRM NIST 3134 = 0‰ (Goldberg et al., 2013).

$$\delta^{98/95}Mo_{NIST} = \left[\left(\frac{\frac{^{98}Mo}{^{95}Mo_{SAMPLE}}}{\frac{^{98}Mo}{^{95}Mo_{NIST\ 3134}}}\right) - 1\right] \cdot 1000 \qquad (1)$$

Long-term machine reproducibility was determined by measurement of an in-house Romil standard, which gave δ^{98}Mo = +0.05 ± 0.05‰ (n = 183). The IAPSO seawater standard gave a δ^{98}Mo composition of +2.09 ± 0.08‰ (n = 43), which is indistinguishable from the mean of published values of +2.08 ± 0.10‰ (given in Goldberg et al., 2013). As this is the first Mo data from Durham University an additional Open University standard (Ou-Mo) was also run; this gave a mean δ^{98}Mo value of -0.35 ± 0.03‰ (n = 11), comparable with values obtained from Imperial College London (0.37 ± 0.04‰) and the Open University (

0.38 ± 0.02‰) (Goldberg et al., 2013). Taken together, these data suggest a long-term external reproducibility (2 s.d.) of ± 0.08‰ or better.

3.3 Results

A complete data table (Table ES1) of major and trace elements is reproduced in the supplementary data, after Kristinsson et al. (2014). Sampling temperatures range from 0°C to 93.2°C and in situ pH is generally alkaline with an mean of 8.4 (Fig. 2) and ranging from 6.9 to 10.0. Aqueous components such as total dissolved solids (TDS), SO_4^{2-}, and SiO_2 increase with temperature with marked increases over 10°C; as such, for ease of discussion, samples >10°C are grouped together and considered as hydrothermally influenced groundwaters.

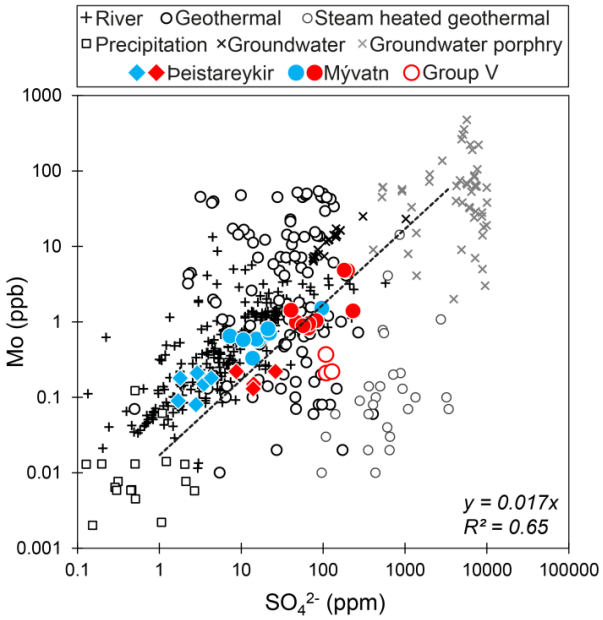

Figure 3: Molybdenum and SO_4^{2-} in precipitation, surface waters, groundwaters, and geothermal systems after Miller et al. (2011). The greyed data are from the literature: river and precipitation data from Miller et al. (2011) and Neubert et al. (2011), geothermal from Kaasalainen & Stefánsson (2012) and Arnórsson & Ívarsson (1985), and groundwaters from Leybourne & Cameron (2008). The coloured data are from this study: filled circles are Mývatn groundwaters whilst the diamonds are from Þeistareykir, blue denotes a sampling temperature of less than 10°C and red, hydrothermally influenced waters. After Miller et al. (2011), a best-fit regression line, forced through the origin, is plotted through the groundwaters from this study (excluding the group V waters as described in the text) and the resulting slope and coefficient of determination fit parameter (R^2) are shown and are in agreement to those reported in Miller et al. (2011) for rivers ($y = 0.01x$, $R^2 = 0.69$).

Table 1: Selected data for Mývatn and Þeistareykir groundwaters.

		Temp °C	pH* *in situ*	Eh* V	Na ppm	Mg ppm	Cl ppm	H_2S ppm	SO_4 ppm	Mo ppb	δ^{98}Mo ‰	2 SD	n
MÝVATN GROUNDWATERS													
M01	Hliðardalslækur	15.9	8.23	0.08	91.3	12.50	26.00	b.d.l	199.00	4.81	0.80	± 0.04	4(2)
M02	AB-2	3.3	8.16	0.60	11.2	5.15	4.36	b.d.l	13.80	0.331	0.04	± 0.08	2
M03	LUD-4	5.4	8.29	0.58	53.6	9.20	12.30	b.d.l	96.20	1.52	0.87	± 0.08	2
M04	LUD-2	5.6	8.55	0.15	18.6	7.60	5.74	b.d.l	16.10	0.565	0.14	± 0.08	2
M05	LUD-3	4.5	8.64	0.51	15.3	7.07	5.29	b.d.l	15.30	0.594	0.14	± 0.08	2
M06	Svelgur	19.2	6.94	0.22	119.0	1.21	54.00	0.05	181.00	4.85	1.30	± 0.08	2
M07	Garðslind	6.5	8.96	0.10	17.4	4.64	2.11	b.d.l	7.33	0.654	0.22	± 0.08	2
M08	Bjarg	19	8.11	0.56	44.3	4.02	9.71	b.d.l	47.10	0.988	0.22	± 0.01	3
M09	Helgavogur	23.3	8.24	0.19	52.3	5.56	8.04	b.d.l	66.20	0.832	0.47	± 0.08	3
M10	Hverfjallsgjá	6.5	8.75	0.48	21.5	6.84	5.08	b.d.l	22.10	0.713	0.13	± 0.08	2
M11	Vogaflói	5	8.79	0.56	21.1	6.26	4.75	b.d.l	21.20	0.812	0.08	± 0.08	2
M12	Langivogur	21.5	8.51	0.47	76.9	3.64	15.10	b.d.l	108.00	0.371	0.81	± 0.08	2
M13	LUD-10	25.3	8.2	0.21	37.3	8.57	4.54	b.d.l	40.50	1.43	0.37	± 0.03	3
M14	Grjótagjá	46.1	8.27	0.17	86.3	3.09	17.70	0.08	109.00	0.206	1.81	± 0.03	5(2)
M15	Stóragjá	26.5	8.23	0.20	61.8	5.58	9.57	b.d.l	81.90	1.04	0.68	± 0.06	3
M16	Vogagjá	40	8.21	0.51	88.0	2.49	17.50	b.d.l	128.00	0.219	1.12	± 0.06	3
M17	Skiljustöð	93.2	8.52	-0.16	250.0	0.01	81.30	22.4	232.00	1.40	0.83	± 0.08	2
M18	AE-10	40.6	8.05	-0.27	42.0	0.99	4.09	0.03	66.80	0.954	0.34	± 0.01	3
M19	LUD-5	4.3	8.68	0.48	13.6	6.55	4.88	b.d.l	10.60	0.579	-0.07	± 0.06	3
M20	LUD-6	33	8.22	0.51	51.7	7.11	5.67	b.d.l	57.00	0.888	0.56	± 0.08	5(2)
ÞEISTAREYKIR GROUNDWATERS													
Þ01	Þeistareykir-vatnsból	0	7.15	0.70	15.2	5.68	5.81	b.d.l	14.20	0.176	0.43	± 0.13	3
Þ02	Þeistareykir-Sæluhús	11.6	8.14	0.57	20.8	3.69	7.41	b.d.l	26.10	0.235	0.25	± 0.08	2
Þ03	ÞR-5	26.6	8.09	0.58	20.8	3.68	7.45	b.d.l	26.20	0.283	0.22	± 0.06	3
Þ04	Krossdalur	3.4	8.68	0.52	9.3	2.67	8.73	b.d.l	3.50	0.181	-0.25	± 0.08	2
Þ05	Fjöll - lind	2.6	10	0.27	16.3	0.05	7.84	b.d.l	4.26	0.209	-0.33	± 0.08	2
Þ06	Fjöll - vatnsból	2.8	9.18	0.42	11.9	0.42	10.40	b.d.l	2.76	0.103	-0.08	± 0.08	2
Þ07	Lón	4.4	7.97	0.62	8.7	2.59	7.68	b.d.l	2.91	0.255	-0.19	± 0.10	3
Þ08	Rifós - Tangabrunnur	10.2	8.24	0.59	14.8	3.41	10.00	b.d.l	8.73	0.269	0.00	± 0.03	3
Þ09	ÞR-15	15.3	8.03	0.54	13.0	3.91	7.50	b.d.l	14.00	0.171	0.30	± 0.12	3
Þ10	ÞR-8	2.5	8.4	-0.28	6.9	1.95	6.95	0.03	1.71	0.097	-0.40	± 0.08	2
Þ11	ÞR-16	5.2	8.95	0.42	8.6	3.37	5.45	b.d.l	1.84	0.189	-0.29	± 0.07	3
IAPSO seawater										10.8	2.09	± 0.08	43(17)

**Calculated using PHREEQC and the minteq.v4 database (Pankhurst and Apello, 2013) at in situ temperature conditions. b.d.l. - below detection limit (0.01 ppm for H_2S). Errors are reported as 2 SD of the mean when n≥3 and as the 2 SD of repeat IAPSO analyses when n<3*

The overall range in Mo concentration in the groundwaters varies from 0.08 ppb to 4.85 ppb (Table 1; Fig 3). In general, the cold groundwaters (sampling temperature <10°C) contain less Mo than the hydrothermally influenced waters. The Þeistareykir waters (diamonds) have a narrow range of relatively low Mo concentrations (0.08 to 0.22 ppb) whilst the Mývatn waters (circles) range from 0.21 to 4.85 ppb. Curiously, although the group V waters are located in the Mývatn groundwater system and are hydrothermally influenced, they have notably lower Mo concentrations (0.21 to 0.37 ppb, Fig. 3) than the other hydrothermal samples.

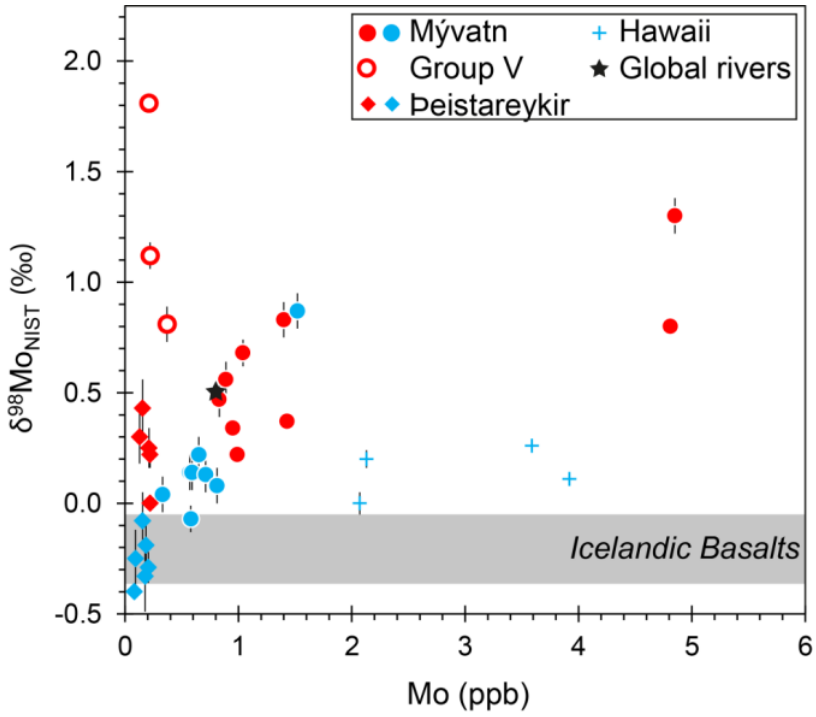

Figure 4: Mo concentration and isotope data for terrestrial groundwaters including those that are geothermally affected (red). All data are from this study save for the four Hawaiian groundwaters (blue crosses) from King et al. (2016). For reference, values for a range of Icelandic basalts (Table 2) and the mean global river composition (Archer & Vance 2008) are plotted.

The groundwaters possess a wide range of δ^{98}Mo isotope compositions, from -0.33‰ to +1.81‰ (Table 1, Fig. 4 & 5). The cold Þeistareykir waters are isotopically very light, with δ^{98}Mo varying from -0.40‰ to -0.08‰, whilst the more hydrothermally influenced waters are isotopically heavier, up to +0.43‰. Similarly, the cold waters from the Mývatn area range from δ^{98}Mo -0.07‰ to +0.22‰ whilst the hydrothermally influenced waters are heavier: between +0.22 and +1.81‰. The exception to this is sample M03 (LUD-4), a cold water well with a high Mo concentration (1.52 ppb), heavy Mo isotope composition of +0.87‰ (Table 1, Fig. 4), and distinctive chemistry including, for example, elevated TDS, SO_4^{2-}, and Al (Table ES1).

The basalts contain from 0.14 ppm to 1.01 ppm Mo, with the hyaloclastite having the highest concentration of 4.67 ppm Mo (Table 2). In comparison, the chalcopyrite contains an order of magnitude more Mo (38 ppm) whilst the pyrite and pyrrhotite contain 0.074 ppm and 0.048 ppm, respectively. The basalts are isotopically light, ranging from -0.09‰ to -0.37‰ whilst the sulfides are all isotopically heavy; the chalcopyrites are +0.9‰ and the pyrite and pyrrhotite +1.55‰ and +1.21‰, respectively.

Table 2: Selected data for complimentary basalt and sulfide samples

		Mo ppm	δ^{98}Mo ‰	2 SD	n
ICELANDIC BASALT*					
RN09-642		1.007	-0.31	± 0.06	4 (2)
RN09-900		0.242	-0.37	± 0.08	2
RN09-1102		0.135	-0.25	± 0.08	2
RN09-1200	(Hyaloclastite)	4.665	-0.09	± 0.03	3 (2)
SULPHIDES					
279-1	Chalcopyrite	38.11	0.92	± 0.03	4
279-8	Chalcopyrite	37.97	0.90	± 0.03	3
279-9	Pyrite	0.074	1.55	± 0.08	1
279-10	Pyrrhotite	0.048	1.21	± 0.08	1

*Errors are reported as 2 SD of the mean when n≥3 and as the 2 SD of repeat IAPSO analyses when n<3. *Bulk rock measurements*

3.4 Discussion

3.4.1 Cold groundwaters

Generally, in these cold Icelandic groundwaters, as the Mo concentrations increase the isotopic composition becomes increasingly heavy (Fig. 4). However, with the exception of sample M03, the cold groundwaters show only a small degree of fractionation away from the average composition of Icelandic basalts (Fig. 4). The Þeistareykir groundwaters and cold Mývatn samples (except M03) are isotopically indistinguishable from igneous rocks ($\delta^{98}Mo_{IGNEOUS}$ -0.3‰ to +0.4‰; e.g. Pearce et al., 2009; Voegelin et al., 2012; Siebert et al., 2015). Icelandic basalts, in particular are isotopically light, and in this study they possess compositions that range from $\delta^{98}Mo_{BASALT}$ -0.09‰ to -0.37‰, comparing favourably with the USGS standard BIR-1 at -0.1‰ (e.g. Burkhardt et al., 2014) and Icelandic lavas at -0.15‰ (Yang et al., 2015). The cold Þeistareykir samples are also isotopically light (-0.40‰ to +0.08‰), similar to the down-well Icelandic basalts measured in this study (Fig. 4).

The mean δ^{98}Mo value of the cold groundwaters in Þeistareykir is -0.26‰ and in Mývatn, +0.08‰. These values are comparable to the basalt-hosted Hawaiian groundwaters measured by King et al. (2016), which have a mean Mo isotope composition of +0.14‰ (range: 0.00‰ to +0.26‰) (Fig. 4). Whilst the waters are isotopically similar, the Mo concentrations in the Icelandic groundwaters are almost an order of magnitude lower than those in Hawaii. The Hawaiian groundwater Mo concentrations range from 1.83 ppb to 4.86 (mean: 3.0 ppb) whilst the maximum Mo in the cold Icelandic waters is 1.52 ppb with a mean of 0.5 ppb (slightly higher than the 0.2 ppb mean of 150 cold groundwaters from an earlier study in north Iceland; Árnórsson & Óskarsson 2007). The Icelandic groundwaters fall between the average global river concentration of 0.8 ppb (Miller et al., 2011) and an Icelandic river average of 0.2 ppb (from 6 catchments in northeast Iceland over some 6 years of monitoring; Eiriksdóttir et al., 2015).

The Icelandic groundwaters also fall within the range of Mo isotope values measured in rivers both locally, in Iceland (δ^{98}Mo from -0.5‰ to +1.4‰ (Pearce et al., 2010), and

globally (-0.35‰ to +2.05‰; summarised in Kendall et al. (2016)). However, on average they are lighter than the global riverine mean of δ^{98}Mo +0.5‰ (Archer & Vance 2008) (Fig. 4 & 8) and the Iceland riverine mean of +0.4‰ (Pearce et al., 2010). If the proportion of direct groundwater discharge is anywhere close to the 40% of river discharge, as suggested by Moore (1996), and the global groundwater mean is isotopically lighter than that of the global river discharge, as indicated by these data and that of King et al. (2016), then the combined input to the oceans may need to be revaluated (see section 4.4). We recognise, however, that current groundwater δ^{98}Mo data remain limited both in terms of their geological setting and their host lithologies.

3.4.2 Groundwater mixing

As with all groundwaters, the chemistry of the Þeistareykir and Mývatn waters is determined by the composition of the source, precipitation, degree of water-rock interaction, mixing with other waters, and the introduction of volcanic gasses (Ármannsson et al., 2000). In the case of these two systems, the influence of hydrothermal waters is significant with mixing and, to a lesser extent, steam-heating known to be important controls on chemistry (Darling & Ármannsson 1989; Ólafsson et al., 2015).

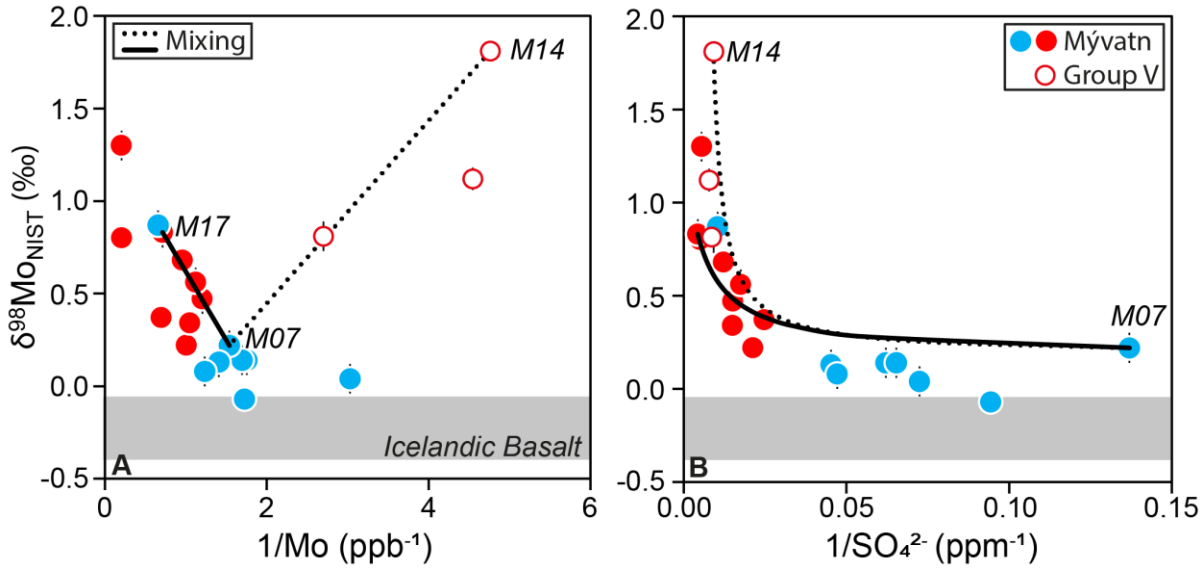

Figure 5: Relationship between Mo isotopes and Mo and SO_4^{2-} concentrations in the Mývatn groundwater system. Cold groundwaters (sampling temperature <10°C) are depicted in blue whilst those that are geothermally influenced are shown in red. The distinct group V waters (as discussed in the main text) are open red circles. For reference, the Mo isotopic range of Icelandic basalts ($\delta^{98}Mo_{BASALT}$ = -0.1 to -0.4‰) is shown as the shaded band (Table 2). There are two mixing lines, both have a common cold groundwater endmember (M07) but two distinct geothermal endmembers: one low [Mo], mid-range SO_4^{2-}, and isotopically heavy (M14, dashed line) and one high [Mo], high SO_4^{2-}, and heavy Mo isotopes (M17solid line).

For the Mývatn waters, the cold groundwater endmember is represented by M07, Garðslind (Fig. 5; Table 1). It is one of the largest cold-water springs in the region and is taken to represent the non-geothermally influenced endmember (Ólafsson et al., 2015). It is not possible to account for all of the Mývatn groundwater data with one simple mixing model (Fig. 5), suggesting that either there are two distinct hydrothermal endmembers, or else that the chemistry of these waters is not controlled by simple mixing alone. The most recent work on the origin of these groundwaters (Ólafsson et al., 2015) concluded that the warm waters may be related to the Krafla hydrothermal fluids as opposed to Námafjall. Sample M17 is therefore taken to represent a geothermal endmember; it is isotopically heavy, has a relatively high Mo concentration (1.4 ppb), and negligible Mg, as is characteristic of hydrothermal waters due to the almost total removal of Mg from solution during high-temperature basalt-water interaction via the formation of Mg-OH silicates (e.g. Bischoff & Dickson 1975).

Mixing between these two endmembers can account for the majority of the Mývatn groundwaters (solid line; Fig. 5). However, the group V waters do not fit this trend (dashed line; Fig. 5); instead they require an isotopically heavy but low Mo concentration endmember. The low Mo concentration is somewhat surprising as these waters are thought to result from straightforward mixing between cold and geothermal groundwaters (Darling & Ármannsson 1989) and Mo is known to be enriched in geothermal waters compared with cold groundwaters and surface waters (Arnórsson & Ívarsson., 1985). Therefore, it is necessary for significant loss of light Mo to have occurred in order to account for the low Mo concentrations seen in these three waters.

Ólafsson et al. (2015) argued that these warm waters are, in part, formed as a consequence of steam-heating. While the behaviour of Mo in the steam (vapour) phase remains poorly understood, several studies suggest that the vapour may contain significant Mo. In fumaroles, Mo can range from 2 to 2.8 ppm and from 1.2 to 168 ppm in inclusions (Hurtig et al., 2014). Even more limited are data on the isotope composition but it is suggested that lighter Mo isotopes accumulate in the vapour whilst heavier isotopes remain in the brine (Kendall et al., 2016). These observations are consistent with preliminary measurements of the vapour phase in geothermal systems from Iceland. All show preferential partitioning of light Mo into the vapour (Neely et al., in prep; Chapter 5) however, Mo concentrations in the vapour phase are relatively low, from 0.30 to 3.27 ppb.

As Mo can partition into vapour with isotope fractionation, it is possible that this process has influenced the composition of the hydrothermally affected waters. However, steam-heating would add isotopically light Mo which cannot explain the isotopically heavy hydrothermal waters. Combined with the indication of relatively low Mo concentrations in the vapour (Neely et al., in prep) this suggests that steam-heating is not a dominant control on the Mo composition of these waters, in agreement with the conclusions of Ólafsson et al., 2015.

3.4.3 Controls on hydrothermal endmember Mo composition

Few minerals contain Mo as a major constituent. Of these sulfides such as molybdenite (MoS_2) and pyrite (FeS_2) dominate, with molybdenite containing approximately 60% Mo by weight and often dominating the mass balance in mineralising systems (Kendall et al.,

2016). The association of Mo and S in sulfides and the high solubility of their oxidised species (MoO_4^{2-} and SO_4^{2-}) indicate that they can be effectively mobilised during oxidative weathering. Indeed, based on a similar positive correlation to that shown in figure 3, Miller et al. (2011) concluded that pyrite weathering is the dominant source of Mo to modern day rivers. The observed agreement between the groundwater data presented in this study and global river data (Fig. 3) may therefore indicate that groundwater Mo in Iceland is similarly controlled by pyrite and sulfide dissolution.

However, the concentration of Mo in mid-ocean ridge basalt (MORB) sulfides has been reported to be much lower than continental sulfides (~0.15 ppm; Patten et al., 2013), with Mo behaving incompatibly during melting and differentiation. This suggests that igneous sulfides may not be a significant source of Mo in this setting, consistent with the low Mo concentrations reported in this study for hydrothermal pyrite and pyrrhotite (see Table 2). In contrast, chalcopyrite is a significant Mo host, containing 38 ppm Mo (Table 2). Molybdenum is also preferentially incorporated into minerals containing Ti^{4+} and Fe^{3+}, thus in basaltic and silicic igneous rocks Mo is often concentrated in ilmenite, titano-magnetite (~10 ppm), and sphene and relatively high Mo concentrations are also found in olivine (~10 ppm), but are lower in pyroxenes (~0.4 ppm) and plagioclase (~0.2 ppm) (see Arnórsson & Óskarsson, 2007). Arnórsson & Óskarsson (2007) found groundwaters to be more concentrated in Mo than comparable surface waters and, in general agreement with this study, that Mo concentration tends to increase with increasing temperature. They concluded that the main source of Mo to Icelandic groundwaters is the incongruent dissolution of basalt, dominated by plagioclase and to a lesser extent pyroxene and basaltic glass due to Mo retention in titano-magnetite and olivine.

As the main source of Mo is likely to be from the dissolution of the isotopically light host basalts, some process is needed to explain the heavy hydrothermal endmember compositions (Fig. 5). There are several processes that could potentially drive the observed fractionation of Mo isotopes in the warm geothermal waters: (1) pedogenesis; (2) changes in redox state; (3) dissolution of primary minerals; (4) the formation of secondary minerals; and (5) dissolution or precipitation of sulfides. To explain the dominant mixing trend in the Mývatn waters (solid line; Fig. 5) the geothermal end member requires an additional source of isotopically heavy Mo whilst the minor, group V endmember mixing (dashed line; Fig 5) requires a loss of isotopically light Mo.

Soils: The retention of light Mo isotopes in soils has been recognised as an important process in driving the preferential enrichment of heavy Mo isotopes in the dissolved phases of pore water, rivers and groundwaters (e.g. Pearce et al., 2010; Siebert et al., 2015; King et al., 2016). Siebert et al. (2015) and King et al. (2016) used selective extraction techniques to show that soil-bound Mo is associated with organic matter and a silicate and/or Ti-oxide residue, as opposed to Mn Fe oxyhydroxides. However, soils in the NVZ of Iceland are generally thin and sandy with much of the groundwater catchment described as a sand desert from Vatnajökull glacier in the south to the Atlantic Ocean in the north (see Figure 5 in Arnalds et al., 2001). Furthermore, as shown in figure 6, the in situ partial pressures of CO_2 in the cold groundwaters (from 10 6 to 10-3.6 bars) are less than that of atmospheric pCO_2 (10 3.4 bars). This suggests that the dissolution and precipitation reactions in these waters take place in isolation from the atmosphere and with little CO_2 contribution from soils (see Figure 4 in Gislason & Eugster 1987). Consequently it is unlikely that soils exert a significant control on groundwater composition in this region due to their lack of development and coverage.

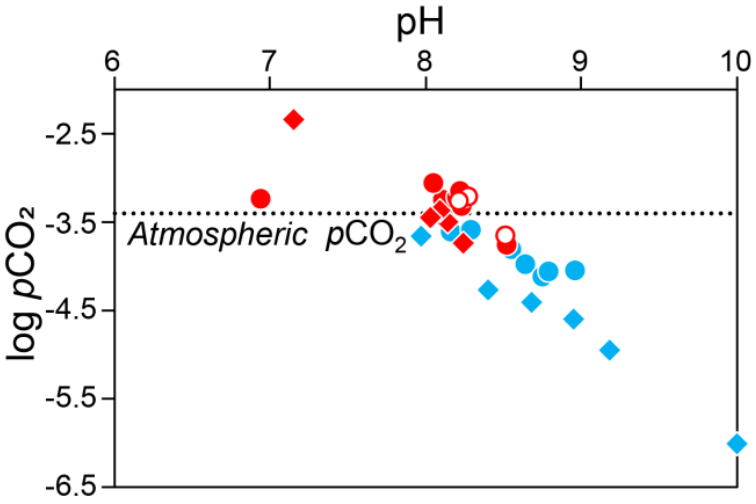

Figure 6: Log pCO_2 for all of the groundwaters. The pH and pCO_2 are calculated for the sampling conditions using PHREEQC (Parkhurst & Appelo 2013) and the minteq.v4 database. The reference line is the pCO_2 of the modern atmosphere.

Redox State: The Eh is relatively difficult to constrain due to the challenges involved in preserving speciation for later laboratory analysis (as demonstrated for Fe speciation in thermal waters; Kaasalainen et al., 2016). For this reason, redox was calculated using several approaches and redox pairs. While absolute values of Eh differ between these approaches the speciation in all of the groundwaters is dominated by molybdate, MoO_4^{2-} (Mo^{6+}), (Fig. 2). A few of the hydrothermally influenced samples approach thiomolybdate speciation ($MoO_{4-x}S_x^{2-}$). However, following classic stable isotope theory, redox reactions tend to enrich light isotopes in the reduced species and those samples approaching reduced Mo speciation retain isotopically heavy Mo signatures. Therefore, despite spanning a wide range of Eh values, the redox conditions do not appear to directly account for the isotope composition of dissolved Mo. However, redox potential does affect the stability and saturation state of mineral phases, which may in turn affect the Mo isotopes of the dissolved phase.

Primary minerals: Dissolution of basalt is thought to be incongruent with respect to Mo (Arnórsson & Óskarsson 2007). Data on the Mo isotope composition for individual minerals remains limited, but there may be significant isotope variation between phases. Initial data from Voegelin et al. (2014) indicate that hornblende and biotite are up to 0.6‰ lighter than bulk-rock. Maintenance of mass balance therefore requires other phases to be isotopically heavier, and enhanced dissolution of these phases could be responsible for the heavier Mo isotope composition and increasing Mo concentration of the main geothermal endmember (M17). An assessment of the saturation state of primary basalt minerals was made using the PHREEQC database (Parkhurst & Appelo, 2013). Plagioclase, hydrated basaltic glass, and olivine tend to be undersaturated whilst pyroxene and magnetite remain oversaturated (Fig. 7, Table ES2). As temperature increases, the tendency for forsterite dissolution becomes dominant over plagioclase, coinciding with increasingly heavy Mo isotope signatures. If olivine retains heavier Mo than plagioclase then incongruent dissolution of these phases may control the Mo isotope signatures of these waters. However, additional Mo isotope data on mineral separates are required to assess this

hypothesis and it seems unlikely that any individual phase could be isotopically heavy enough and in sufficient enough abundance to drive waters to almost δ^{98}Mo +2‰ without other processes playing an important role.

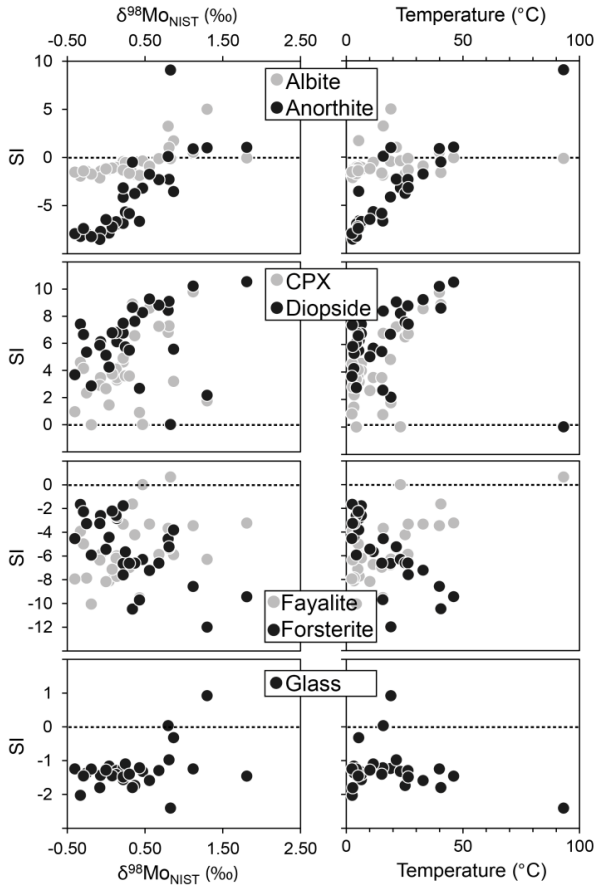

Figure 7: Basalt primary mineral saturation indices (SI) in the Mývatn and Þeistareykir groundwaters plotted against both the Mo isotope composition and sampling temperature of the waters. Saturation indices are calculated using the PHREEQC database and SI >0 suggests that precipitation of the phase is likely whilst SI <0 indicates the likelihood of dissolution.

Secondary minerals: The formation of secondary phases or the adsorption of Mo onto such phases provides a potential mechanism to remove light Mo from solution (as is required to form the group V waters). The formation of secondary phases has been used to explain some of the Mo isotope variation in rivers, with adsorption of light Mo onto Mn-Fe oxyhydroxides driving the waters to heavier values (e.g. Archer & Vance, 2008; Miller et al., 2011). In this study, the most common Mn phases are significantly undersaturated in the groundwaters (Table ES2), whilst Fe phases only tend to be oversaturated in the cold groundwaters. From the calculated saturation indices, there is no indication that the formation of these secondary phases in the group V waters is any more likely than in the other hydrothermal waters (Table ES2). With the hydrothermally influenced waters being generally undersaturated for both Fe- and Mn- oxyhydroxides, their formation is considered to exert little influence on the Mo isotopes in these groundwaters.

Sulfides: Calculating the saturation state of sulfide minerals in the cold groundwaters is difficult due to the absence of measureable reduced S in the system (Table 1; ES1). However, the oxidising nature of these fluids (Fig. 2) would suggest that they are undersaturated with respect to sulfide minerals. It is known that the mixing of hydrothermal waters with cold waters leads to molybdenite undersaturation and therefore favours dissolution of Mo sulfides (Arnórsson & Ívarsson 1985). Consequently, the main mixing trend in Fig. 5 could in part be explained by the dissolution of sulfide phases, increasing the Mo concentration in these waters. Molybdenites show a large isotopic variation, ranging from $\delta^{98}Mo_{MOLYBDENITE}$ -1.6‰ to +2.3‰ (Breillat et al., 2016) and the hydrothermally sourced chalcopyrite, pyrite, and pyrrhotite measured in this study are all isotopically heavy ($\delta^{98}Mo$ = +0.9 to +1.5‰; Table 2, Fig. 8). Chalcopyrite appears to be a significant host of heavy Mo (38 ppm and $\delta^{98}Mo$ +0.9‰), and although both the pyrite and pyrrhotite have significantly less Mo (<0.1 ppm Mo) they are significantly enriched with Mo isotope compositions of +1.5‰ and +1.2‰ respectively. The dissolution of such phases could indeed be a source of heavy Mo to the hydrothermal endmembers. However, saturation state calculations systematically show that the hydrothermally influenced waters are oversaturated for sulfide minerals (Table ES2), indicating that their precipitation is more likely than dissolution and therefore sulfides are unlikely to be controlling the composition of the main hydrothermal endmember (M17).

Alternatively, it is possible that the precipitation of sulfides from reducing, sulfide-bearing waters may instead remove Mo from solution as indicated by the minor group V mixing trend (Fig. 5). When redox is defined using sulfur speciation and trace levels of H_2S are assumed to be present in the hydrothermally influenced waters (at levels of 0.01 ppm to 0.01 ppb) then the hydrothermal samples tend towards sulfide (molybdenite, pyrite, and chalcopyrite) saturation (Table ES2). Whilst molybdenite has not been found in active geothermal systems in Iceland, it is known to occur in some New Zealand geothermal systems and has been identified in hydrothermally altered Tertiary basalt formations at Reydarártindur in southeast Iceland (Árnorsson & Ívarsson 1985). Although the sulfides measured in this study are all isotopically heavy, Tossell (2005) calculated that aqueous Mo-sulfide complexes are >2‰ lighter than oxidised complexes and Greber et al. (2014) suggested that light Mo is preferentially incorporated in molybdenite during crystallization leaving behind a residually heavier hydrothermal fluid. If isotopically light, sulfide formation could generate the M14 endmember and the group V waters, but cannot be responsible for the main groundwater trend.

At this stage, it is not clear what role, if any, sulfide plays in controlling the Mo chemistry of the waters studied here. Sulfides span a large isotope range and are only sometimes significant hosts of Mo. Whilst both sulfide dissolution and precipitation are potentially contributing factors to the Mo chemistry of these waters, due to the saturation state calculations it is considered more likely that sulfides are forming in these waters, thereby removing Mo from solution.

The mechanisms controlling the compositions of these waters appear to be complex. There are potentially two distinct hydrothermal endmembers as shown on the mixing diagrams (Fig. 5): both are isotopically heavy but one possesses high Mo concentrations and the other, low concentrations. We suggest that an important control on Mo in the groundwaters is the incongruent dissolution of basalt. The hydrothermal waters are increasingly influenced by the dissolution of olivine over plagioclase with corresponding heavier Mo isotope compositions. However, it is unlikely that silicate dissolution alone could control

the composition of the hydrothermal endmember as it would require extraordinary fractionation between these minerals at high temperatures when forming the basalts. The group V waters are likely to be more strongly influenced by Mo removal mechanisms involving the precipitation of isotopically light phases, such as molybdenite or other sulfide minerals.

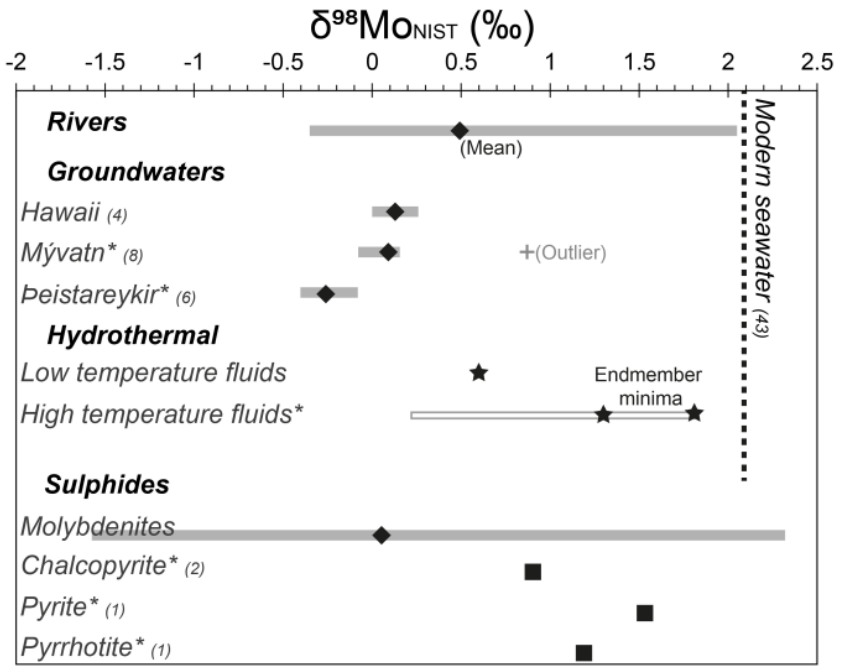

Figure 8: Molybdenum isotope compositions for sources of Mo to the modern oceans. The grey bars denote the range whilst the black diamonds show mean values and the stars minimum estimates of the hydrothermal endmembers. The grey outline for the high temperature fluids shows the range of values measured for the mixed fluids in this study. River data is summarised in Kendall et al. (2016), Hawaii groundwater data from King et al. (2016), and the low temperature hydrothermal fluids from McManus et al. (2002). In addition, the individual sulfide values from this study are plotted (black squares) with the entire molybdenite range (from Breillat et al., 2016) for comparison.

3.4.4 Ocean mass balance

Although the mechanisms driving groundwater compositions remain complex the new data here allows a more detailed assessment of the Mo budget of the oceans. Typically, the source of Mo to the ocean is considered to be dominated by rivers, with a minor (~10%) hydrothermal component contributing the remaining flux (McManus et al., 2002), and the sinks of Mo comprise euxininc, suboxic, and oxic sedimentary deposition (e.g. Kendall et al., 2016). There are currently two approaches to evaluating the Mo input composition: (1) the assumption that over long time scales riverine flux will represent the average crustal value (e.g. Asael et al., 2013); and (2) the direct measurement of the riverine compositions (e.g. Archer & Vance 2008). These two approaches result in slightly different estimates of the Mo isotope input to the oceans. The continental crust has a bulk composition of

between δ^{98}Mo +0.1‰ and +0.35‰ and a maximum of +0.15‰ for the upper continental crust alone (Willbold et al., 2017). The riverine average has a higher δ^{98}Mo value of +0.5‰ (Archer & Vance 2008) and when combined with a poorly constrained hydrothermal input of δ^{98}Mo +0.6‰ (McManus et al., 2002) results in a Mo input of ca. +0.5‰ (Eq. 2).

$$\delta^{98}Mo_{input} = f_{river} \times \delta^{98}Mo_{river} + f_{hydrothermal} \times \delta^{98}Mo_{hydrothermal} \quad (2)$$

If, as the data from these Icelandic cold groundwaters suggest (see section 4.1), the concentration of Mo in groundwaters is similar to that of rivers, and groundwaters contribute up to 40% of the riverine water flux as suggested by Moore (1996), then groundwaters may account for nearly 30% of the total Mo flux to the oceans (e.g. Rivers: 65%; Groundwater: 27%; Hydrothermal: 8%). The available Mo isotope data for groundwaters indicate that they are isotopically lighter (δ^{98}Mo -0.1‰) than river compositions, thus necessitating a revaluation of the Mo ocean input (Eq. 3).

$$\delta^{98}Mo_{input} = f_{river} \times \delta^{98}Mo_{river} + f_{hydrothermal} \times \delta^{98}Mo_{hydrothermal} + f_{groundwater} \times \delta^{98}Mo_{groundwater} \quad (3)$$

The result is a Mo input to the oceans of δ^{98}Mo +0.35‰ which if correct, brings this combined Mo input closer to that of the estimate based upon crustal values. Furthermore, the data from King et al. (2016) indicate that groundwaters may actually contain around four times more Mo than the riverine average, in which case their contribution ($f_{groundwater}$) would increase, potentially even becoming the dominant source, and the total Mo input would be lighter still, more closely matching that of the crustal values. However, whilst groundwater data remain so limited both in terms of potential flux to the oceans and the isotope composition it is not possible to accurately constrain these values.

Despite high temperature hydrothermal systems generally not being considered a significant source of Mo to the oceans these terrestrial hydrothermal systems maintain relatively high Mo concentrations (up to 4.8 ppb). Without exception they all show preferential enrichment of heavy δ^{98}Mo in the hydrothermal fluid with minimum endmember fluids of δ^{98}Mo +1.30‰ to +1.81‰. If this is indicative of the processes contributing to the evolution of MOR hydrothermal fluids then the hydrothermal portion of the Mo input to the oceans may be heavier than previously estimated. Within the modern ocean budget hydrothermal contributions are minor; increasing the hydrothermal Mo isotope composition to an extreme of δ^{98}Mo +2.0‰ only increases the combined input ($\delta^{98}Mo_{input}$) by some 0.1‰. However, during early periods of Earth's history when hydrothermal fluids may have comprised a greater proportion of the oceanic inputs the accurate characterisation of these fluids is of increasing importance for ocean chemistry. Whilst there is only one other direct study of hydrothermal fluids, the significance of these systems and reactions at both low and high temperatures remains, at best, uncertain (cf. McManus et al., 2002).

3.5 Conclusions

A comprehensive study of the Mo isotopic composition of waters from two hydrothermally influenced groundwater systems in northeast Iceland demonstrates variations in δ^{98}Mo that range from 0.40‰ to +1.81‰. This represents a significant increase in the available data for both cold and hydrothermally influenced groundwaters, with the main findings being:

1) Cold groundwaters are isotopically light, ranging from δ^{98}Mo -0.40‰ to +0.22‰ (mean: $\delta^{98}Mo_{GROUNDWATER}$ -0.1‰), and are comparable with the Mo composition of groundwaters from Hawaii (mean δ^{98}Mo +0.14‰) reported in King et al. (2016). On average the groundwaters are isotopically lighter than rivers and have Mo isotope signatures that are similar to their basaltic host-rocks ($\delta^{98}Mo_{BASALT}$ -0.4‰ to -0.1‰).

2) Hydrothermally influenced groundwaters have higher dissolved Mo concentrations (up to 4.81 ppb) and heavier Mo isotope compositions than the regional cold groundwaters ($\delta^{98}Mo_{HYDROTHERMAL}$ 0.00‰ to +1.81‰). Mixing between the cold groundwaters and hydrothermal endmembers (+1.81‰ and +0.83‰) is the main control on the Mo composition of the groundwater samples. The incongruent dissolution of basalt and dissolution and precipitation of sulfide minerals are both processes capable of controlling hydrothermal endmember Mo compositions.

3) With the inclusion of a direct groundwater contribution to the Mo flux to the oceans the combined groundwater and river input is revaluated to δ^{98}Mo +0.35‰, in closer agreement with estimates based upon the crustal composition alone. However, whilst groundwater data remain limited these estimates should be interpreted with caution

References

ARNALDS, O., GISLADOTTIR, F. O. & SIGURJONSSON, H. 2001. Sandy deserts of Iceland: an overview. Journal of Arid Environments, 47, 359-371.

ARCHER, C. & VANCE, D. 2008. The isotopic signature of the global riverine molybdenum flux and anoxia in the ancient oceans. Nature Geoscience, 1, 597-600.

ÁRMANNSSON, H., KRISTMANNSDÓTTR, H. & ÓLAFSSON, M. 2000. Geothermal influence of groundwater in the Lake Mývatn area, North Iceland World Geothermal Congress, 28 May - 10 June 2000 Kyushu - Tohoku, Japan.

ARNÓRSSON, S. & ÍVARSSON, G. 1985. Molybdenum in Icelandic geothermal waters. Contributions to Mineralogy and Petrology, 90, 179-189.

ARNÓRSSON, S. & ÓSKARSSON, N. 2007. Molybdenum and tungsten in volcanic rocks and in surface and< 100 C ground waters in Iceland. Geochimica et Cosmochimica Acta, 71, 284-304.

ASAEL, D., TISSOT, F. L. H., REINHARD, C. T., ROUXEL, O., DAUPHAS, N., LYONS, T. W., PONZEVERA, E., LIORZOU, C. & CHÉRON, S. 2013. Coupled molybdenum, iron and uranium stable isotopes as oceanic paleoredox proxies during the Paleoproterozoic Shunga Event. Chemical Geology, 362, 193-210.

BARLING, J., ARNOLD, G. L. & ANBAR, A. D. 2001. Natural mass-dependent variations in the isotopic composition of molybdenum. Earth and Planetary Science Letters, 193, 447-457.

BARLING, J. & ANBAR, A. D. 2004. Molybdenum isotope fractionation during adsorption by manganese oxides. Earth and Planetary Science Letters, 217, 315-329.

BREILLAT, N., GUERROT, C., MARCOUX, E. & NÉGREL, P. 2016. A new global database of δ98Mo in molybdenites: A literature review and new data. Journal of Geochemical Exploration, 161, 1-15.

BURKHARDT, C., HIN, R. C., KLEINE, T. & BOURDON, B. 2014. Evidence for Mo isotope fractionation in the solar nebula and during planetary differentiation. Earth and Planetary Science Letters, 391, 201-211.

CHURCH, T. M. 1996. An underground route for the water cycle. Nature, 380, 579-580.

DARLING, W. G. & ÁRMANNSSON, H. 1989. Water-rock interaction Stable isotopic aspects of fluid flow in the Krafla, Námafjall and Theistareykir geothermal systems of northeast Iceland. Chemical Geology, 76, 197-213.

DE RONDE, C. E. J., CHANNER, D. M. D., FAURE, K., BRAY, C. J. & SPOONER, E. T. C. 1997. Fluid chemistry of Archean seafloor hydrothermal vents: Implications for the composition of circa 3.2 Ga seawater. Geochimica et Cosmochimica Acta, 61, 4025-4042.

EIRIKSDOTTIR, E. S., GISLASON, S. R. & OELKERS, E. H. 2015. Direct evidence of the feedback between climate and nutrient, major, and trace element transport to the oceans. Geochimica et Cosmochimica Acta, 166, 249-266.

GISLASON, S.R. & EUGSTER, H.P. 1987. Meteoric water-basalt interactions: II. A field study in NE Iceland. Geochim. Cosmochim. Acta 51, pp. 2841-2855.

GOLDBERG, T., ARCHER, C., VANCE, D. & POULTON, S. W. 2009. Mo isotope fractionation during adsorption to Fe (oxyhydr)oxides. Geochimica et Cosmochimica Acta, 73, 6502-6516.

GOLDBERG, T., GORDON, G., IZON, G., ARCHER, C., PEARCE, C. R., MCMANUS, J., ANBAR, A. D. & REHKÄMPER, M. 2013. Resolution of inter-laboratory discrepancies in Mo isotope data: an intercalibration. Journal of Analytical Atomic Spectrometry, 28, 724-735.

GREBER, N. D., PETTKE, T. & NÄGLER, T. F. 2014. Magmatic–hydrothermal molybdenum isotope fractionation and its relevance to the igneous crustal signature. Lithos, 190–191, 104-110.

GUDMUNDSSON, B. T. & ARNÓRSSON, S. 2002. Geochemical monitoring of the Krafla and Námafjall geothermal areas, N-Iceland. Geothermics, 31, 195-243.

GUDMUNDSSON, B. T. & ARNÓRSSON, S. 2005. Secondary mineral–fluid equilibria in the Krafla and Námafjall geothermal systems, Iceland. Applied Geochemistry, 20, 1607-1625.

HURTIG, N. C. & WILLIAMS-JONES, A. E. 2014. An experimental study of the solubility of MoO 3 in aqueous vapour and low to intermediate density supercritical fluids. Geochimica et Cosmochimica Acta, 136, 169-193.

KAASALAINEN, H. & STEFÁNSSON, A. 2012. The chemistry of trace elements in surface geothermal waters and steam, Iceland. Chemical Geology, 330–331, 60-85.

KAASALAINEN, H., STEFANSSON, A. & DRUSCHEL, G. K. 2016. Determination of Fe (II), Fe (III) and Fetotal in thermal water by ion chromatography spectrophotometry (IC-Vis). International Journal of Environmental Analytical Chemistry, 96, 1074-1090.

KENDALL, B., DAHL, T., ANABAR, A. 2016. Good Golly, Why Moly? The Stable Isotope Geochemistry of Molybdenum, Reviews in Mineralogy and Geochemistry, 82, 683-732.

KING, E. K., THOMPSON, A., CHADWICK, O. A. & PETT-RIDGE, J. C. Molybdenum sources and isotopic composition during early stages of pedogenesis along a basaltic climate transect. Chemical Geology.

KRISTINSSON, S. G., ÓSKARSSON, F., ÓLAFSSON, M. & ÓLADÓTTIR, A. A. 2014. Háhitasvæðin í Kröflu, Námafjalli og á Þeistareykjum: Vöktun á yfirborðsvirkni og grunnvatni árið 2014 (The high temperature areas of Krafla, Námafjall and Þeistareyki: monitoring of groundwater an surface activity in 2014). ÍSOR (Íslenskar Orkurannsóknir) Icelandic GeoSurvey. LV-2014-132 ÍSOR2014/058

LEYBOURNE, M. I. & CAMERON, E. M. 2008. Source, transport, and fate of rhenium, selenium, molybdenum, arsenic, and copper in groundwater associated with porphyry–Cu deposits, Atacama Desert, Chile. Chemical Geology, 247, 208-228.

LOWELL, R. P. & KELLER, S. M. 2003. High-temperature seafloor hydrothermal circulation over geologic time and Archean banded iron formations. Geophysical research letters, 30.

MCMANUS, J., NÄGLER, T. F., SIEBERT, C., WHEAT, C. G. & HAMMOND, D. E. 2002. Oceanic molybdenum isotope fractionation: Diagenesis and hydrothermal ridge-flank alteration. Geochemistry, Geophysics, Geosystems, 3, 1-9.

MILLER, C. A., PEUCKER-EHRENBRINK, B., WALKER, B. D. & MARCANTONIO, F. 2011. Re-assessing the surface cycling of molybdenum and rhenium. Geochimica et Cosmochimica Acta, 75, 7146-7179.

MOORE, W. S. 1996. Large groundwater inputs to coastal waters revealed by 226Ra enrichments. Nature, 380, 612-614.

NAKAGAWA, Y., TAKANO, S., FIRDAUS, M. L., NORISUYE, K., HIRATA, T., VANCE, D. & SOHRIN, Y. 2012. The molybdenum isotopic composition of the modern ocean. Geochemical Journal, 46, 131.

NEUBERT, N., HERI, A., VOEGELIN, A., NÄGLER, T., SCHLUNEGGER, F. & VILLA, I. 2011. The molybdenum isotopic composition in river water: constraints from small catchments. Earth and planetary science letters, 304, 180-190.

ÓLAFSSON, M., FRIDRIKSSON, T., HAFSTAD, T. H., GYLFADÓTTIR, S. S., ÓSKARSSON, F. & ÁRMANNSSON, H. The Groundwater in the Mývatn Area: Influence of Geothermal Utilization at Námafjall and Origin of the Warm Groundwater Component. World Geothermal Congress 2015, 19-25 April 2015 Melbourne, Australia.

ÓSKARSSON, F., ÁRMANNSSON, H., ÓLAFSSON, M., SVEINBJÖRNSDÓTTIR, Á. E. & MARKÚSSON, S. H. 2013. The Theistareykir Geothermal Field, NE Iceland: Fluid Chemistry and Production Properties. Procedia Earth and Planetary Science, 7, 644-647.

PARKHURST, D.L., & APPELO, C.A.J., 2013, Description of input and examples for PHREEQC version 3—A computer program for speciation, batch-reaction, one-dimensional transport, and inverse geochemical calculations: U.S. Geological Survey Techniques and Methods, book 6, chap. A43, 497 p., available only at https://pubs.usgs.gov/tm/06/a43/.

PATTEN, C., BARNES, S.-J., MATHEZ, E. A. & JENNER, F. E. 2013. Partition coefficients of chalcophile elements between sulfide and silicate melts and the early crystallization history of sulfide liquid: LA-ICP-MS analysis of MORB sulfide droplets. Chemical Geology, 358, 170-188.

PEARCE, C. R., COHEN, A. S., COE, A. L. & BURTON, K. W. 2008. Molybdenum isotope evidence for global ocean anoxia coupled with perturbations to the carbon cycle during the Early Jurassic. Geology, 36, 231-234.

PEARCE, C. R., COHEN, A. S. & PARKINSON, I. J. 2009. Quantitative Separation of Molybdenum and Rhenium from Geological Materials for Isotopic Determination by MC-ICP-MS. Geostandards and Geoanalytical Research, 33, 219-229.

PEARCE, C. R., BURTON, K. W., VON STRANDMANN, P. A., JAMES, R. H. & GÍSLASON, S. R. 2010. Molybdenum isotope behaviour accompanying weathering and riverine transport in a basaltic terrain. Earth and Planetary Science Letters, 295, 104-114.

RAD, S. D., ALLÈGRE, C. J. & LOUVAT, P. 2007. Hidden erosion on volcanic islands. Earth and Planetary Science Letters, 262, 109-124.

SIEBERT, C., PETT-RIDGE, J. C., OPFERGELT, S., GUICHARNAUD, R. A., HALLIDAY, A. N. & BURTON, K. W. 2015. Molybdenum isotope fractionation in soils: Influence of redox conditions, organic matter, and atmospheric inputs. Geochimica et Cosmochimica Acta, 162, 1-24.

SVEINBJORNSDOTTIR, Á., ÁRMANNSSON, H., ÓLAFSSON, M., ÓSKARSSON, F., MARKÚSSON, S. & MAGNUSDOTTIR, S. 2013. The Theistareykir geothermal field, NE Iceland. Isotopic characteristics and origin of circulating fluids. Procedia Earth and Planetary Science, 7, 822-825.

TAYLOR S. R. and MCLENNAN, S. M. (1985) The Continental Crust: Its Composition and Evolution. Blackwell Scientific Public.

TOSSELL, J. A. 2005. Calculating the partitioning of the isotopes of Mo between oxidic and sulfidic species in aqueous solution. Geochimica et Cosmochimica Acta, 69, 2981-2993.

VOEGELIN, A. R., NÄGLER, T. F., PETTKE, T., NEUBERT, N., STEINMANN, M., POURRET, O. & VILLA, I. M. 2012. The impact of igneous bedrock weathering on the Mo isotopic composition of stream waters: Natural samples and laboratory experiments. Geochimica et Cosmochimica Acta, 86, 150-165.

VOEGELIN, A. R., PETTKE, T., GREBER, N. D., VON NIEDERHÄUSERN, B. & NÄGLER, T. F. 2014. Magma differentiation fractionates Mo isotope ratios: Evidence from the Kos Plateau Tuff (Aegean Arc). Lithos, 190–191, 440-448.

WASYLENKI, L. E., WEEKS, C. L., BARGAR, J. R., SPIRO, T. G., HEIN, J. R. & ANBAR, A. D. 2011. The molecular mechanism of Mo isotope fractionation during adsorption to birnessite. Geochimica et Cosmochimica Acta, 75, 5019-5031.

WILLBOLD, M. & ELLIOTT, T. 2017. Molybdenum isotope variations in magmatic rocks. Chemical Geology, 449, 253-268.

YANG, J., SIEBERT, C., BARLING, J., SAVAGE, P., LIANG, Y.-H. & HALLIDAY, A. N. 2015. Absence of molybdenum isotope fractionation during magmatic differentiation at Hekla volcano, Iceland. Geochimica et Cosmochimica Acta, 162, 126-136.

Acknowledgments

The geochemistry team at ÍSOR are thanked for sample collection and along with Landsvirkjun for permission to publish the sample information. Geoff Nowell, in particular, is thanked for his generous help in the preparation and isotopic analysis of the samples and Chris Ottley for assistance with ICP-MS analysis. We acknowledge financial support from Initial Training Network, MetTrans, grant number 290336 from the European Research Council.

Author contributions

R.A.N., S.R.G., and K.W.B., designed the study. M.O., coordinated sampling and major and trace element analysis. R.A.N. lead the Mo isotope analysis with guidance from A.J.M-W. and C.R.P. (A.J.M-W. analysed the sulfides). R.A.N. coordinated the project and lead authorship of the paper.

Electronic supplements

Table ES1: Complete dissolved element data from the 2014 report on Mývatn and Þeistareykir.

Data reproduced from 'Groundwater and surface activity monitoring ' report, ÍSOR-2014/058 by the Icelandic Geosurvey for Landsvirkjun (Tables 12 & 16).

Table ES2: Calculated saturation state of the groundwaters.

Calculations were performed in PHREEQC with thermodynamic additions from Gysi & Stefansson (2011). Measured total Fe was used (as opposed to Fe speciation data). Redox was defined using sulfur speciation.

GYSI, A. P. & STEFÁNSSON, A. 2011. CO2–water–basalt interaction. Numerical simulation of low temperature CO2 sequestration into basalts: Geochimica et Cosmochimica Acta, v. 75, no. 17, p. 4728-4751.

Table ES1: Complete groundwater data

Paper ID	Station name	Sample number		Location		Date	Temperature	pH /ref. Temp
				Latitude	Longitude		(°C)	
M01	Hliðardalslækur	20140293	V-2356	65.630833	-16.773067	9.9.2014	15.9	8.16 / 22.6
M02	AB-2	20140294	B-57842	65.631708	-16.773970	9.9.2014	3.3	8.00 / 23.2
M03	LUD-4	20140295	B-58504	65.624773	-16.803274	9.9.2014	5.4	8.10 / 22.0
M04	LUD-2	20140296	B-58502	65.588422	-16.827410	9.9.2014	5.6	8.44 / 21.2
M05	LUD-3	20140297	B-58503	65.612385	-16.813065	9.9.2014	4.5	8.45 / 21.6
M06	Svelgur	20140298	M-20004	65.640274	-16.851123	9.9.2014	19.2	6.80 / 21.7
M07	Garðslind	20140299	K-556	65.552501	-16.968874	9.9.2014	6.5	8.87 / 21.8
M08	Bjarg	20140300	H-10080	65.640275	-16.915006	10.9.2014	19	8.08 / 22.5
M09	Helgavogur	20140301	H-10082	65.633611	-16.922502	10.9.2014	23.3	8.25 / 22.0
M10	Hverfjallsgjá	20140302	K-559	65.605848	-16.893306	10.9.2014	6.5	8.57 / 21.8
M11	Vogaflói	20140303	K-558	65.610997	-16.920045	11.9.2014	5	8.62 / 22.2
M12	Langivogur	20140304	H-10088	65.616667	-16.916667	11.9.2014	21.5	8.50 / 22.1
M13	LUD-10	20140305	B-58510	65.626119	-16.839131	11.9.2014	25.3	8.24 / 21.3
M14	Grjótagjá	20140306	H-10085	65.626389	-16.882778	11.9.2014	46.1	8.33 / 21.7
M15	Stóragjá	20140310	H-10083	65.638334	-16.909720	12.9.2014	26.5	8.28 / 21.7
M16	Vogagjá	20140311	H-10087	65.618889	-16.889446	12.9.2014	40	8.40 / 21.9
M17	Skiljustöð	20140312	M-20008	65.705337	-16.765919	12.9.2014	93.2	9.85 / 22.0
M18	AE-10	20140395	B-57890	65.681296	-16.774979	12.11.2014	40.6	8.23 / 21.2
M19	LUD-5	20140396	B-58505	65.614879	-16.770150	12.11.2014	4.3	8.48 / 21.6
M20	LUD-6	20140397	B-58506	65.614814	-16.853074	12.11.2014	33	8.33 / 21.9
Þ01	Þeistareykir-vatnsból	20140307	M-20409	65.881709	-16.932724	11.9.2014	15.7	7.11 / 21.8
Þ02	Þeistareykir-Sæluhús	20140308	H-10124	65.877561	-16.960227	11.9.2014	11.6	8.05 / 22.0
Þ03	ÞR-5	20140309	B-60365	65.898087	-16.966069	11.9.2014	26.6	8.14 / 21.2
Þ04	Krossdalur	20140313	K-2745	66.079883	-16.729300	13.9.2014	3.4	8.45 / 22.5
Þ05	Fjöll - lind	20140317	K-2742	66.070350	-16.959383	13.9.2014	2.6	9.65 / 21.5
Þ06	Fjöll - vatnsból	20140316	K-568	66.081866	-16.958171	13.9.2014	2.8	8.91 / 21.2
Þ07	Lón	20140315	K-2744	66.097450	-16.921850	13.9.2014	4.4	7.84 / 22.0
Þ08	Rifós - Tangabrunnur	20140314	K-2743	66.102400	-16.907817	13.9.2014	10.2	8.11 / 22.2
Þ09	ÞR-15	20140403	B-60376	65.963094	-16.910100	13.11.2014	15.3	7.98 / 21.9
Þ10	ÞR-8	20140404	B-60368	65.958865	-16.987384	13.11.2014	2.5	8.18 / 22.2
Þ11	ÞR-16	20140405	B-60377	65.867748	-17.028110	13.11.2014	5.2	8.73 / 21.3

Table ES1: Complete groundwater data

Paper ID	Conductivity @ 25°C (µS cm-1)	CO2 ppm	H2S ppm	B ppm	SiO2 ppm	Na ppm	K ppm	Mg ppm	Ca ppm	F ppm	Cl ppm	SO4 ppm	Al ppb	As ppb
M01	730	96.8	b.d.l	0.31	179	91.3	10.9	12.5	37.9	0.4	26	199	321	9.05
M02	156	49.1	b.d.l	0.06	27.6	11.2	1.54	5.15	10.2	0.2	4.36	13.8	4.58	0.537
M03	404	66.9	b.d.l	0.18	46.6	53.6	2.29	9.2	14.2	0.27	12.3	96.2	223	4.6
M04	216	72	b.d.l	0.08	23.4	18.6	1.97	7.6	12.3	0.16	5.74	16.1	11	b.d.l
M05	192	62.5	b.d.l	0.07	22.3	15.3	1.79	7.07	11.1	0.17	5.29	15.3	10.4	b.d.l
M06	683	6.9	0.05	1.58	590	119	20.2	1.21	2.44	0.78	54	181	2020	157
M07	155	54.4	b.d.l	0.05	19.3	17.4	1.34	4.64	7.04	0.17	2.11	7.33	10.5	b.d.l
M08	322	79	b.d.l	0.1	58.2	44.3	3.68	4.02	16.2	0.24	9.71	47.1	5.79	0.091
M09	408	107	b.d.l	0.11	70.9	52.3	4.64	5.56	24.8	0.26	8.04	66.2	5.25	b.d.l
M10	220	66	b.d.l	0.08	22.7	21.5	1.84	6.84	11.7	0.2	5.08	22.1	8.74	b.d.l
M11	210	62.7	b.d.l	0.09	22.3	21.1	1.73	6.26	10.9	0.21	4.75	21.2	6.5	b.d.l
M12	475	76.5	b.d.l	0.29	119	76.9	6.3	3.64	15.3	0.34	15.1	108	16	b.d.l
M13	313	94.9	b.d.l	0.07	28.7	37.3	3.74	8.57	14.6	0.34	4.54	40.5	6.09	b.d.l
M14	515	89.8	0.08	0.36	149	86.3	7.82	3.09	14.8	0.38	17.7	109	11.5	b.d.l
M15	456	111	b.d.l	0.17	84.6	61.8	5.44	5.58	26.1	0.27	9.57	81.9	7.04	b.d.l
M16	533	76.1	b.d.l	0.39	143	88	7.15	2.49	15.7	0.37	17.5	128	24.8	b.d.l
M17	1208	29.8	22.4	0.88	605	250	30.6	0.01	2.68	1.19	81.3	232	1400	6.8
M18	345	81.9	0.03	0.18	49.7	42	1.51	0.99	28.5	0.15	4.09	66.8	9.12	b.d.l
M19	172	56.3	b.d.l	0.17	21.3	13.6	1.82	6.55	9.92	0.18	4.88	10.6	4.9	b.d.l
M20	384	106	b.d.l	0.2	62.7	51.7	5.51	7.11	17.2	0.28	5.67	57	7.25	b.d.l
Þ01	212	82.4	b.d.l	0.06	49.3	15.2	1.61	5.68	17.5	0.06	5.81	14.2	1.51	b.d.l
Þ02	202	51.8	b.d.l	0.08	52	20.8	1.48	3.69	12.2	0.1	7.41	26.1	5.1	b.d.l
Þ03	201	51.4	b.d.l	0.09	51.9	20.8	1.48	3.68	12.2	0.1	7.45	26.2	5.62	b.d.l
Þ04	103	25.6	b.d.l	0.09	21.9	9.25	0.81	2.67	5.7	0.1	8.73	3.5	5.68	b.d.l
Þ05	102	17.2	b.d.l	0.06	9.9	16.3	0.03	0.05	2.7	0.03	7.84	4.26	16.7	0.117
Þ06	104	23.6	b.d.l	0.07	12.3	11.9	0.11	0.42	7.12	0.03	10.4	2.76	4.83	b.d.l
Þ07	92.3	27.7	b.d.l	0.08	20.9	8.74	0.9	2.59	4.33	0.08	7.68	2.91	5.31	0.062
Þ08	139	38.6	b.d.l	0.09	31.3	14.8	1.28	3.41	6.28	0.11	10	8.73	5.85	b.d.l
Þ09	158	44	b.d.l	0.13	35.5	13	1.18	3.91	11	0.07	7.5	14	3.15	b.d.l
Þ10	73.4	18.6	0.03	0.11	17.5	6.86	0.54	1.95	3.6	0.05	6.95	1.71	11.5	b.d.l
Þ11	94.8	29.3	b.d.l	0.1	22.4	8.57	1.14	3.37	4.25	0.1	5.45	1.84	7.7	0.098

Table ES1: Complete groundwater data

Paper ID	Ba	Cd	Co	Cr	Cu	Fe	Hg	Mn	Mo	Ni	Pb	Sr	Zn	TDS
	ppb	ppb	ppb	ppb	ppb	ppb	ppb	ppb	ppb	ppb	ppb	ppb	ppb	ppm
M01	2.03	0.011	0.177	0.906	0.682	49.3	0.005	71.7	4.81	1.85	0.024	46.1	2.58	641
M02	0.296	0.002	0.005	0.442	0.594	4.83	b.d.l	1.68	0.331	0.19	0.01	11.8	2.72	111
M03	0.542	0.003	0.01	0.406	1.19	29.3	b.d.l	1.45	1.52	0.172	0.011	18.6	1.05	289
M04	0.285	b.d.l	b.d.l	1.17	1.6	1.31	b.d.l	0.043	0.565	0.504	b.d.l	14.7	0.802	128
M05	0.277	b.d.l	0.006	0.903	0.545	8.23	b.d.l	0.703	0.594	0.476	b.d.l	12.2	0.473	117
M06	1.06	0.032	0.225	4.88	2.52	385	0.004	9.29	4.85	8.13	0.014	11.9	5.53	1109
M07	0.162	b.d.l	b.d.l	1.02	0.322	0.54	b.d.l	b.d.l	0.654	0.38	b.d.l	8.56	1.09	92
M08	0.75	0.003	0.025	0.639	1.47	2.35	b.d.l	0.177	0.988	0.289	b.d.l	24.9	1.12	244
M09	1.56	b.d.l	b.d.l	0.87	0.682	b.d.l	b.d.l	b.d.l	0.832	0.195	b.d.l	34.4	0.428	309
M10	0.253	0.004	0.007	1.44	1.23	3.18	b.d.l	0.086	0.713	0.417	0.021	15.4	0.841	123
M11	0.308	b.d.l	0.008	1.26	0.948	0.92	b.d.l	0.036	0.812	0.14	b.d.l	13.5	0.368	127
M12	1.99	b.d.l	b.d.l	0.488	0.298	1.03	b.d.l	0.046	0.371	0.051	b.d.l	22.7	0.376	400
M13	4.92	0.003	0.067	0.092	b.d.l	13.6	b.d.l	43.1	1.43	0.358	b.d.l	30.8	1.24	202
M14	2.64	b.d.l	b.d.l	0.047	0.281	1.69	b.d.l	5.43	0.206	0.183	b.d.l	22.2	0.985	450
M15	1.76	b.d.l	0.02	0.49	0.493	1.22	0.003	0.18	1.04	0.893	b.d.l	37.4	0.566	344
M16	1.83	b.d.l	b.d.l	0.274	0.339	2.15	b.d.l	0.066	0.219	0.13	b.d.l	20.3	1.46	452
M17	2.72	b.d.l	b.d.l	0.106	0.103	5.58	0.014	0.998	1.4	0.286	0.025	21.7	1.11	1344
M18	1.06	0.003	0.056	3.23	0.331	48.7	b.d.l	9.68	0.954	3.59	0.015	52.1	2	267
M19	0.194	b.d.l	b.d.l	0.926	0.718	7.79	b.d.l	0.406	0.579	0.369	0.019	10.6	1.68	113
M20	3.21	b.d.l	0.012	0.567	0.266	9.11	b.d.l	0.593	0.888	0.755	0.057	51.8	0.76	290
Þ01	0.481	b.d.l	0.007	0.372	0.121	9.75	b.d.l	1	0.176	0.207	b.d.l	19.2	0.857	160
Þ02	0.186	b.d.l	0.011	0.976	0.515	5.28	b.d.l	0.13	0.235	0.258	0.025	15.4	2.89	159
Þ03	0.236	b.d.l	0.012	0.894	0.385	33.6	b.d.l	0.298	0.283	0.916	0.032	16	6.6	150
Þ04	0.073	b.d.l	b.d.l	0.677	0.304	0.92	b.d.l	0.153	0.181	0.277	b.d.l	8.1	0.571	79
Þ05	0.027	b.d.l	0.009	0.168	b.d.l	1.03	b.d.l	0.046	0.209	0.321	b.d.l	0.603	0.493	61
Þ06	0.022	b.d.l	0.006	0.321	b.d.l	1.03	b.d.l	0.035	0.103	0.253	b.d.l	0.632	0.754	66
Þ07	0.121	b.d.l	0.006	0.572	0.483	1.04	b.d.l	0.072	0.255	0.373	b.d.l	5.93	0.387	69
Þ08	0.126	b.d.l	0.008	0.94	0.348	1.09	b.d.l	b.d.l	0.269	0.222	b.d.l	10.5	0.754	102
Þ09	0.219	0.003	0.006	0.584	0.655	4.13	b.d.l	0.221	0.171	0.41	0.023	13.2	2.66	129
Þ10	0.087	b.d.l	b.d.l	0.377	0.294	3.29	b.d.l	0.08	0.097	0.158	0.014	5.87	1.7	66
Þ11	0.079	b.d.l	b.d.l	0.784	0.661	5.75	b.d.l	0.118	0.189	0.254	0.029	4.74	1.04	81

Table ES1: Complete groundwater data *Recalculated to NIST = 0.25‰ for literature comparison*

Paper ID	Fe2+ ppb	Fe3+ ppb	$\delta^{98}Mo_{NIST0}$ ‰	2 SD	n	$\delta^{98}Mo_{NIST0.25}$ ‰	2 SD	n
M01	21.5	32.1	0.80	± 0.04	4(2)	1.05	± 0.04	4(2)
M02	b.d.l	62.7	0.04	± 0.08	2	0.29	± 0.08	2
M03	b.d.l	40.4	0.87	± 0.08	2	1.12	± 0.08	2
M04	10.5	1618.9	0.14	± 0.08	2	0.39	± 0.08	2
M05	b.d.l	24.9	0.14	± 0.08	2	0.39	± 0.08	2
M06	750.5	184.2	1.30	± 0.08	2	1.55	± 0.08	2
M07	4.6	1729.7	0.22	± 0.08	2	0.47	± 0.08	2
M08	b.d.l	13.1	0.22	± 0.01	3	0.47	± 0.01	3
M09	9.6	1690.7	0.47	± 0.08	3	0.72	± 0.08	3
M10	b.d.l	12.9	0.13	± 0.08	2	0.38	± 0.08	2
M11	b.d.l	473	0.08	± 0.08	2	0.33	± 0.08	2
M12	b.d.l	5.2	0.81	± 0.08	2	1.06	± 0.08	2
M13	1.4	525.2	0.37	± 0.03	3	0.62	± 0.03	3
M14	6.9	825.7	1.81	± 0.03	5(2)	2.06	± 0.03	5(2)
M15	4.1	1436.7	0.68	± 0.06	3	0.93	± 0.06	3
M16	b.d.l	13.4	1.12	± 0.06	3	1.37	± 0.06	3
M17	1.8	14	0.83	± 0.08	2	1.08	± 0.08	2
M18	-	-	0.34	± 0.01	3	0.59	± 0.01	3
M19	-	-	-0.07	± 0.06	3	0.18	± 0.06	3
M20	-	-	0.56	± 0.08	5(2)	0.81	± 0.08	5(2)
Þ01	b.d.l	25.4	0.43	± 0.13	3	0.68	± 0.13	3
Þ02	b.d.l	17.8	0.25	± 0.08	2	0.50	± 0.08	2
Þ03	b.d.l	41.4	0.22	± 0.06	3	0.47	± 0.06	3
Þ04	b.d.l	30.7	-0.25	± 0.08	2	0.00	± 0.08	2
Þ05	b.d.l	14.2	-0.33	± 0.08	2	-0.08	± 0.08	2
Þ06	b.d.l	20.2	-0.08	± 0.08	2	0.17	± 0.08	2
Þ07	b.d.l	42.1	-0.19	± 0.10	3	0.06	± 0.10	3
Þ08	b.d.l	743.5	0.00	± 0.03	3	0.25	± 0.03	3
Þ09	-	-	0.30	± 0.12	3	0.55	± 0.12	3
Þ10	-	-	-0.40	± 0.08	2	-0.15	± 0.08	2
Þ11	-	-	-0.29	± 0.07	3	-0.04	± 0.07	3

Table ES2: Calculated saturation sate of the groundwater.

	Primary basalt minerals								
	Plagioclase feldspar		**Pyroxene**			**Olivine**		**Basaltic Glass**	**Magnetite**
Sample	Albite	Anorthite	CPX	Diopside	Enstatite	Fayalite	Forsterite		
	$NaAlSi_3O_8$	$CaAl_2Si_2O_8$	$Ca_{0.7}Mg_{0.84}Fe_{0.46}(SiO_3)_2$	$MgCa(SiO_3)_2$	$MgSiO_3$	Fe_2SiO_4	Mg_2SiO4	$SiAl_{0.36}O_2(OH)$	Fe_3O_4
M01	3.23	0.08	6.80	8.42	-2.45	-3.68	-4.57	0.03	6.24
M02	-1.24	-7.87	1.44	4.23	-4.58	-8.13	-4.44	-1.17	3.50
M03	1.69	-3.56	3.19	5.55	-3.84	-5.90	-3.82	-0.32	6.73
M04	-0.93	-6.62	3.28	6.29	-3.48	-7.73	-2.85	-1.29	3.91
M05	-1.03	-6.94	3.45	6.11	-3.58	-5.99	-2.70	-1.30	6.24
M06	4.99	0.98	1.75	2.15	-5.46	-6.29	-12.00	0.92	2.06
M07	-1.28	-6.86	4.61	7.47	-2.87	-6.10	-1.78	-1.57	5.14
M08	-0.44	-4.15	4.90	6.74	-3.32	-6.78	-6.66	-1.23	2.37
M09	-0.39	-3.21		8.25	-2.54		-6.30	-1.32	
M10	-1.05	-6.70	4.08	6.79	-3.23	-6.21	-2.60	-1.41	6.57
M11	-1.12	-7.25	3.73	6.76	-3.27	-7.13	-2.22	-1.45	4.38
M12	1.02	-2.29	7.27	9.08	-2.14	-5.35	-5.25	-0.98	3.83
M13	-1.75	-3.77	6.54	7.61	-2.63	-4.23	-6.61	-1.74	6.26
M14	-0.06	1.03	10.46	10.53	-1.23	-3.24	-9.45	-1.46	6.39
M15	-0.14	-2.32	7.24	8.80	-2.25	-5.89	-6.61	-1.29	3.42
M16	0.52	0.88	9.79	10.21	-1.50	-3.46	-8.59	-1.25	6.43
M17	-0.14	9.06				0.64		-2.41	11.28
M18	-1.61	-0.51	8.89	8.64	-2.60	-1.63	-10.48	-1.80	9.86
M19	-1.44	-7.70	3.45	6.11	-3.57	-5.90	-2.61	-1.44	6.30
M20	-0.93	-1.77	8.59	9.25	-1.82	-3.33	-7.23	-1.59	7.09
Þ01	-1.88	-6.65	0.89	2.67	-5.33	-9.53	-9.72	-1.21	-2.57
Þ02	-0.56	-5.67	3.58	5.72	-3.86	-6.74	-5.67	-1.10	2.33
Þ03	-1.33	-3.18	6.77	7.47	-2.84	-3.33	-7.61	-1.49	7.24
Þ04	-1.45	-7.92	2.33	5.34	-4.04	-7.87	-3.29	-1.37	3.29
Þ05	-1.96	-8.22	4.58	7.40	-3.57	-3.93	-1.66	-2.03	9.61
Þ06	-2.14	-8.53	2.89	5.85	-4.25	-6.36	-3.27	-1.80	5.83
Þ07	-1.75	-8.23	-0.01	2.85	-5.22	-10.07	-5.94	-1.25	0.17
Þ08	-1.21	-6.46	2.64	5.11	-4.06	-8.18	-5.45	-1.28	0.39
Þ09	-1.67	-5.84	3.58	5.48	-3.91	-6.98	-6.62	-1.41	2.13
Þ10	-1.54	-7.93	0.94	3.67	-4.85	-7.95	-4.55	-1.25	3.28
Þ11	-1.42	-7.40	4.14	6.63	-3.26	-5.00	-2.27	-1.46	7.38

Table ES2: Calculated saturation sate of the groundwater.

	Manganese (oxyhydr)oxides				Iron (oxyhydr)oxides			
Sample	Birnessite	Bixbyite	Hausmannite	Manganite	Maghemite	Ferrihydrite	Goethite	Lepidocrocite
M01	-26.34	-24.06	-25.30	-11.40	-5.43	-3.12	-0.35	-0.89
M02	-19.33	-20.76	-24.45	-8.35	1.23	-0.39	2.48	2.44
M03	-18.97	-20.00	-23.53	-8.22	3.29	0.74	3.60	3.47
M04	-19.95	-21.77	-26.10	-9.12	1.84	0.03	2.89	2.74
M05	-18.02	-18.74	-21.87	-7.48	4.06	1.09	3.95	3.85
M06	-29.54	-30.37	-35.03	-14.90	-8.69	-4.60	-1.86	-2.53
M07					2.46	0.38	3.23	3.05
M08	-29.01	-28.94	-32.68	-14.17	-8.21	-4.37	-1.62	-2.28
M09								
M10	-18.35	-19.42	-23.10	-8.05	3.76	1.03	3.88	3.70
M11	-18.45	-20.00	-24.01	-8.17	2.87	0.51	3.37	3.26
M12	-28.69	-28.03	-31.42	-13.97	-7.38	-3.84	-1.11	-1.87
M13	-26.05	-22.40	-23.14	-11.54	-5.90	-2.94	-0.24	-1.13
M14	-25.69	-20.19	-20.80	-12.38	-6.76	-2.53	0.02	-1.56
M15	-28.28	-26.81	-29.83	-13.86	-7.85	-3.86	-1.17	-2.10
M16	-27.74	-24.73	-27.35	-14.10	-6.45	-2.61	-0.01	-1.40
M17	-23.11	-11.39	-8.97	-11.55	-7.71	-1.46	0.82	-2.03
M18	-26.02	-21.09	-21.83	-12.34	-4.44	-1.58	1.01	-0.40
M19	-18.20	-19.12	-22.42	-7.65	4.12	1.10	3.97	3.88
M20	-27.34	-24.38	-26.47	-13.28	-5.68	-2.50	0.14	-1.02
Þ01	-30.24	-31.80	-36.86	-15.25	-10.79	-5.80	-3.03	-3.57
Þ02	-29.67	-30.84	-35.12	-14.33	-7.94	-4.57	-1.77	-2.15
Þ03	-28.25	-26.75	-29.75	-13.85	-5.34	-2.60	0.09	-0.85
Þ04	-18.71	-20.24	-24.05	-8.10	2.17	0.09	2.96	2.91
Þ05	-14.95	-14.68	-16.61	-5.23	1.96	-0.06	2.82	2.80
Þ06	-17.69	-18.96	-22.46	-7.40	3.18	0.56	3.44	3.41
Þ07	-21.20	-24.12	-29.43	-10.16	-0.92	-1.41	1.45	1.36
Þ08					-9.23	-5.29	-2.47	-2.79
Þ09	-29.38	-29.89	-33.88	-14.26	-8.28	-4.57	-1.79	-2.32
Þ10	-30.60	-33.07	-37.74	-14.42	-8.61	-5.35	-2.47	-2.48
Þ11	-17.75	-18.53	-21.79	-7.46	4.65	1.41	4.27	4.15

Table ES2: Calculated saturation sate of the groundwater.

Sample	Sulphides			Carbonates				log $p\,CO_2$
	Molybdenite MoS_2	Pyrite FeS_2	Chalcopyrite $CuFeS_2$	Dolomite D	Dolomite O	Calcite	Aragonite	
M01	10.54	5.72	11.01	-0.72	-0.13	0.06	-0.14	-3.32
M02				-2.85	-2.21	-0.97	-1.20	-3.61
M03				-2.06	-1.43	-0.65	-0.88	-3.59
M04				-1.31	-0.67	-0.26	-0.49	-3.81
M05				-1.53	-0.89	-0.37	-0.60	-3.98
M06	16.16	7.83	13.64	-7.98	-7.41	-3.69	-3.89	-3.24
M07				-1.08	-0.45	-0.17	-0.40	-4.35
M08	10.30	4.80	9.88	-1.54	-0.97	-0.32	-0.51	-3.25
M09	8.91			-0.48	0.08	0.19	0.01	-3.22
M10				-1.16	-0.53	-0.19	-0.41	-4.05
M11				-1.24	-0.60	-0.21	-0.44	-4.12
M12	7.94	4.48	8.02	-0.80	-0.24	0.04	-0.15	-3.65
M13	8.63	5.37		-0.50	0.05	-0.04	-0.22	-3.22
M14	3.00	3.60	6.09	-0.11	0.36	0.20	0.06	-3.21
M15	8.14	4.40	8.07	-0.26	0.29	0.29	0.11	-3.18
M16	3.90	3.91	6.75	-0.43	0.06	0.15	0.00	-3.26
M17	-6.61	0.57	-3.66			0.24	0.19	-3.76
M18	6.37	6.24	8.22	-0.71	-0.22	0.33	0.18	-3.06
M19				-1.63	-0.99	-0.43	-0.66	-4.06
M20	6.51	4.96	8.03	0.04	0.55	0.23	0.07	-3.15
Þ01	13.95	5.64	10.85	-3.46	-2.87	-1.30	-1.50	-2.34
Þ02	11.67	5.53	10.61	-2.39	-1.79	-0.71	-0.93	-3.50
Þ03	7.43	5.31	9.69	-1.54	-1.00	-0.43	-0.60	-3.37
Þ04				-2.98	-2.34	-1.02	-1.25	-4.41
Þ05				-2.83	-2.18	-0.38	-0.62	-6.01
Þ06				-2.90	-2.26	-0.51	-0.75	-4.95
Þ07				-4.23	-3.59	-1.71	-1.94	-3.66
Þ08	12.22	5.03	9.81	-2.86	-2.25	-1.06	-1.27	-3.74
Þ09	10.72	5.09	10.30	-2.49	-1.90	-0.83	-1.03	-3.45
Þ10	14.82	6.56	10.88	-4.15	-3.50	-1.63	-1.87	-4.27
Þ11				-2.24	-1.60	-0.78	-1.01	-4.60

4 Quantifying the effect of primary productivity on molybdenum isotopes in a natural environment: Lake Mývatn, Iceland

Rebecca A. Neely[1], Carl-Magnus Mörth[2], Sigurdur R. Gislason[1], Peter Torssander[2], Eydís S. Eiríksdóttir[1], Christopher R. Pearce[3], Kevin W. Burton[4]

[1]Institute of Earth Science, University of Iceland, Sturlugata 7, 101 Reykjavík, Iceland

[2]Institute for Geology and Geochemistry, Stockholm University, 106 91 Stockholm, Sweden

[3]National Oceanography Centre Southampton, University of Southampton Waterfront Campus, European Way, Southampton, SO14 3ZH, UK.

[4]Department of Earth Sciences, Durham University, Science Labs, Durham DH1 3LE, UK

Nitrogen fixation is catalysed by the nitrogenase enzyme and its most common and efficient form contains molybdenum (Mo) in the FeMoco (Fe_7MoS_9C) cofactor. These enzymes facilitate the fixation of atmospheric nitrogen, making it biologically available to the wider ecosystem. In the aqueous environment this fixation is primarily carried out by cyanobacteria that are capable of causing significant Mo isotope fractionations. Here we present seasonal Mo isotope data from the riverine output of one of the most biologically productive lakes in the northern hemisphere. Large biological $\delta^{98/95}$Mo fractionations are observed for the first time in the natural aqueous environment, with lake output values increasing from +0.2‰ (relative to SRM NIST 3134= 0‰) during the ice-covered months to a high of +0.5‰ in September, coincident with an observed cyanobacteria bloom. Box model calculations indicate that these variations are driven by the removal of isotopically light Mo with an enrichment factor of ε -1.5‰ between the removed Mo and the Lake waters. Abiotic processes are unlikely to be the origin of this isotope fractionation due to the extremely high lacustrine pH inhibiting both adsorption of Mo onto Fe-Mn (oxyhydr)oxide surfaces and the absence of any associated Li isotope fractionation. Consequently these results demonstrate for the first time in the natural aqueous environment the biological fractionation of Mo isotopes of ca. ε -1.5‰, associated with cyanobacteria growth.

4.1 Introduction

The importance and use of molybdenum (Mo) in biological systems was first recognised in the 1930's when it was discovered that Mo could stimulate biological nitrogen fixation (Bortels 1930 in Stiefel 1997). By the 1970s, the presence of Mo in the crucial nitrogenase enzyme and its ubiquity in the biogeochemical cycling of nitrogen, sulfur, and carbon was fully recognised (c.f. Stiefel 1997). In the N-cycle the predominance of Mo is notable; it is essential for nearly all organisms and forms the catalytic centre of a large variety of enzymes such as nitrogenase and nitrate reductases (e.g. Schwarz et al., 2009). Despite being the most abundant gas in Earth's atmosphere, nitrogen (N_2) is too inert to be used directly by most organisms as a relatively large amount of energy is required to break the N triple bond. The nitrogen must be bound to hydrogen or oxygen to form more reactive compounds before it is then incorporated into living cells. Consequently biological fixation, catalysed by the nitrogenase enzyme, is the main process through which new nitrogen is added to ecosystems. There are a number of different nitrogen-fixing enzymes that all require iron but the most common nitrogenase also requires Mo at its active site in the form of the FeMoco, Fe_7MoS_9C, cofactor (Bellenger et al., 2011).

As such, Mo has played a significant role in the Earth's history. Whilst other processes such as hydrothermal reduction, photochemical reactions, and lightning are capable of fixing nitrogen, the evolution of nitrogenase is considered a major breakthrough in facilitating the radiation of life with biological fixation of nitrogen, facilitated by Mo, dated back to 3.2 Ga (Stueken et al., 2015). In addition, the significance of Mo in the Earth's ecosystems and biogeochemical cycles is highlighted by its capacity to limit (and conversely, therefore, to stimulate) primary productivity. Goldman (1960) demonstrated that molybdate (MoO_4^{2-}) additions to Castle Lake, California, lead to increased photosynthetic rates. Later, the significance of Mo facilitated N-fixation in the soils of forests was demonstrated by Silvester et al. (1989) in the Pacific northwest, USA, and Barron et al. (2009) in tropical forests, Panama. These studies showed that nitrogen fixation and nitrogenase activity is enhanced by the additions of Mo, with Barron et al. (2009) demonstrating that fixation did not respond to additions of phosphorus alone but required Mo to be present.

Mo is an ideal cofactor in enzymes for carbon, nitrogen, and sulfur metabolism due to its redox sensitivity (Frausto da Silva and Williams, 2001). This redox response has also made Mo of great interest in other Earth Science applications (e.g. Kendall et al., 2016), though its use in low temperature environments has been somewhat restricted to oceanic paleoredox reconstructions, including the study of riverine inputs and ocean sediments. The effects of biological utilisation on Mo isotopes have been the subject of fewer studies, and those are often restricted to laboratory experiments.

In general, it is energetically favourable for biological material to utilise lighter isotopes (e.g. Wierderhold et al., 2015) causing the cells to become enriched in light isotopes while the growth media becomes increasingly enriched in the heavy isotopes: resulting in isotopic fractionation. This has been demonstrated for Mo in several studies; Nägler et al. (2004) showed that marine cyanobactieria preferentially use light Mo resulting in ε^{98}Mo (enrichment factor) values from -0.1‰ to -0.5±0.1‰, whilst Liermann et al. (2005) and Wasylenki et al. (2007) reported similar results for Mo isotope fractionation in soil bacteria (-0.8±0.4‰ and -0.5±0.2‰ respectively). Zerkle et al. (2011) showed that the magnitude

of isotope fractionation in the freshwater cyanobacteria Anabaena variabilis depends on the stage of cell growth and the source of nitrogen, with fractionation being greater (up to 0.9‰) with a N_2 source as opposed to NO_3^- (-0.3±0.2‰) for the same experiment. Compared with the total environmental variation in Mo isotopes (δ^{98}Mo -1.75 to +2.1‰; Kendall et al., 2016), these studies clearly demonstrate that large biological fractionation of δ^{98}Mo occurs. However, whether this isotope fractionation process is as large and resolvable in natural environments remains to be determined.

This study examines the effects of primary productivity in Lake Mývatn, Iceland on δ^{98}Mo. Previous studies have made use of this natural laboratory to demonstrate large Si isotope fractionation by diatoms (Opfergelt et al., 2012) and an absence of biological incorporation or isotope fractionation of Li (Pogge von Strandmann et al., 2016). Thus this work builds on the wealth of information already available to assess the impact of biological incorporation of Mo on the lacustrine δ^{98}Mo composition.

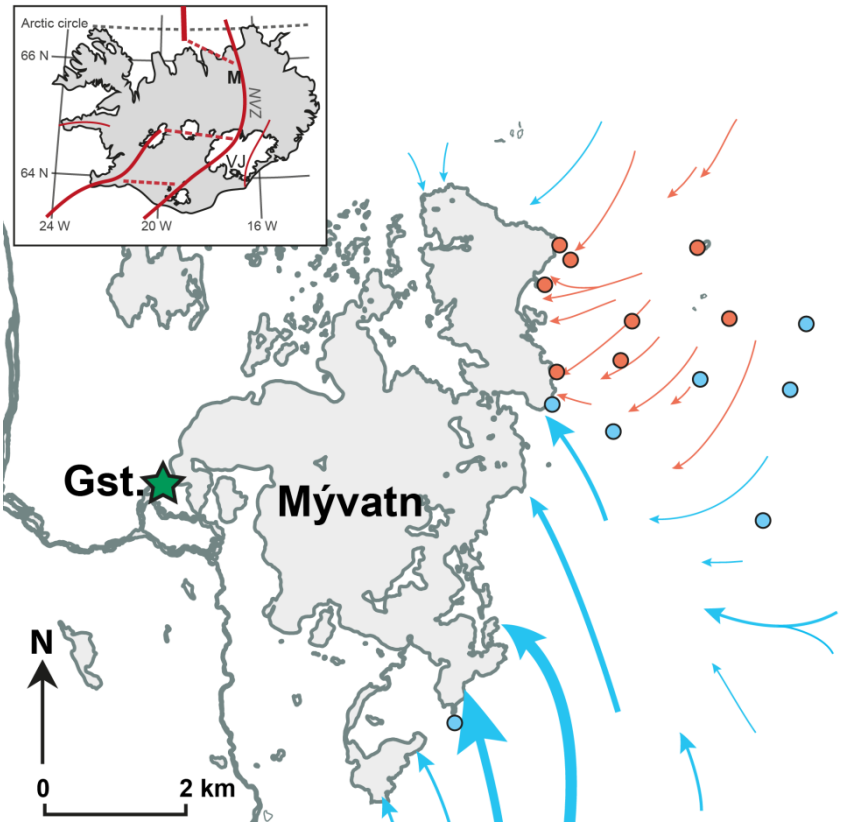

Figure 1: The inset map shows the location of Lake Mývatn (M) in Iceland relative to the plate boundaries (solid red lines are volcanic zones, dashed red lines are fracture zones after Thordarson & Larsen 2007). The lake outlet sampling location, Geirastaðaskurður, is marked by the green star. The groundwater source to the lake are represented by the arrows, blue representing cold groundwaters and red indicating warm, geothermally affected waters (Ólafsson et al., 2015). The groundwater system extends from Vatnajökull (VJ) glacier to the Atlantic Ocean and the filled circles show where corresponding groundwater samples have been taken as reported in Neely et al. (Submitted 2017).

4.2 Geological setting and methods

4.2.1 Geological setting

Lake Mývatn is a 37 km^2, shallow eutrophic lake situated at 65°35'N 17°00'W, just below the Arctic Circle (Fig. 1). It is 278 m above sea level with a mean depth of ~2.5 m and has a water residence time of less than one month (Jónasson 1979; Jónasson & Adalsteinsson 1979). Located in the northern volcanic zone of Iceland, the surrounding young, porous lavas limit surface runoff resulting in a lake that is almost entirely sourced by groundwater. The groundwater entering Lake Mývatn is part of a large (~1500 km^2) system extending from Vatnajökull in the south to the Atlantic Ocean in the north (Ólafsson et al., 2015). As the groundwater approaches the lake, some of it is heated by direct mixing (and steam heating) with the Krafla and Námafjall geothermal fluids. These warm groundwaters then enter the northern basin of the lake at rate of 11 m^3s^{-1} whilst the cold groundwaters enter the southern basin at 25 m^3s^{-1} (Ólafsson et al., 2015). The groundwaters are nutrient rich and, when taken with the relatively high solar radiation over the summer months, they make Lake Mývatn one of the most productive lakes in the northern hemisphere, despite being ice-covered for ~190 days of the year (Jónasson 1979; Ólafsson 1979; Adalsteinsson 1979).

In a marked contrast to the stable groundwater input (Kristmannsdóttir & Ármannson 2004; Thorbergdóttir & Gislason 2004a), the biological succession and productivity in the lake show fluctuations with no straightforward correlation to external signals (Einarsson et al., 2004). Primary production has been estimated at 3800 kcal m^{-2} a^{-1} of which some 15% comes from phytoplankton (Jónasson 1979). It is dominated by benthic organisms such as diatoms, filamentous green algae (Cladophora glomerata), and also cyanobacteria (*Anabaena flos-aquae*) blooms (Einarsson et al., 2004). The seasonal succession is typically is characterised by a diatom peak in the month following the break-up of ice, a cyanobacteria bloom during the summer, and another diatom peak in the autumn (Jónasson and Adalsteinsson, 1979; Opfergelt et al., 2011). Invertebrates such as the non-biting midge larvae (Tanytarsus gracilentus) also contribute substantially: and through the binding of sediment via silk secretion, impact the benthic environment of this detritus-driven ecosystem (Ólafsson & Paterson 2004). It is of note, although not considered in this paper that this ecosystem supports many and diverse higher trophic level organisms such as fish (e.g. arctic charr; salvelinus alpinus) and ducks (e.g. tufted duck; Aythya fuligula).

4.2.2 Sample Collection

The Lake Mývatn outlet was sampled at monthly intervals at Geirastaðaskurður (Fig. 1), before the river mixes with other surface waters, in order to obtain a record of seasonal variations associated with biological productivity within the lake. The sample collection procedures are outlined in detail by Opfergelt et al. (2011) and Eiríksdóttir et al., (2008), with 11 samples collected between March 2000 and March 2001. During this sampling period the ice began to break up in the middle of April and Lake Mývatn was completely ice-free by 9th May. The physical conditions during sampling and major- and trace-element concentrations are taken from Eiriksdóttir et al. (2008) (Table ES1).

Table 1: Selected data for the Lake Mývatn outlet time series at Geirastaðaskurður

		Temp	pH	Eh	Na	Mg	Cl	SO4	$\delta^{34}S$	Mo	$\delta^{98}Mo$	2 SD	n
		°C	*in situ*	V	ppm	ppm	ppm	ppm	‰	ppb	‰		
MÝVATN OUTLET, GEIRASTAÐASKURÐI													
00-A013	03/03/2000	1.2	8.37	0.28	23.1	4.0	3.92	19.60	3.37	0.84	0.27	± 0.08	2
00-A023	11/04/2000	0.0	9.01	0.22	17.9	3.6	3.67	12.37	2.22	0.60	0.13	± 0.05	3
00-A031	08/05/2000	6.0	8.52	0.25	17.3	3.2	3.12	14.08	2.02	0.78	0.17	± 0.05	3
00-A044	07/06/2000	12.3	9.64	0.15	20.2	3.7	3.57	16.68	1.67	1.01	0.1	± 0.06	3
00-A053	12/07/2000	15.7	9.94	0.14	21.9	3.5	3.48	15.70	2.2	0.83	0.13	± 0.02	3
00-A062	09/08/2000	15.5	9.79	0.13	23.8	4.0	3.95	17.56	3.43	0.76	0.29	± 0.03	3
00-A071	14/09/2000	8.3	9.35	0.18	21.6	3.7	3.62	15.57	4.64	0.66	-	± -	
00-A080	17/10/2000	1.4	8.72	0.24	21.9	3.8	3.35	12.27	2.85	0.70	0.28	± 0.03	3
00-A089	21/11/2000	0.6	8.31	0.27	22.3	3.8	3.52	14.32	2.35	0.83	-	± -	
01-A006	06/01/2001	0.9	8.33	0.28	22.4	3.9	3.22	14.53	2.44	0.82	0.13	± 0.04	3
01-A015	03/03/2001	0.5	8.43	0.27	20.3	3.4	2.92	11.40	2.29	0.82	0.15	± 0.05	3
IAPSO seawater										10.8	2.09	± 0.08	43(17)

A complete data table for the Lake Mývatn time series is reproduced in the electronic supplements after Eiríksdóttir et al., (Table ES1). Mo isotope data are as described in the text; they are reported with errors of two standard deviations from the mean when n≥3. When n< 3, the 2SD of repeat IAPSO analyses is used (±0.08‰). "n" is the number of measurements made from one aliquot save for IAPSO which has been through chemistry 17 times and analysed a total of 43 times

4.2.3 Sulfur isotope chemistry and analysis

Column chemistry for sulfur purification was carried out at the Institute of Earth Sciences, University of Iceland whilst analysis was carried out at the Department of Geological Sciences, Stockholm University. Sulfate in the water samples was collected and by anion exchange resin (chloride form, Sigma-Aldrich, 20-50 mesh) in small columns using a method slightly modified from Andersson et al. (1992). Each column was filled with approximately 9 ml wet weight resin before 1L of the sample was allowed to pass through at a rate of 3-5 ml water per minute. The resin in the columns was pre-rinsed with a 200 ml 0.5 M NaCl solution and after that rinsed with 100 ml Milli-Q water. After the sulfate was collected on the resin the columns were eluted with 200 ml of 0.5M NaCl into a clean beaker. The solution was acidified with HCl to a pH of about 2, heated on a hot plate and allowed to boil for approximately one minute. After boiling the beaker was moved to a water bath (temperature of about 90°) where 5 ml 0.25 M BaCl solution was added and BaSO4 precipitated. Samples were left in the water bath for two hours and after cooling, the samples were filtered and rinsed, and the precipitated $BaSO_4$ was collected on polycarbonate filters and dried in an oven at 60°C overnight. The $BaSO_4$ was recovered by scraping the filter and storing the precipitated $BaSO_4$ in small glass bottles. For sulfur isotope analysis, approximately 0.5 mg $BaSO_4$ was weighed into small tin capsules and combined with an equal amount of V_2O_5. The isotope ratios were measured by using a Carlo Erba NC2500 elemental analyzer connected through a Conflo open split interface to a Finnigan Delta Plus mass spectrometer. The reference gas was calibrated by using IAEA-S-1, IAEA-S-2, and several in house standards. Standards were run at start and end of each run and every 10th sample. Isotope values are reported in the usual δ-notation, $\delta^{34}S$ (‰) = (R/Rstd -1) x 1000. The precision was better than ±0.2‰ based on standard measurements.

4.2.4 Molybdenum isotope chemistry and analysis

All sample preparation and δ^{98}Mo measurements were conducted at the Department of Earth Science, Durham University. Mo concentrations were initially determined by ICP-MS before each sample was weighed and spiked with a ^{97}Mo-^{100}Mo double-spike to yield a ~1:1 ratio of spike to natural Mo. 50 100 ng of natural Mo was processed per sample. Chemical separation of Mo was achieved using a single pass anion exchange procedure detailed in Pearce et al. (2009). An additional 12 ml 0.5 M HF matrix elution step was included to ensure complete removal of Zn before the final Mo elution in 3 M HNO_3.

Molybdenum isotope compositions were measured by MC-ICP-MS (Thermo-Finnegan 'Neptune') equipped with an Aridus II desolvating nebuliser. Samples were aspirated at ~35 µl min^{-1} using a Cetac nebuliser and the maximum sensitivity was ~400 v ppm^{-1}. Measurements were made in low resolution, static mode with 1 block of 50 cycles. Total procedural blanks for aqueous samples were < 1 ng and data reduction was carried out offline using a deconvolution routine (Pearce et al. 2009) based on the Newton-Raphson method. All Mo isotope compositions are reported in delta notation in parts-per-thousand relative to a reference solution (eq.1) with errors of 2 standard deviations from the mean. In this study the reference solution is SRM NIST 3134 (Greber et al., 2012; Goldberg et al., 2013), and all Mo isotope data in this paper are referenced to NIST 3134 - recalculated, where necessary based on data from Goldberg et a. (2013).

$$\delta^{98/95}Mo_{NIST} = \left[\left(\frac{\frac{^{98}Mo}{^{95}Mo_{SAMPLE}}}{\frac{^{98}Mo}{^{95}Mo_{NIST\ 3134}}}\right) - 1\right] \cdot 1000 \qquad (1)$$

δ^{98}Mo reproducibility was determined by measurement of the in-house Romil standard, which gave $\delta^{98}Mo_{NIST}$ = +0.05 ± 0.05‰, n=183. IAPSO seawater was run as an additional unknown standard, yielding a $\delta^{98}Mo_{NIST}$ composition of +2.09 ± 0.08‰ (n=43, nchem=17), which is comparable with the mean of published values of +2.08 ± 0.10‰ (Gerber et al., 2012; Pearce et al., 2009; Siebert et al., 2003). An additional Open University standard (OU-Mo) was also run, with the $\delta^{98}Mo_{NIST}$ value of -0.35 ± 0.03‰ (n=11) being comparable with the mean value of this standard obtained at Imperial College London (-0.37 ± 0.04‰) and the Open University (-0.38 ± 0.02‰) (Goldberg et al., 2013). Taken together, these data indicate a long term external reproducibility of ± 0.08‰ or better for the δ^{98}Mo isotope data reported in this study.

In situ pH and Eh values, at the measured sampling temperature of the waters, were calculated by PHREEQC version 3.0.6 (Pankhurst and Apello, 2013) using the minteq.v4 database. Redox was defined by (i) the measured nitrogen speciation, and (ii) assuming atmospheric oxygen saturation at the measured water temperature. The results from each approach show that oxidised MoO_4^{2-} dominates all of the samples (Fig. 2). This supports previous data for Icelandic waters below 200°C (Arnórsson and Ívarsson 1985).

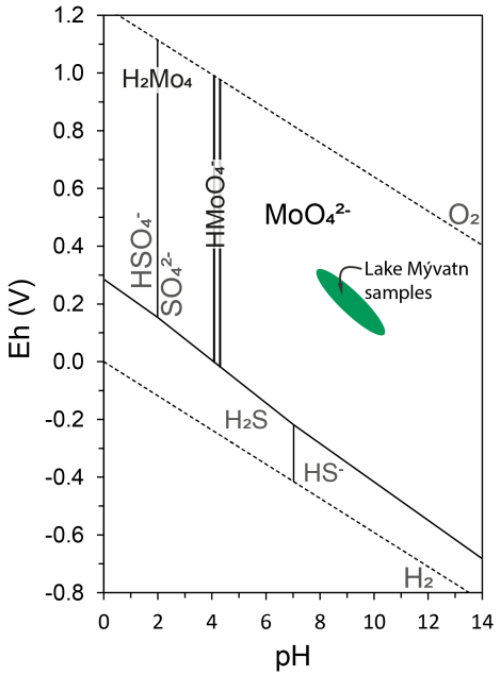

Figure 2: pH-Eh diagram at 25°C, 10^5 Pa for the S-O-H system with available, oxidised, Mo data superimposed. Mo speciation below the SO42- - H2S transition is not well characterised although it is thought to be dominated by oxythiomolybdate species (Erikson & Helz 2000). Calculated in situ pH and Eh for the lake samples are plotted and all are dominated by MoO_4^{2-}. Calculations are based on the minteq.v4 database within PHREEQC (Parkhurst & Appelo, 2013). The stability field for water lies between the two dashed lines.

4.3 Results

A complete dataset for the sampling period is given in the electronic supplements (Table ES1; Eiríksdóttir et al., 2008). The most relevant data for this study and the new Mo data are detailed in table 1.

Mo concentrations in the lake outlet vary from a minimum of 0.60 ppb to a summer maximum of 1.01 ppb (Table 1, Fig. 3a). The Mo concentration is stable during the winter, ice-covered months at ~0.8 ppb. Accompanying ice break-up from the middle of April there is Mo depletion to 0.6 ppb (Fig. 3a). Following the onset of ice break-up there is a single concentration peak in June to 1.0 ppb before a sustained concentration reduction over the late summer months, between June and November. Over the sampled time series, the measured δ^{98}Mo variation is small (δ^{98}Mo from +0.10 to +0.29‰) but distinguishable from the 2SD of repeat analyses and the long term reproducibility (Fig. 3b). Unfortunately, due to sample size limitations and the fact that the Mo concentration is low (0.66 ppb), the September sample was not able to be analysed for Mo isotopes. However, based on the correlation with sulfur isotopes (Fig. 3c) it was estimated to δ^{98}Mo +0.5‰, making this a significantly enriched sample, coincident with Mo depletion in the lake.

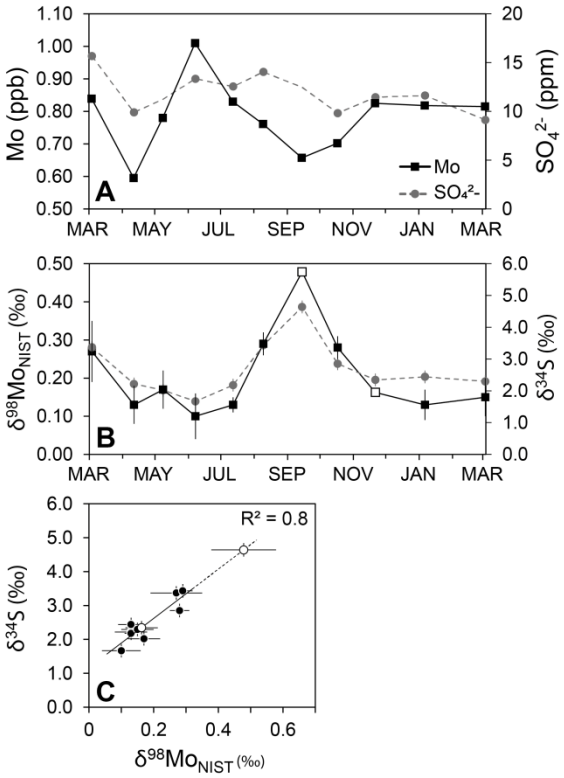

Figure 3: (A) Variation in dissolved Mo and S concentrations in Lake Mývatn from March 2000 to March 2001. (B) Covariation of Mo and S isotopes in Lake Mývatn with a shift to heavier isotopes in both systems in the late summer months (August–October). Sulfur isotopes (Eiríksdóttir et al., 2008) are represented by the grey dashed line and $\delta^{34}S$ values are on the right hand y-axis; Mo isotopes are shown with the solid black line, with 2SD errors plotted, and $\delta^{98}Mo$ values on the left hand y-axis. The open squares in the Mo isotope data are for those samples that were unable to be measured but are inferred from the sulfur data according to plot (C): correlation between the two systems (R^2 = 0.8 for the measured, filled black circles alone). Again, the open circles represent the inferred Mo isotope composition.

As shown in figure 2, sulfate is the dominant sulfur species in these samples. Measured sulfate concentrations vary between 11.4 and 19.6 ppm, but do not co-vary with Mo nor show clear seasonal variation (Fig. 3a). In contrast, $\delta^{34}S$ isotopes are at their lightest during the spring and winter months ($\delta^{34}S$: +2‰) rising from July to a significant September peak of +4.6‰.

Whilst the concentrations of sulfate and Mo do not appear to be covariant, figures 3b and c show the clear correlation between the stable isotopes of both S and Mo, reaching coincident peaks in the late summer, far exceeding their analytical uncertainties.

4.4 Discussion

Lake Mývatn shows strong seasonal variation in nutrient concentrations due to its high latitude resulting in high summer insolation and associated biological processes. For example: NO_3 and Si concentrations are reduced in the summer months due to enhanced utilisation in primary productivity mainly controlled by diatom and cyanobacteria growth (Fig. 8; Opfergelt et al., 2011). Despite both S and Mo being essential components of living cells (Canfield 2001; Glass et al., 2012) only Mo shows reduced summer concentrations (Fig. 3a). Conversely, their isotopes do show a strong seasonality with a late summer peak in which the lake waters enriched in heavy isotopes of both S and Mo relative to winter values (Fig. 3b).

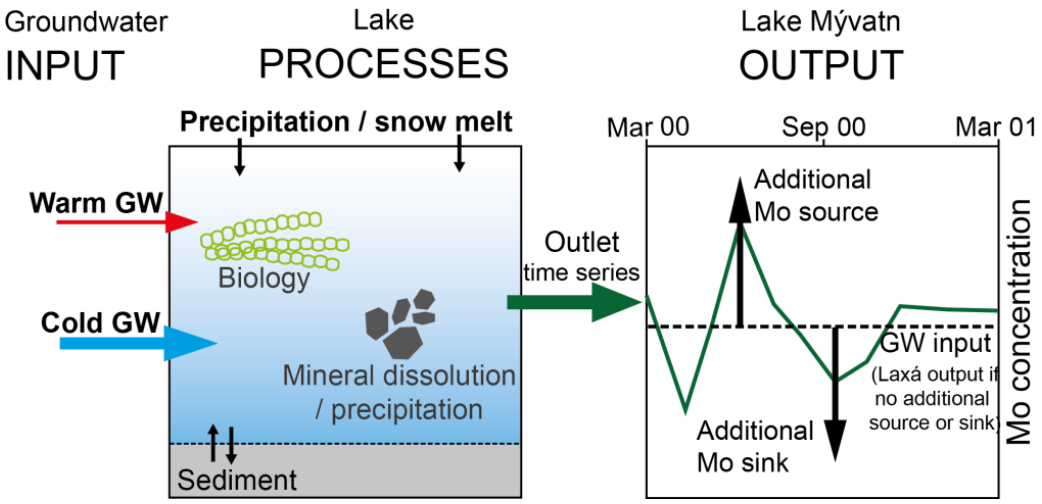

Figure 4: Schematic for the processes affecting Mo isotopes in Lake Mývatn and the concepts underpinning the Mo isotope numerical modelling. The major source of Mo to Mývatn is from the groundwaters (GW). In addition there is direct precipitation/snow-melt and sediment-water column exchange processes (although both are negligible in this case). If the Mo transits through the lake with no further processing then the time series Lake output will be the dashed, unchanging horizontal line depicted in the right-hand graph. However, if additional sources and sinks (such as biology and mineral precipitation/dissolution) affect the Mo then the Lake outlet Mo concentration will be modified as shown by the green line. These changes in concentration are used to drive the Mo isotope model.

4.4.1 Modelling Mo variations in Lake Mývatn

The box model used to characterise Mo behaviour in Lake Mývatn is shown in Fig. 4 schematic. This model assumes an open system in which the principal sources and sinks of Mo can be characterised through direct measurement, calculation, and literature data.

Potential sources of Mo into Lake Mývatn come from the groundwaters, direct precipitation, and exchange with the sediments. Cold groundwaters feed into the southern

basin (25 m^3s^{-1}) and geothermally influenced waters enter the northern basin (11 m^3s^{-1}) (Ólafsson et al., 2015). Due to its location in the rain shadow of Vatnajökull, precipitation amounts to some 0.5 m^3s^{-1} (Ólafsson 1979) which, with concentrations of 0.007 ppb (King et al., 2016), makes little impact on the lake's Mo budget. Although exchange of solutes across the sediment-water interface is high for some nutrients and elements (Jónasson 1979; Jónasson & Adalsteinsson 1979; Ólafsson 1979 in Gíslason et al., 2004), the sediments are only a minor sink for Mo at 4×10^2 mg Mo s^{-1} (calculated from Gíslason et al., 2004) compared with the groundwater flux of 28 mg Mo s^{-1} (this study). Therefore, through the characterisation of the Mývatn groundwaters it is possible to estimate the chemical composition of the total Mo input into the lake (c.f. Opfergelt et al., 2011 and Pogge von Strandmann et al., 2016).

The estimated cold input is the mean chemical composition of all of the Mývatn groundwaters with a sampling temperature of less than 10°C, yielding $[Mo]_{COLD}$ 0.7 ppb and $\delta^{98}Mo_{COLD}$ +0.2‰ (Neely et al., Submitted 2017, Chapter 3). Due to the chemical variability in the geothermally affected waters, the δ^{98}Mo composition of groundwater input to the northern basin is calculated using only those springs located directly around the lake, resulting in $[Mo]_{HOT}$ 0.8 ppb and $\delta^{98}Mo_{HOT}$ +0.5‰ (Neely et al., Submitted 2017, Chapter 3). The proportionally combined input to Lake Mývatn is therefore 0.8 ppb Mo and δ^{98}Mo +0.2‰ (calculated from equations 2 and 3 where X is the concentration of Mo, F is the fraction, and δ is the Mo isotope signature with the subscripts denoting cold groundwaters (c), geothermally affected waters (h), and combined lake input (in)).

$$X_{in}=F_c\,X_c+(1-F_c)X_h \quad (2)$$

$$\delta_{in}=\left(F_c\cdot\delta_c\cdot\frac{X_c}{X_{in}}\right)+\left((1-F_c)\cdot\delta_h\cdot\frac{X_h}{X_{in}}\right) \quad (3)$$

This characterisation of the Lake Mývatn input, when combined with the seasonal samples from the lake output, enables an assessment of the processes controlling the Mo isotope composition of the lake (Fig. 4). Crucially, the groundwater supply to the lake is stable and constant with time (Arnórsson & Ívarsson 1985; Kristmannsdóttir & Ármannsson 2004; Thorbergsdóttir & Gíslason 2004), meaning that any differences in the composition of the lake output and the groundwater input must reflect a processes that occurs within the lake itself.

The evolution of the Mo isotope composition of the lake (δ_{OUT}) is best described by an open, steady state model. As in Opfergelt et al. (2011), this can be modelled using equation 4

$$\delta_{OUT} = \delta_{in} - \varepsilon_{UP}\cdot(1-F) \quad (4)$$

where δin is the calculated groundwater isotopic composition, F is the fraction of Mo remaining (calculated from the ratio of $[Mo]_{out}$ that changes with time, and $[Mo]_{in}$ that is assumed to be constant at 0.8 ppm), and ε_{UP} is the assigned enrichment factor (where $\varepsilon_{UP} \sim \delta_{UPTAKE} - \delta_{DISSOLVED}$). Hence, negative values for the enrichment factor indicate that the dissolved phase is heavier than the removed phase.

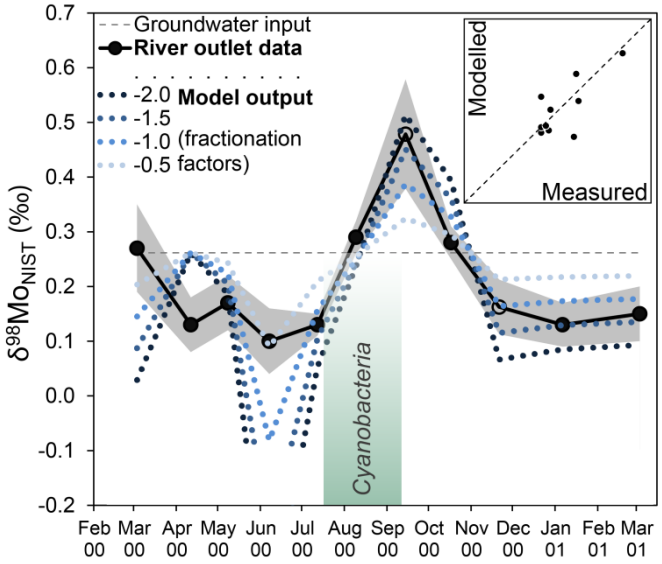

Figure 5: The measured seasonal variation in Mo isotopes (solid black with grey shaded 2SD error envelope) compared to the model output (blue dotted lines), assuming the stated fractionation factors from -0.5 to -2.0‰. A fractionation factor of 0‰ is forced through the month of April due to the dilution of the lake without associated isotopic affect. The groundwater input (grey dashed line) is assumed to be stable with time. The two open black circles in the measured time series data represent data points calculated from extrapolation of the $\delta^{34}S$ and $\delta^{98}Mo$ relationship. In the inset, the modelled data (ε_{UP} -1.5‰) is compared with the measured Mo isotopes from the river outlet; a perfect fit would sit on the 1:1 dashed line. The actual regression line is y=1.1x-0.07, R^2=0.5.

The measured Mo isotope composition at the lake outlet is compared with the model output in Fig. 5 and ES1. When negative enrichment factors of between -0.5 and -2.0‰ are applied the model replicates the measured time series data. The greatest discrepancy between the model and measured data occurs in April (Fig. ES1). During this period the ice cover begins to disperse and Eiriksdóttir et al. (2008) suggest that dilution of Lake Mývatn occurs over the 2-3 week period that the lake becomes ice-free. Assuming a pure water composition and instantaneous melting, the modelled level of dilution requires the addition of 22×10^6 m^3 meltwater or the equivalent of approximately 60 cm thickness of ice over the area of Lake Mývatn. This is reasonable given that the Myvatn ice thickness was measured at 40-50 cm in February 2000 (Thorbergsdottir et al., 2004) and can routinely reach 70 cm (Ólasson 1979). It is also supported by an increase in the River Laxá discharge from a stable mean of 36.0 m^3 s^{-1} to 47.5 m^3 s^{-1} in April 2000 (Eiriksdóttir et al., 2008). As dilution will not affect isotope composition, an enrichment factor of 0‰ has been applied in the model for April. With a water residence time in the lake of less than one month (Jónasson & Adalsteinsson 1979), dilution is unlikely to have persisted beyond April.

4.4.2 The late summer molybdenum isotope peak

Two processes have the potential to explain the changing Mo isotope composition of the Lake Mývatn output: biological uptake and adsorption onto mineral surfaces. In the case of biologically driven isotope fractionation, the cyanobacteria, Anabaena flos-aque, is known to bloom in the lake between late July and early September (Einarsson et al., 2004; Thorbergsdottir et al., 2004; Eiríksdóttir et al., 2008). Experiments have shown that Anaaena achieves optimal growth in solutions with a dissolved Mo concentration of 4 to 192 ppb (Glass et al., 2012) and can fractionate Mo isotopes through the preferential uptake of light isotopes with associated biological enrichment factors between -0.2 and -1.0‰ (Zerkle et al., 2011).

Blooms of *A. Flos-aquae* have long been known to occur in Lake Mývatn, and systematic observations of these blooms have been made since 1970 (Einarsson et al., 2004). Secchi depth measurements (which quantify water clarity and can be used as a proxy for bloom density) indicate that there was a small cyanobacteria bloom in 2000 when the *A. flos-aquae* density was relatively low (Einarsson et al., 2004; Thorbergsdottir et al., 2004). Corresponding with this bloom from late July to early September (Eiríksdóttir et al., 2008) was a small, but sustained, reduction in Mo concentration and a shift to heavy Mo isotope compositions at the lake outlet (Figs. 3a & b).

The model data best fit with the measured data when an enrichment factor of -1.5‰ is assigned (Fig 5). This is consistent with biological isotope fractionation, where the preferential uptake of light Mo isotopes by *A. flos-aquae* results in a dissolved reservoir enriched in heavier Mo isotopes. The largest biological δ^{98}Mo fractionation reported in laboratory experiments thus far is -1.0‰, and was associated with nitrogen limitation; a common occurrence in natural bloom events (Zerkle et al., 2011). Nitrogen is known to be a limiting nutrient in Lake Mývatn, with a N:P ratio consistently below the Redfield ratio (16), and the almost complete utilisation of NO_3 occurring by August (Fig. 8). It is therefore likely that biological fixation of atmospheric N_2 became increasingly important to the Lake Mývatn ecosystem during this period of cyanobacterial growth. With significant N-limitation within the lake, it is also reasonable to envision that the isotope enrichment factors would be at the extreme end of those observed in laboratory experiments.

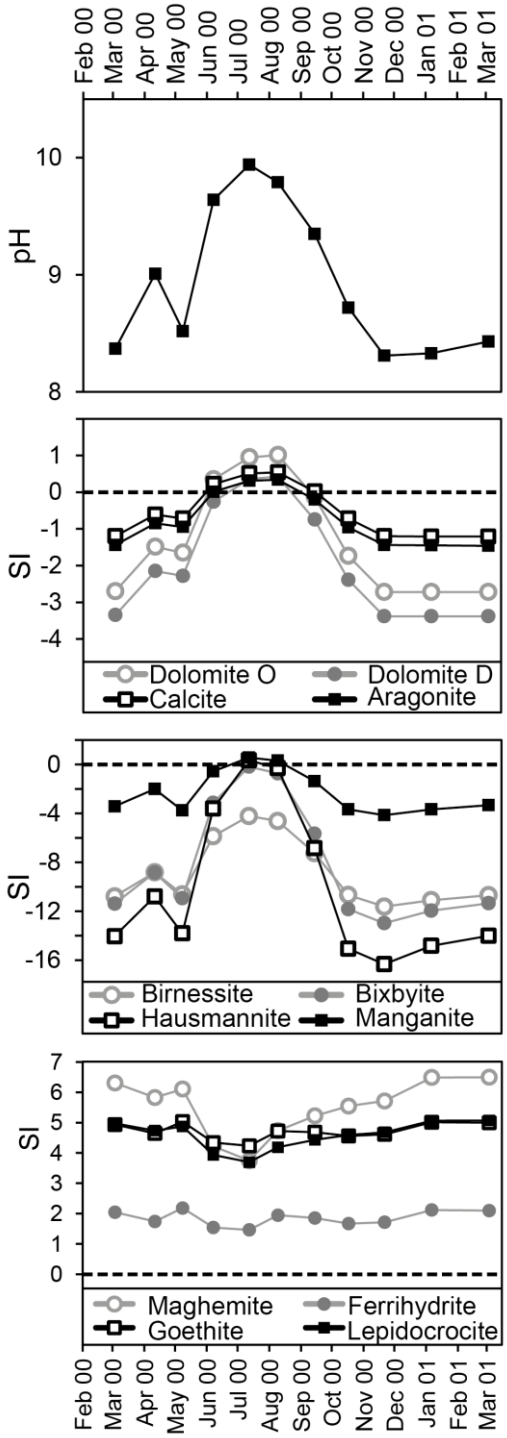

Figure 6: In situ pH and saturation indices (SI) for selected mineral phases in the Lake Mývatn outlet: Carbonates (ordered and disordered dolomite ($CaMg(CO_3)$), and calcite and aragonite ($CaCO_3$)), Manganese (oxyhydr)oxides (Birnessite (MnO_2), Bixbyite (Mn_2O_3), Hausmannite (Mn_3O_4), and Manganite (MnOOH)), and Iron (oxyhydr)oxides (Maghemite (Fe_2O_3), Ferrihydrite ($Fe(OH)_3$, and Goethite and Lepidocrocite (FeOOH)). Positive SI suggests oversaturation and potential for precipitation; negative SI suggests undersaturation and tendency for dissolution. Saturation Index calculated using PHREEQC (Parkhurst & Appelo, 2013) with the waters in equilibrium with atmospheric O_2.

If the Mo isotope composition of the lake is affected by the formation of secondary minerals then they are most likely to be Fe and Mn (oxyhydr)oxides. These secondary phases are known to be important in controlling the Mo isotope composition in low temperature, aqueous environments (e.g. Miller et al., 2011; Matern & Mansfeldt 2015; Goldberg et al., 1996; Wasylenki et al., 2011; Barling & Andbar 2004; Goldberg et al., 2009). Similar to the biological process, adsorption onto these minerals removes light Mo from solution. Typical isotope enrichment factors are between -2 and -3‰ (Barling et al., 2001, 2004) with isotope fractionation specifically associated with adsorption to Fe (oxyhydr)oxides from -0.8 to 2.2‰ (Goldberg et al., 2009). As the ice breaks up, light is able to penetrate the lake, and the biotic response causes the pH to increase from 8.4 to almost pH 10 at the height of summer (Table 1, Fig. 6). These changes in pH change mineral saturation states, with the carbonate phases that were undersaturated in the winter becoming oversaturated in the summer (Fig. 6). However, little or no δ^{98}Mo fractionation has been observed accompanying abiogenic carbonate formation (Voegelin et al., 2009).

Mn phases (except Birnessite) also reach saturation in the summer, whilst Fe phases remain oversaturated throughout the year (Fig. 6). These phases are associated with δ^{98}Mo fractionation, thus it is possible that during the summer pH peak, the saturation of some Mn phases results in their precipitation and adsorption of light Mo from the dissolved phase. However, although increased pH may facilitate the increased saturation state of these Mn phases, also limits the adsorption of Mo, as several studies have shown that Mo adsorption onto Fe and Mn (oxyhrdr)oxides is at a maximum at low pH (<4) and decreases to negligible levels at the lake pH conditions of 9 and 10 (e.g. Goldberg et al., 1996, Barling et al., 2004; Matern & Mansfeldt 2015). Consequently the precipitation of Fe and Mn (oxyhrdr)oxides is not thought to have driven the observed variations in δ^{98}Mo in Lake Mývatn. This is supported by the fact that secondary phase formation is known to significantly fractionate Li isotopes (Burton and Vigier 2012), thus the negligible variation of δ^{7}Li in the same lake waters (Pogge von Strandmann et al., 2016) supports the hypothesis that secondary phase formation is not a significant controlling factor in the modification of lake water Mo chemistry.

The overlap in timing between mineral saturation and cyanobacteria blooms, and the observation that both of these mechanisms are capable of driving δ^{98}Mo fractionation in the same direction, make it difficult to distinguish these processes based on Mo isotope data alone. However, the high summer pH inhibition of Mo adsorption onto secondary phases and lack of associated δ^{7}Li fractionation in the lake waters give support to biological isotope fractionation playing the dominant role in controlling the δ^{98}Mo composition of the lake.

4.4.3 June Mo concentration peak

The peak in lacustrine Mo concentration (Fig. 3a) suggests an additional source of isotopically light Mo to the lake in June. In shallow lakes such as Mývatn, bottom sediments can play a major role in releasing nutrients to the overlying water column due to wind-induced resuspension, diffusive flux, biological activity, and bioturbation (e.g. Einarsson et al., 2004). Sediment resuspension is known to affect nutrient loading in Lake Mývatn through oxidation and dissolution of said sediments. When wind speeds exceed 8.5 m s^{-1}, the sediment (diatmoaceous gyttja) is prone to resuspension and mobilisation

(Einarsson et al., 2004), exposing it to the oxidising water column and the increased potential for dissolution. Meteorological data provided by the Icelandic Meteorological Office for the weather station at Mývatn shows a strong wind speed peak (>8.5 m s^{-1}) in May 2000. This peak (Fig. 7), capable of disturbing the Mývatn sediments, is coincident with an increase in particulate organic carbon (POC) however, the peak in Mo occurs slightly later than the POC peak.

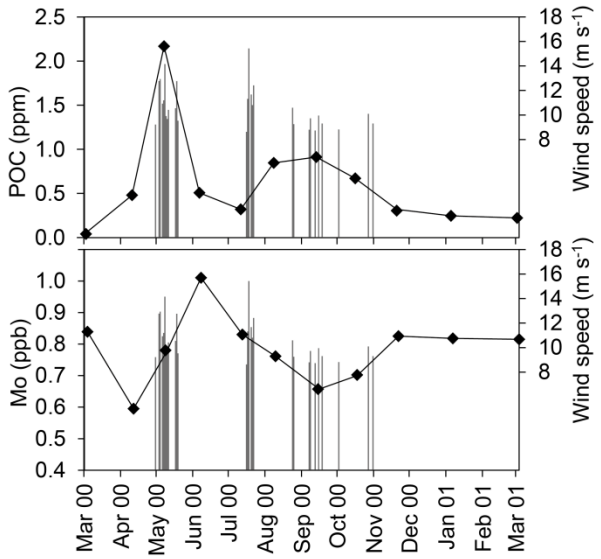

Figure 7: Relating wind speed to potential sediment resuspension events. Mean daily wind speed >8.5 m s^{-1} (the minimum threshold for wind driven resuspension (Einarsson et al., 2004)) is plotted and superimposed are the concentrations for POC (particulate organic carbon) and Mo for the Lake Mývatn outlet. The meteorological data, from the weather station Mývatn, were kindly supplied by the Icelandic Meteorological Office.

If the source of this Mo peak is from the sediments then it is likely associated with sulfides precipitated in the anoxic sediments. The concentration of dissolved S within the pore waters of the bottom sediment of Lake Mývatn is a factor of 20 to 50 lower than in the lake water above, and dissolved Mo is a factor of 2 lower in these interstitial waters (Gislason et al., 2004). This suggests removal of both aqueous S and Mo into sulfides at an early stage of diagenesis under reducing conditions within these sediments. Using the interstitial sediment water data from Gíslason et al. (2004) with the addition of detection limit H_2S (0.01 ppm) due to the observed smell (Thorbersdóttir et al., 2004), it is possible to make an assessment of the mineral saturation state of the sediments. Using the measured Eh to define redox, many sulfide minerals (e.g. molybdenite, pyrite, and chalcopyrite) are supersaturated in the sediment waters (Table ES2). When these sediments are disturbed by the wind-driven resuspension event they are exposed to the oxygenated lake-waters. The resulting oxidation may lead to the dissolution of some minerals rich in Mo, a possible cause of the summer concentration peaks in Mo and other trace metals such as Fe and Al (trace element data in Table ES2 and plots in Eiríksdóttir et al., 2008).

4.4.4 Sulfur isotope variation

Despite the strong case for the direct biological assimilation of Mo controlling the Mo isotope composition of Lake Mývatn, the correlation between the sulfur and molybdenum isotopes may demand an explanation that can account for both datasets. In the case of sulfur, the groundwater input far exceeds the measured sulfate concentration in the lake. Using the same reasoning as for the groundwater Mo, the sulfate input to Lake Mývatn is some 38 ppm (Neely et al., submitted 2017, Chapter 3) whilst the concentration in the lake is, at most, 19.6 ppm (Table 1; Fig. 3a). As such, there must be a large sink of S in the lake. Gislason et al. (2004) demonstrated a diffusive flux from the lake waters to the sediment of 3×10^{-14} mol cm^{-2} s^{-1} however, to account for the discrepancy between the groundwater sulfate input and the lake's concentration, there must be a total net removal of 2×10^{-8} mol cm^{-2} s^{-1}, considerably greater than the suggested diffusive flux. In such a biologically active lake, this sulfate removal is most obviously attributed to either sulfur assimilation and/or bacterial sulfate reduction (BSR). However, the observed sulfate removal is associated with a total S isotope enrichment factor of -3 to -5‰ (i.e. the removed S is isotopically lighter than the residual S in the lake waters). This enrichment factor is considerably less than expected for BSR – typically -10‰ to -30‰ and too high to support assimilation alone, usually -1 to -2 ‰ (Canfield, 2001). The possibility that these two processes are occurring in tandem is therefore considered: that both direct assimilation and bacterial reduction are occurring at the same time with a combined isotopic shift in between the expected enrichment factors. Using a simple box model to test this approach for the lake it was assumed that the enrichment factor for assimilation was -1.5‰ and for BSR, -15‰. For the tandem approach to be true the sulfate removal would have to be dominated by assimilation (potentially associated with the Mo assimilation already demonstrated with Mo isotopes) with a contribution from BSR causing the overall S isotope shift to be more enriched in residual ^{34}S-sulfate than via assimilation alone. The results from this simple box modelling show that to be the case, close to 60% of the sulfate is removed by assimilation and the rest by BSR. Of course, a significant variable in this calculation is the modelled BSR enrichment factor of -15‰, if pushed to still plausible, even lighter values then the proportion removed by assimilation would be even greater.

4.5 Summary & Conclusions

Presented here is a thorough study of Mo geochemistry in the biologically productive Lake Mývatn, Iceland. It contributes to the mounting literature demonstrating the different responses of stable isotopes to biological activity within the lake (fig. 8). Lithium isotopes are not biologically affected (Pogge von Strandmann et al., 2016) whilst Si records the growth and dissolution of diatoms (Opfergelt et al., 2011), and Mo, the cyanobacteria bloom within the lake. Via monitoring and simple numerical modelling of seasonal variations in bulk chemistry, and S and Mo isotopes, a number of lacustrine processes have been explored. Firstly, of note, is the striking correlation between Mo and S isotopes with no covariation in concentrations. Mo is initially diluted by the ice break-up and melting resulting in reduced concentrations. When ice-free, the lake is susceptible to wind-driven sediment resuspension; this is invoked as the cause of a Mo release in June as a result of the reduced sediment sulfides being exposed to the oxygenated lake. However, the major shift in Mo isotopes, from δ^{98}Mo +0.13‰ to +0.5‰ occurs in the late summer

corresponding to a sustained reduction in Mo concentration, from 0.8 ppb to 0.6 ppb, and the onset of the cyanobacteria bloom (known to assimilate and fractionate Mo; Zerkle et al., 2011). Through simple numerical and geochemical modelling the major findings of this work are:

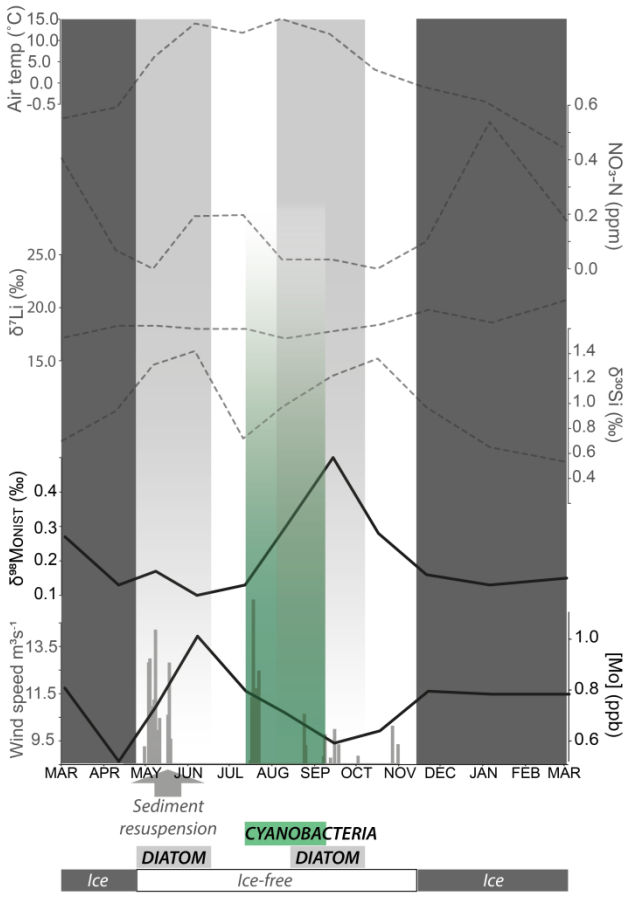

Figure 8: Lake Mývatn composite figure including the new Mo data (heavy black lines) and literature data (grey). Air temperature and NO_3-N are from Eiríksdóttir et al. (2008), Li isotopes from Pogge von Strandmann et al. (2016), and Si isotopes from Opfergelt et al. (2011). The Mo data are from this study and the wind speed data are from the Mývatn weather station, kindly supplied by the Icelandic Meteorological Office. The ice-covered period is blocked out by dark grey whilst the significant biological events are highlighted: two diatom blooms (light grey) and the cyanobacteria bloom (green).

1) The δ^{98}Mo variations at the Lake outlet are best replicated with an enrichment factor of -1.5‰ between the removed material and the residual lake waters. This is attributed to biological fractionation by cyanobacteria, preferentially removing light isotopes at a time of extreme nitrogen limitation. Given the complex nature of this natural system this enrichment factor agrees remarkably well with those measured in laboratory settings for cyanobacteria (-0.9‰; Zerkle et al., 2011).

2) Abiotic processes, such as adsorption onto Fe-Mn (oxyhydr)oxides, are rejected as controlling Mo isotope fractionation in Lake Mývatn. Due to the high lacustrine pH, the adsorption of Mo onto secondary phases is inhibited and, in addition, no significant changes in δ^7Li were recorded (Pogge von Strandmann et al., 2016) as would be expected with secondary phase formation.

3) These observations are the first time that the biological fractionation of Mo isotopes has been documented in a natural aqueous environment. It is possible that marine N_2-fixing cyanobacteria could produce similar scale δ^{98}Mo fractionations as they use proteins homologous to the freshwater organisms (Zerkle et al., 2011). If these fractionations are recorded in sediments then the implications could be two-fold. Firstly, as these fractionations are of a similar magnitude to those produced in other sedimentary settings, biological fractionations may need to be considered when interpreting δ^{98}Mo variations observed in the sedimentary record. Secondly, within lake sediments they may be useful additional proxies for paleolimnology studies.

References

ADALSTEINSSON, H. 1979. Zooplankton and Its Relation to Available Food in Lake Mývatn. Oikos, 32, 162-194.

ANDERSSON, P. S., TORSSANDER, P. & INGRI, J. Sulfur isotope ratios in sulfate and oxygen isotopes in water from a small watershed in Central Sweden. Hydrobiologica 235/236, 205–217 (1992).

ARNÓRSSON, S. & ÍVARSSON, G. 1985. Molybdenum in Icelandic geothermal waters. Contributions to Mineralogy and Petrology, 90, 179-189.

BARLING, J., ARNOLD, G. L. & ANBAR, A. D. 2001. Natural mass-dependent variations in the isotopic composition of molybdenum. Earth and Planetary Science Letters, 193, 447-457.

BARLING, J. & ANBAR, A. D. 2004. Molybdenum isotope fractionation during adsorption by manganese oxides. Earth and Planetary Science Letters, 217, 315-329.

BARRON, A. R., WURZBURGER, N., BELLENGER, J. P., WRIGHT, S. J., KRAEPIEL, A. M. L. & HEDIN, L. O. 2009. Molybdenum limitation of asymbiotic nitrogen fixation in tropical forest soils. Nature Geosci, 2, 42-45.

BELLENGER, J. P., WICHARD, T., XU, Y. & KRAEPIEL, A. 2011. Essential metals for nitrogen fixation in a free-living N2-fixing bacterium: chelation, homeostasis and high use efficiency. Environmental microbiology, 13, 1395-1411.

BORTELS, H. 1930. Molybdän als Katalysator bei der biologischen Stickstoffbindung. Archiv für Mikrobiologie, 1, 333-342.

BURTON, K. W. & VIGIER, N. 2012. Lithium Isotopes as Tracers in Marine and Terrestrial Environments. In: BASKARAN, M. (ed.) Handbook of Environmental Isotope Geochemistry: Vol I. Berlin, Heidelberg: Springer Berlin Heidelberg.

CANFIELD, D. 2001. Biogeochemistry of sulfur isotopes. In: Valley, J.W. and Cole D.R. (Eds), Stable isotope geochemistry, vol 43, Mineralogical Society of America, pp. 607-636.

EINARSSON, Á., STEFÁNSDÓTTIR, G., JÓHANNESSON, H., ÓLAFSSON, J. S., GÍSLASON, G. M., WAKANA, I., GUDBERGSSON, G. & GARDARSSON, A. 2004. The ecology of Lake Myvatn and the River Laxá: variation in space and time. Aquatic Ecology, 38, 317-348.

EIRÍKSDÓTTIR, E. S., GÍSLASON, S. R., ELEFSEN, S. Ó., HARÐARDÓTTIR, J., HREINSSON, E. Ö., TORSSANDER, P. & SVEINBJÖRNSDÓTTIR, Á. E. 2008. Efnasamsetning, rennsli og aurburður í útfalli Mývatns (Chemical composition, discharge, and suspended load of the lake Mývatn outflow). Náttúrurannsóknastöð við Mývatn.

ERICKSON, B. E. & HELZ, G. R. 2000. Molybdenum(VI) speciation in sulfidic waters: Stability and lability of thiomolybdates. Geochimica et Cosmochimica Acta, 64, 1149-1158.

FRAUSTO DA SILVA, J.J.R., WILLIAMS, R.J.P. 2001. The Biological Chemistry of the Elements. Oxford University Press, New York.

GÍSLASON, S. R., EIRÍKSDÓTTIR, E. S. & OLAFSSON, J. S. 2004. Chemical composition of interstitial water and diffusive fluxes within the diatomaceous sediment in Lake Myvatn, Iceland. Aquatic Ecology, 38, 163-175.

GLASS, J. B., AXLER, R. P., CHANDRA, S. & GOLDMAN, C. R. 2012. Molybdenum limitation of microbial nitrogen assimilation in aquatic ecosystems and pure cultures. Frontiers in microbiology, 3.

GOLDBERG, S., FORSTER, H. S. & GODFREY, C. L. 1996. Molybdenum Adsorption on Oxides, Clay Minerals, and Soils. Soil Science Society of America Journal, 60, 425-432.

GOLDBERG, T., GORDON, G., IZON, G., ARCHER, C., PEARCE, C. R., MCMANUS, J., ANBAR, A. D. & REHKÄMPER, M. 2013. Resolution of inter-laboratory discrepancies in Mo isotope data: an intercalibration. Journal of Analytical Atomic Spectrometry, 28, 724-735.

GOLDMAN, C. R. 1960. Molybdenum as a factor limiting primary productivity in Castle Lake, California. Science, 132, 1016-1017.

GREBER, N. D., SIEBERT, C., NÄGLER, T. F. & PETTKE, T. 2012. δ98/95Mo values and Molybdenum Concentration Data for NIST SRM 610, 612 and 3134: Towards a Common Protocol for Reporting Mo Data. Geostandards and Geoanalytical Research, 36, 291-300.

JÓNASSON, P. M. 1979. The Lake Mývatn Ecosystem, Iceland. Oikos, 32, 289-305.

JÓNASSON, P. M. & ADALSTEINSSON, H. 1979. Phytoplankton Production in Shallow Eutrophic Lake Mývatn, Iceland. Oikos, 32, 113-138.

KENDALL, B., DAHL, T., ANABAR, A. 2016. Good Golly, Why Moly? The Stable Isotope Geochemistry of Molybdenum, Reviews in Mineralogy and Geochemistry, 82, 683-732.

KING, E. K., THOMPSON, A., CHADWICK, O. A. & PETT-RIDGE, J. C. Molybdenum sources and isotopic composition during early stages of pedogenesis along a basaltic climate transect. Chemical Geology.

KRISTMANNSDÓTTIR, H. & ÁRMANNSSON, H. 2004. Groundwater in the Lake Myvatn area, northern Iceland: Chemistry, origin and interaction. Aquatic Ecology, 38, 115-128.

LIERMANN, L. J., GUYNN, R. L., ANBAR, A. & BRANTLEY, S. L. 2005. Production of a molybdophore during metal-targeted dissolution of silicates by soil bacteria. Chemical Geology, 220, 285-302.

MATERN, K. & MANSFELDT, T. 2015. Molybdate adsorption by birnessite. Applied Clay Science, 108, 78-83.

MILLER, C. A., PEUCKER-EHRENBRINK, B., WALKER, B. D. & MARCANTONIO, F. 2011. Re-assessing the surface cycling of molybdenum and rhenium. Geochimica et Cosmochimica Acta, 75, 7146-7179.

NÄGLER, T.F., MILLS M.M., SIEBERT, C. 2004 Biological fractionation of Mo isotopes duringN2 fixation by Trichodesmium sp. IMS 101. Geochimica et Cosmochimica Acta, 68, A364.

NEELY, R.A., GISLASON, S.R., ÓLAFSSON, M., MCCOY-WEST, A.J., PEARCE, C.R., BURTON, K.W., SUBMITTED 2017. Molybdenum isotope behaviour in groundwaters and terrestrial hydrothermal systems, Iceland. Submitted to EPSL

ÓLAFSSON, J. 1979. The Chemistry of Lake Mývatn and River Laxá. Oikos, 32, 82-112.

ÓLAFSSON, J. S. & PATERSON, D. M. 2004. Alteration of biogenic structure and physical properties by tube-building chironomid larvae in cohesive sediments. Aquatic Ecology, 38, 219-229.

ÓLAFSSON, M., FRIDRIKSSON, T., HAFSTAD, T. H., GYLFADÓTTIR, S. S., ÓSKARSSON, F. & ÁRMANNSSON, H. The Groundwater in the Mývatn Area: Influence of Geothermal Utilization at Námafjall and Origin of the Warm Groundwater Component. World Geothermal Congress 2015, 19-25 April 2015 2015 Melbourne, Australia.

OPFERGELT, S., EIRIKSDOTTIR, E., BURTON, K., EINARSSON, A., SIEBERT, C., GISLASON, S. & HALLIDAY, A. 2011. Quantifying the impact of freshwater diatom productivity on silicon isotopes and silicon fluxes: Lake Myvatn, Iceland. Earth and Planetary Science Letters, 305, 73-82.

PARKHURST, D.L., & APPELO, C.A.J., 2013, Description of input and examples for PHREEQC version 3—A computer program for speciation, batch-reaction, one-dimensional transport, and inverse geochemical calculations: U.S. Geological Survey Techniques and Methods, book 6, chap. A43, 497 p., available only at https://pubs.usgs.gov/tm/06/a43/.

PEARCE, C. R., COHEN, A. S. & PARKINSON, I. J. 2009. Quantitative Separation of Molybdenum and Rhenium from Geological Materials for Isotopic Determination by MC-ICP-MS. Geostandards and Geoanalytical Research, 33, 219-229.

POGGE VON STRANDMANN, P. A. E., BURTON, K. W., OPFERGELT, S., EIRÍKSDÓTTIR, E. S., MURPHY, M. J., EINARSSON, A. & GISLASON, S. R. 2016. The effect of hydrothermal spring weathering processes and primary productivity on lithium isotopes: Lake Myvatn, Iceland. Chemical Geology.

SCHWARZ, G., MENDEL, R. R. & RIBBE, M. W. 2009. Molybdenum cofactors, enzymes and pathways. Nature, 460, 839-847.

SIEBERT, C., NÄGLER, T. F., VON BLANCKENBURG, F. & KRAMERS, J. D. 2003. Molybdenum isotope records as a potential new proxy for paleoceanography. Earth and Planetary Science Letters, 211, 159-171.

SILVESTER, W. B. 1989. Molybdenum limitation of asymbiotic nitrogen fixation in forests of Pacific Northwest America. Soil Biology and Biochemistry, 21, 283-289.

STIEFEL, E. I. 1997. Chemical keys to molybdenum enzymes*. Journal of the Chemical Society, Dalton Transactions, 3915-3924.

STUEKEN, E. E., BUICK, R., GUY, B. M. & KOEHLER, M. C. 2015. Isotopic evidence for biological nitrogen fixation by molybdenum-nitrogenase from 3.2 Gyr. Nature, 520, 666-669.

THORBERGSDÓTTIR, I. M. & GÍSLASON, S. R. 2004a. Internal loading of nutrients and certain metals in the shallow eutrophic Lake Myvatn, Iceland. Aquatic Ecology, 38, 191-208.

THORBERGSDÓTTIR, I. M., GÍSLASON, S. R., INGVASON, H. R. & EINARSSON, A. 2004b. Benthic oxygen flux in the highly productive subarctic Lake Myvatn, Iceland: In situ benthic flux chamber study. Aquatic Ecology, 38, 177-189.

THORDARSON, T. & LARSEN, G. 2007. Volcanism in Iceland in historical time: Volcano types, eruption styles and eruptive history. Journal of Geodynamics, 43, 118-152.

VOEGELIN, A. R., NÄGLER, T. F., SAMANKASSOU, E. & VILLA, I. M. 2009. Molybdenum isotopic composition of modern and Carboniferous carbonates. Chemical geology, 265, 488-498.

WASYLENKI, L., ANBAR, A., LIERMANN, L., MATHUR, R., GORDON, G. & BRANTLEY, S. 2007. Isotope fractionation during microbial metal uptake measured by MC-ICP-MS. Journal of Analytical Atomic Spectrometry, 22, 905-910.

WASYLENKI, L. E., WEEKS, C. L., BARGAR, J. R., SPIRO, T. G., HEIN, J. R. & ANBAR, A. D. 2011. The molecular mechanism of Mo isotope fractionation during adsorption to birnessite. Geochimica et Cosmochimica Acta, 75, 5019-5031.

WIEDERHOLD, J. G. 2015. Metal Stable Isotope Signatures as Tracers in Environmental Geochemistry. Environmental Science & Technology, 49, 2606-2624.

ZERKLE, A., SCHEIDERICH, K., MARESCA, J., LIERMANN, L. & BRANTLEY, S. 2011. Molybdenum isotope fractionation by cyanobacterial assimilation during nitrate utilization and N2fixation. Geobiology, 9, 94-106.

Acknowledgements

Geoff Nowell, in particular, is thanked for his generous help in the preparation and isotopic analysis of the samples and Chris Ottley for assistance with ICP-MS analysis. We acknowledge financial support from Initial Training Network, MetTrans, grant number 290336 from the European Research Council and thank the Icelandic Meteorological Office who kindly supplied the meteorological data from the weather station at Mývatn

Author contributions

K.W.B., R.A.N., and S.R.G., conceived the project. Samples were collected by E.S.E. Sulfur isotope analyses were coordinated by P.T. and C-M.M. whilst Mo isotopes were analysed by R.A.N. with some assistance from C.R.P. Data interpretation and writing was led by R.A.N. with significant inputs from C-M.M. for S-isotopes.

Electronic supplement information

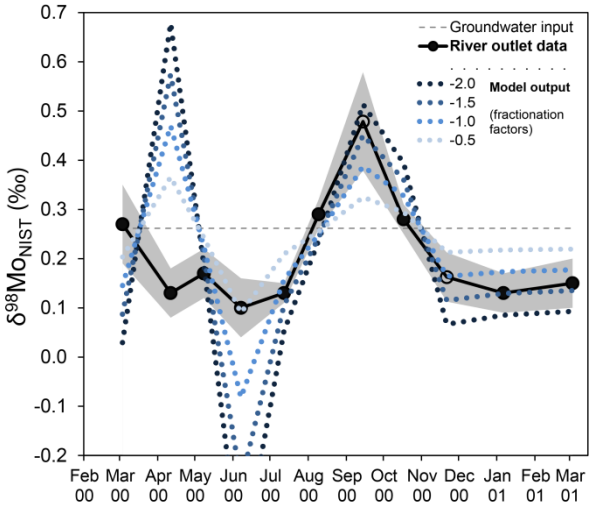

Figure ES1: The model output before the April snow-melt and subsequent dilution has been taken into account. Therefore, this model output demonstrates the big discrepancy between the measured data (black) and the model output (blue dotted lines) in April 2000.

Table ES1: Table ES1: Complete dissolved and suspended element data for the Lake Mývatn outlet at Geirastaðaskurður

EIRÍKSDÓTTIR, E. S., GÍSLASON, S. R., ELEFSEN, S. Ó., HARÐARDÓTTIR, J., HREINSSON, E. Ö., TORSSANDER, P. & SVEINBJÖRNSDÓTTIR, Á. E. 2008. Efnasamsetning, rennsli og aurburður í útfalli Mývatns (Chemical composition, discharge, and suspended load of the lake Mývatn outflow). Náttúrurannsóknastöð við Mývatn.

Table ES2: Calculated saturation state for the outlet waters. Calculated in PHREEQC with O2 saturation

Table ES3: Saturation state of sediment interstitial waters from Gislason et al., 2004. Redox set by sulfur speciation

GÍSLASON, S. R., EIRÍKSDÓTTIR, E. S. & OLAFSSON, J. S. 2004. Chemical composition of interstitial water and diffusive fluxes within the diatomaceous sediment in Lake Myvatn, Iceland. Aquatic Ecology, 38, 163-175.

Table ES1: Complete dissolved and suspended element data for the Lake Mývatn outlet at Geirastaðaskurður

Sample	Date	Time	Water temp	Air temp	measured pH	Ref. Temp	Conductivity	SiO2	Na	K	Ca	Mg
			°C	°C		T °C	µS/sm	mmol/kg	mmol/kg	mmol/kg	mmol/kg	mmol/kg
00-A013	03/03/2000	13:15	1.2	-8.3	8.14	19.1	171.4	0.384	1.005	0.040	0.196	0.164
00-A023	11/04/2000	11:30	0.0	-5.7	8.69	21.9	139.4	0.260	0.779	0.029	0.158	0.147
00-A031	08/05/2000	19:57	6.0	6.0	8.31	22.6	134.5	0.174	0.753	0.028	0.149	0.132
00-A044	07/06/2000	15:00	12.3	14.0	9.45	25.0	158.2	0.091	0.879	0.031	0.176	0.154
00-A053	12/07/2000	17:00	15.7	11.8	9.86	20.7	163.1	0.040	0.953	0.034	0.176	0.144
00-A062	09/08/2000	16:15	15.5	15.1	9.67	23.4	176.5	0.077	1.035	0.040	0.202	0.165
00-A071	14/09/2000	15:00	8.3	11.5	9.15	22.4	160.6	0.079	0.940	0.037	0.178	0.154
00-A080	17/10/2000	15:15	1.4	3.1	8.43	22.9	158.7	0.146	0.953	0.038	0.184	0.156
00-A089	21/11/2000	14:45	0.6	-0.9	8.08	20.6	165.5	0.276	0.970	0.039	0.193	0.156
01-A006	06/01/2001	10:00	0.9	-4.4	8.11	19.4	158.9	0.374	0.974	0.036	0.189	0.159
01-A015	03/03/2001	09:05	0.5	-15.0	8.18	20.0	139.2	0.318	0.883	0.035	0.159	0.141

Sample	Alk	DIC	SO4	δ34S	Cl	F	TDS	DOC	POC	PON	C/N	P	PO4-P
	meq./kg	mmol/kg	mmol/kg	‰	mmol/kg	µmol/kg	mg/kg	mmol/kg	µg/kg	µg/kg	mol	µmol/kg	µmol/kg
00-A013	1.342	1.368	0.204	3.37	0.111	14.32	162	0.017	42	<1.5	32.7	1.550	1.32
00-A023	1.107	1.123	0.129	2.22	0.104	11.68	128	0.025	482	53.1	10.6	0.946	0.815
00-A031	1.049	1.067	0.147	2.02	0.088	10.53	118	0.042	2171	356.8	7.10	0.620	0.349
00-A044	1.190	1.322	0.174	1.67	0.101	13.53	136	0.075	509	74.4	7.98	0.339	0.283
00-A053	1.252	1.618	0.163	2.2	0.098	13.34	149	0.175	322	37.6	10.0	0.859	0.544
00-A062	1.358	1.614	0.183	3.43	0.111	13.84	158	0.117	848	140.4	7.05	0.694	0.268
00-A071	1.277	1.348	0.162	4.64	0.102	8.58	137	0.075	915	152.1	7.02	0.465	0.283
00-A080	1.246	1.267	0.128	2.85	0.095	12.12	136	0.050	673			0.252	0.123
00-A089	1.313	1.343	0.149	2.35	0.099	13.45	152	0.027	307	37.2	9.61	0.613	0.549
01-A006	1.298	1.325	0.151	2.44	0.091	12.61	154	<0.008	247	46.5	6.21	1.498	1.33
01-A015	1.194	1.216	0.119	2.29	0.082	12.50	137	0.023	225	30.2	8.68	1.456	1.46

Table ES1: Complete dissolved and suspended element data for the Lake Mývatn outlet at Geirastaðaskurður

Sample	NO3-N	NO2-N	NH4-N	Ntot	Ptot	Al	Fe	B	Mn	Sr	As	Ba	Cd
	µmol/kg	µmol/kg	µmol/kg	µmol/kg	µmol/kg	µmol/kg	µmol/kg	µmol/kg	µmol/kg	µmol/kg	nmol/kg	nmol/kg	nmol/kg
00-A013	2.06	0.052	3.803	4.60	1.361	0.330	0.412	2.960	0.080	0.118	<0.294	1.755	0.015
00-A023	0.35	0.049	<0.200	6.65	0.784	0.326	0.394	1.166	0.024	0.091	<3.03	1.820	0.041
00-A031	<0.15	0.071	0.995	4.60	0.495	0.302	0.328	1.258	0.013	0.079	<2.18	2.046	0.037
00-A044	0.98	0.039	0.299	5.07	0.289	0.404	0.247	1.452	0.009	0.096	<2.46	2.235	0.033
00-A053	1.01	0.050	0.490	10.21	0.697	1.08	0.283	2.683	0.016	0.100	<0.133	0.998	0.017
00-A062	0.17	0.086	<0.200	11.05	0.646	0.486	0.636	2.868	0.026	0.109	0.574	1.471	0.030
00-A071	0.17	<0.04	<0.200	8.03	1.004	0.261	0.408	2.914	0.010	0.095	<0.133	1.740	0.015
00-A080	<0.15	0.056	<0.200	4.27	0.222	0.150	0.184	2.646	0.004	0.098	<0.133	1.886	0.012
00-A089	0.51	0.067	0.624	3.82	0.598	0.178	0.217	2.775	0.023	0.101	<0.133	1.886	0.015
01-A006	2.75	0.072	1.324	3.59	1.376	0.467	0.519	2.525	0.059	0.095	<0.133	1.522	<0.009
01-A015	0.89	0.062	1.961	5.45	1.472	0.378	0.491	1.776	0.065	0.081	<0.133	0.990	<0.009

Sample	Co	Cr	Cu	Ni	Pb	Zn	Hg	Mo	Ti
	nmol/kg	nmol/kg	nmol/kg	nmol/kg	nmol/kg	nmol/kg	nmol/kg	nmol/kg	nmol/kg
00-A013	0.166	23.7	4.17	2.39	0.068	3.64	<0.011	8.75	2.67
00-A023	0.339	19.0	10.86	3.12	0.187	25.08	<0.011	6.20	5.58
00-A031	0.490	14.3	6.07	4.96	0.192	20.65	<0.011	8.13	8.77
00-A044	0.591	11.19	9.19	2.91	0.132	10.15	<0.011	10.53	9.48
00-A053	1.013	10.7	9.74	3.07	0.097	11.45	<0.011	8.65	15.64
00-A062	0.784	8.15	7.54	2.73	0.074	3.61	<0.011	7.93	12.13
00-A071	0.550	7.10	6.14	2.18	0.087	4.66	<0.011	6.85	10.67
00-A080	0.321	10.3	4.61	3.17	0.040	3.38	<0.011	7.32	3.34
00-A089	0.246	12.9	4.12	2.62	0.068	4.95	<0.011	8.60	3.40
01-A006	0.112	22.9	5.40	2.27	0.068	6.16	<0.011	8.53	1.80
01-A015	0.112	21.3	3.15	6.56	0.043	1.16	<0.011	8.49	2.40

Table ES1: Complete dissolved and suspended element data for the Lake Mývatn outlet at Geirastaðaskurður

Sample	[a] Si	[a] δ^{30}Si	[a] 2SD	[a] n	[b] Li	[b] δ^{7}Li	[b] 2SD
	mM	‰			nM	‰	
00-A013	0.41	0.70	0.08	9	180	17.2	0.8
00-A023	0.30	0.94	0.07	9	137	18.3	0.3
00-A031	0.22	1.31	0.07	9	177	18.3	0.7
00-A044	0.10	1.42	0.06	9	146	18.0	0.5
00-A053	0.05	0.72	0.09	9	237	18.0	0.3
00-A062	0.09	0.97	0.03	9	167	17.1	0.2
00-A071	0.10	1.22	0.12	9	217	17.8	0.5
00-A080	0.16	1.36	0.08	9	155	18.4	0.1
00-A089	0.31	0.97	0.15	9	116	19.8	0.2
01-A006	0.41	0.65	0.12	9	153	18.6	0.2
01-A015	0.34	0.53	0.17	9	236	20.8	0.6

a – From Opfergelt et al., 2011

b – from Pogge von Strandmann et al., 2016

Table ES2: Calculated saturation state for the outlet waters. Calculated in PHREEQC with O_2 saturation

	Manganese (oxyhydr)oxides				Iron oxyhydr(oxides)			
Sample	Birnessite	Bixbyite	Hausmannite	Manganite	Maghemite	Ferrihydrite	Goethite	Lepidocrocite
In equilibrium with atmospheric O2								
00-A013	-10.78	-11.37	-14.02	-3.42	6.31	2.04	4.94	4.98
00-A023	-8.82	-8.83	-10.77	-2.00	5.83	1.74	4.65	4.74
00-A031	-10.61	-10.91	-13.77	-3.74	6.11	2.18	5.04	4.88
00-A044	-5.86	-3.13	-3.59	-0.55	4.22	1.54	4.34	3.93
00-A053	-4.21	-0.17	0.37	0.56	3.75	1.46	4.23	3.70
00-A062	-4.61	-0.70	-0.27	0.32	4.74	1.95	4.72	4.19
00-A071	-7.24	-5.65	-6.84	-1.37	5.23	1.85	4.68	4.43
00-A080	-10.67	-11.82	-15.06	-3.66	5.55	1.67	4.56	4.59
00-A089	-11.62	-12.97	-16.33	-4.14	5.72	1.71	4.61	4.68
01-A006	-11.10	-11.95	-14.83	-3.67	6.49	2.12	5.01	5.07
01-A015	-10.68	-11.35	-14.00	-3.32	6.49	2.10	5.00	5.07

	Carbonates			
Sample	Dolomite D	Dolomite O	Calcite	Aragonite
In equilibrium with atmospheric O2				
00-A013	-3.35	-2.7	-1.2	-1.44
00-A023	-2.15	-1.49	-0.61	-0.85
00-A031	-2.28	-1.65	-0.72	-0.95
00-A044	-0.26	0.35	0.22	0.01
00-A053	0.36	0.95	0.51	0.31
00-A062	0.42	1.01	0.54	0.34
00-A071	-0.75	-0.13	0.02	-0.2
00-A080	-2.39	-1.74	-0.72	-0.96
00-A089	-3.38	-2.72	-1.2	-1.44
01-A006	-3.38	-2.72	-1.21	-1.45
01-A015	-3.38	-2.72	-1.21	-1.46

Table ES3: Saturation state of sediment interstitial waters from Gislason et al., 2004. Redox set by sulfur speciation

	Sulphides			Manganese (oxyhydr)oxides					
Sample	Molybdenite MoS_2	Pyrite FeS_2	Chalcopyrite $CuFeS_2$	Birnessite	Bixbyite	Hausmannite	Ferrihydrite	Goethite	Lepidocrocite
Interstital waters - Addition of DL H2S, redox defined by S species									
98-M004	12.81	6.54	12.49	-27.7	-25.95	-28.15	-3.68	-0.94	-1.66
98-M003	13.57	7.04	12.17	-27.74	-26.08	-28.31	-3.67	-0.93	-1.62
98-M002	13.21	6.37	11.55	-27.48	-25.47	-27.35	-3.91	-1.17	-1.86
98-M001	13.05	6.82	12.12	-27.49	-25.46	-27.32	-3.54	-0.8	-1.5

5 Molybdenum isotope fractionation in hydrothermal systems: phase segregation and subsequent vapour transport

Rebecca A. Neely[1], Sigurdur R. Gislason[1], ISOR[2], Christopher R. Pearce[3], Kevin W. Burton[4]

[1]Institute of Earth Science, University of Iceland, Sturlugata 7, 101 Reykjavík, Iceland

[2] ÍSOR, Iceland GeoSurvey, Orkugardur, Grensásvegur 9, IS-109, Reykjavík, Iceland

[3]National Oceanography Centre Southampton, University of Southampton Waterfront Campus, European Way, Southampton, SO14 3ZH, UK.

[4]Department of Earth Sciences, Durham University, Science Labs, Durham DH1 3LE, UK

Molybdenite deposits are economically significant and geologically interesting as they can be invoked as an indicator of the average continental input to the oceans. Numerous studies have shown that molybdenites (MoS_2) possess highly diverse Mo isotope compositions, from δ^{98}Mo -1.6‰ to +2.3‰ (see Breillat et al., 2016). Studies attribute this variation to: temperature, fractional crystallisation, variations in source magma and redox conditions, and vapour phase formation and transport. Whilst experimental and field studies have been made on Mo concentration and speciation in the vapour phase, none have directly measured the Mo isotope composition of vapour, despite it being considered a fluid capable of transporting significant quantities of ore components in its own right. Here we present data for the Mo composition of the vapour phase, and corresponding liquid phase, for four geothermal fields in Iceland. One, Reykjanes, is recharged by seawater; one is recharge by a 2:1 seawater-meteoric mix (Svartsengi); and the final two are meteoric in origin (Krafla and Námafjall). The vapour phase contains up to 3 ppb Mo and is isotopically lighter than the corresponding liquid. The reservoirs show a large variation in isotopic composition $\delta^{98}Mo_{LIQUID}$ +0.1‰ to +2.9‰ whilst the range is reduced in the vapour: $\delta^{98}Mo_{VAPOUR}$ -0.4‰ to +0.7‰. Rayleigh fractionation is used to model the evolution of the fluids through progressive phase segregation with the measured fractionation factors from $\varepsilon_{V\text{-}L}$ 0.2 to -2.92. The theoretical compositions of molybdenites precipitating from these fluids encompass the entire range of measured Mo isotope compositions for MoS_2 but are more easily formed from the high salinity seawater fluids than from the dilute fluids which require more than 50% vapour formation before reasonable molybdenite compositions are achieved.

5.1 Introduction

Molybdenite (MoS_2) is the most significant host of molybdenum in the Earth's crust and an important ore mineral (e.g. Wang et al., 2016), containing approximately 60% Mo by weight (e.g. Kendall et al., 2016). As the only economically viable mineral source of Mo, molybdenite deposits are clearly of economic significance (e.g. Greber et al., 2011; Breillat et al., 2016) utilised in a variety of applications from alloying steel to increase its strength through to its addition to fertiliser as an essential micronutrient. Multiple studies have shown that molybdenites possess large variations in Mo isotope composition (e.g. Wieser et al., 2003; Hannah et al., 2007; Mathur et al 2010; Greber et al., 2011, 2014: Shafiei et al., 2015; Wang et al., 2016; Yao et al., 2016), from δ^{98}Mo -1.6‰ to +2.3‰ with a mean of 0.04±1.04‰ as summarised in Breillat et al. (2016). These large variations occur at every scale: within single deposits, outcrops, hand specimens, and individual minerals (Greber et al., 2014). The cause of these variations has been attributed to a number of processes: temperature (see Breillat et al., 2016), fractional crystallisation (Hannah et al., 2007; Greber et al., 2014), variations in source magma and redox conditions (Greber et al., 2014; Greber et al., 2011; Mathur et al., 2010; Wang et al., 2016); and vapour phase formation and transport (Shafiei et al., 2015; Yao et al., 2016).

Porphyry deposits, specifically, are significant molybdenite sources and alone demonstrate large Mo isotope variations: from δ^{98}Mo -1.0 to +1.0‰ (compiled in Breillat et al., 2016). These systems can be approximated to fossilised versions of modern-day hydrothermal and geothermal systems (e.g. Henley & Ellis 1983) and as such, the study of these accessible hydrothermal fluids, used as analogues, can inform our interpretation of exhumed ore deposits (e.g. Karingithi et al., 2010). And, whilst molybdenite has not been found in active geothermal systems in Iceland it is known to occur in some New Zealand geothermal systems and has been identified in hydrothermally altered Tertiary basalt formations at Reydarfirtindur in southeast Iceland (Arnórrsson & Ívarsson 1985)

This study is focussed on the role played by vapour in the transport of Mo. The aqueous-vapour phase is a common state of crustal fluids, and boiling and vapour–liquid separation are ubiquitous phenomena occurring during the formation of a wide range of metal ore types, from porphyry to epithermal (see Pokrovski et al., 2008). Indeed, early work by Henley and McNabb (1978) proposed a vapour plume as a transport medium for the metals in porphyry-type deposits. However, historically it has generally been assumed that metals concentrate in the dense liquid phase and that boiling promotes the partitioning of volatiles alone. However, Barnes (2015) and references therein highlight the increasing body of evidence that metal solubility in gases in epithermal and porphyry ores is sufficient for significant vapour transport of Ag, Au, As, Cu, and Mo (e.g. Kouzmanov & Pokrovski 2012). The vapour phase is now viewed as a fluid capable of transporting important quantities of ore components in its own right (Heinrich et al., 1999).

For Mo specifically, a number of experimental studies have shown that metal species are stable in aqueous vapours and that, in all cases, metal solubility is orders of magnitude higher than that predicted from volatility data (e.g. Rempel et al., 2006, 2008; Hurtig & Williams-Jones, 2014). This is supported by both modelling (Hurtig & Williams-Jones, 2015) and field studies investigating the concentrations of metals in the vapour phase of

fluid inclusions (e.g. Heinrich et al., 1992, 1999) and fumarolic condensates (e.g. Williams-Jones & Heinrich., 2005). Whilst it is now well established that the vapour phase can play a significant role in the concentration of metals in economic deposits it is not yet clear how it may affect Mo isotope compositions.

In this study, both liquid- and vapour- phase fluids are sampled from four geothermal systems in Iceland: Reykjanes, Svartsengi, Námafjall (Bjarnarflag field), and Krafla (the Leirbotnar and Hvíthólar fields). The location of these areas can be seen in figure 1. All of these areas have been exploited for geothermal power; HS Orka runs Reykjanes (100 MW) and Svartsengi (75 MW) power plants whilst Landsvirkjun operates Bjarnarflag (3 MW) and Krafla (60 MW) plants.

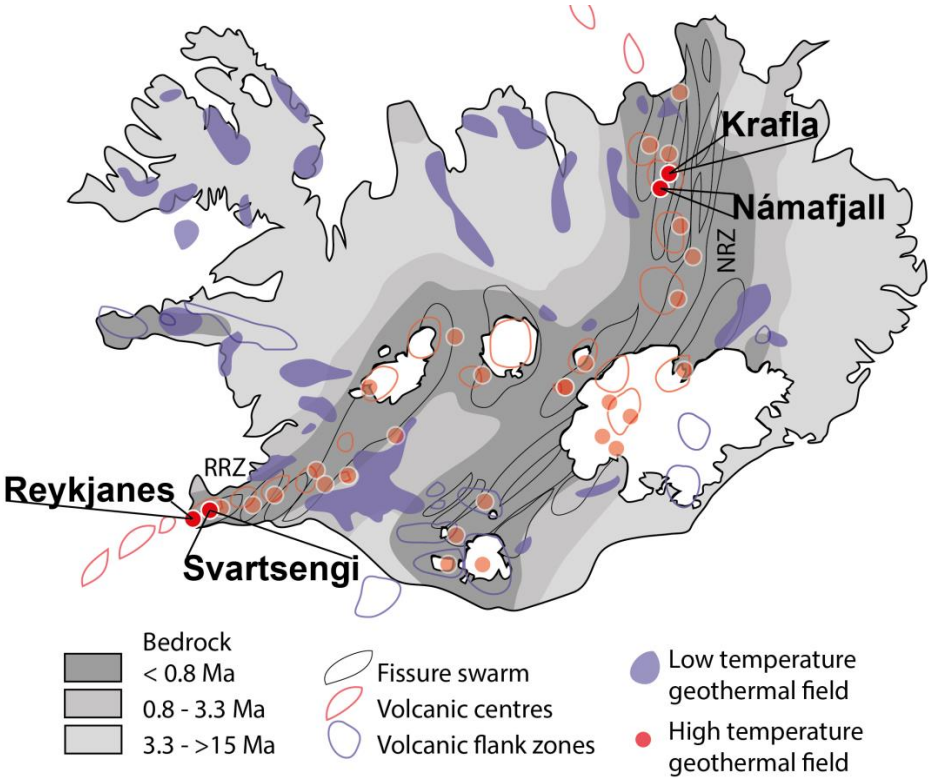

Figure 1: Map locating the four geothermla systems in Iceland in relation to major volcanic features. Reykjanes and Svartsengi are located in the Reykjanes rift zone (RRZ), which when off-shore forms the Reykjanes ridge, part of the mid-Atlanitc ridge. Krfla and Námafjall are located in the nortehrn rizt zone (NRZ)

5.1.1 Geological setting

The Icelandic basalt plateau rises ~3000 m above the surrounding seafloor and is situated at the junction of the Mid-Atlantic Ridge (MAR) and the Greenland-Iceland-Faroe ridge. It is thought to result from the interaction between the Mid-Atlantic Ridge and a deep mantle plume. There are 20 known, active, high-temperature geothermal areas in Iceland and another eight potential areas, all located in the active volcanic zone (Arnórsson 1995).

The Reykjanes Ridge, part of the MAR-system, lies south west of Iceland and extends on shore at the south western tip of the Reykjanes Peninsula (Fridriksson et al., 2006). The Reykjanes and Svartsengi geothermal areas lie within this volcanic system (Jakobsson et al., 1978), at the south western tip of the Reykjanes Peninsula (Fig. 1). As a seawater-recharged hydrothermal system, Reykjanes can be considered as analogous to seafloor hydrothermal systems with respect to host rock type and low water/rock interaction (Hjardardóttir et al., 2010; Marks et al., 2010), whilst Svartsengi is a mixed reservoir, approximately one third meteoric and two thirds seawater (Ragnarsdóttir et al., 1984). The Reykjanes Peninsula comprises young, highly permeable basalt formations and is tectonically active, transected by an intense NE-SW fault zone (Björnsson et al., 1970). As a volcanic system it is characterised by oblique extensional tectonics and episodic fissure eruptions (Jakobsson et al., 1978; Thordarson and Larsen, 2007). Heat is provided to the geothermal systems of the Reykjanes Peninsula via dikes intruded at depth as the area lacks the central volcanoes more often associated with geothermal activity in Iceland (Gudmundsson & Thórhallsson, 1968; Gudmundsson, 1995).

Whilst both Reykjanes and Svartsengi are recharged by seawater and a seawater/meteoric mix, both Krafla and Námafjall geothermal systems are recharged with meteoric water alone. The Krafla geothermal area is located within the caldera of the active Krafla central volcano in the neovolcanic zone of axial rifting in N-Iceland (Fig. 1). The main fissure swarm that intersects the Krafla caldera formed approximately 100 ka. It is 5-8 km in width and some 100 km long. Postglacial volcanism in the region has been divided into two periods. The first ended some 8 ka whilst the second period started approximately 3 ka and is ongoing. A major, modern, volcanic-rifting episode of the Krafla system started 20th December 1975; nine volcanic eruptions occurred over the subsequent nine years with the last in September 1984. The Krafla geothermal system is a high-temperature geothermal field with an aerial extent of approximately 7 km^2 (Thórarinsson, 1980) whilst surface features such as fumaroles and ground alterations cover some 15 km^2. The Krafla system is a heterogonous reservoir and is subdivided into three distinctive wellfields: Leirbotnar, Sudurhlídar, and Hvíthólar. This study samples three wells from Leirbotnar and one from Hvíthólar.

The Bjarnarflag field is part of the Námafjall high temperature area and is part of the same fissure system as Krafla. The geothermal area lies outside of the Krafla caldera, on the eastern edge of the main fissure swarm associated with the Krafla central volcano (Sæmundsson, 1991). In general the fluids are dilute, Na-Cl type and have low gas content with TDS from 700 to 1300 ppm and pH between 7 and 8 (Ólafsson & Ármannson 2013).

5.2 Methods

5.2.1 Sampling

All of the samples in this study come from geothermal power plant production wells. The sampled systems are extensively and routinely monitored by the Icelandic GeoSurvey (ÍSOR), and the companies that operate the wells. For this study, additional samples from Reykjanes and Svartsengi were taken during routine monitoring by ÍSOR (for HS Orka) and specific sampling was carried out at Krafla and Bjarnarflag by agreement with Landsvirkjun.

All of the samples come from two-phase wells in which depressurisation boiling in the wells of producing aquifers causes cooling and degassing of the aquifer fluid. Thus, the fluid composition is altered between the undisturbed reservoir and the wellhead sampling (see Karingithi et al., 2010) making it extremely important to sample both the liquid and vapour to enable back-calculation of the reservoir conditions. As such both the liquid and vapour phases were collected at the wellhead by way of a Webre separator (fig. 2) and the pressure drop from the wellhead to the separator was minimised so that secondary flashing (boiling) of the fluids was avoided. All liquid samples and the condensed vapour samples for Mo isotope analysis were cooled through a stainless steel cooling coil. Liquid-phase samples were then filtered through 0.2 µm cellulose acetate filters into LDPE bottles except for those samples for trace metal and Mo isotope analysis which were sampled into acid cleaned HDPE. All equipment was pre-contaminated before sampling. Samples for major cations and trace metals were degassed and acidified with Suprapur HNO_3 after sampling. Anion samples were not treated save for an SO_4^{2-} sample to which zinc acetate was added to remove H_2S as ZnS (which is then filtered from the sample prior to analysis by ion-chromatography). The pH, alkalinity, and H_2S measurements were made within hours of sampling (if not on site). Dry steam was collected into evacuated gas sampling bulbs prepared with KOH (or NaOH) solution (Giggenbach 1975). The non-condensable gases (H_2, N_2, Ar, O_2, and CH_4) were analysed by gas chromatography. Both CO_2 and H_2S dissolve quantitatively in the alkaline solution and were determined by titration of the KOH (or NaOH) solution with HCl and $Hg(CH_3COO)_2$ respectively.

To complement these samples the IAPSO Atlantic seawater standard was also analysed. This is dual purpose, as an external standard for Mo isotope analysis and as a representative sample of seawater.

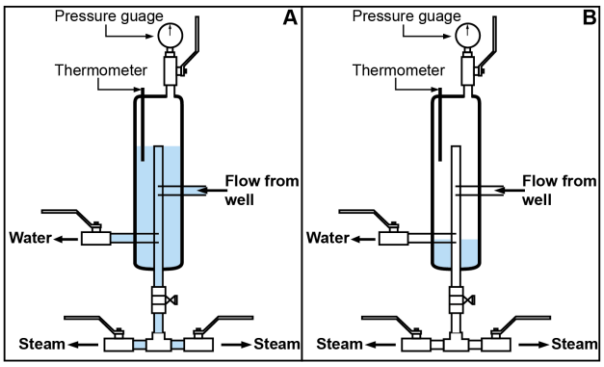

Figure 2: Webre separator used to sample two-phase fluids from wellheads. Figure based on details in Arnórsson et al. (2006). Inset A depicts water phase sampling; the steam valves are fully open but the water valve is only slightly open, thus ensuring the separator fills with the liquid phase. This is reversed for vapour phase sampling; the steam valves are only partially open whilst the water valve is fully open, resulting in little liquid in the separator (inset B) and ensuring that an uncontaminated, dry vapour phase is sampled.

5.2.2 Molybdenum isotope preparation and analysis

All Mo sample preparation and measurements were undertaken in the Department of Earth Science, Durham University, UK. Preliminary Mo concentrations were determined by ICP-MS (inductively coupled plasma mass spectrometry). A volume of each sample was then weighed and spiked with a ^{97}Mo-^{100}Mo double-spike (Siebert et al., 2001) to yield a ~1:1 ratio of spike to natural Mo (Rudge et al., 2009) with 50 to 100 ng of natural Mo. Chemical separation of Mo was achieved using a single pass anion exchange procedure detailed in Pearce et al. (2009). An additional 12 ml 0.5 M HF matrix elution step was included to ensure complete removal of Zn before the final Mo elution in 3 M HNO_3.

Molybdenum isotope compositions were measured using a multi-collector ICP-MS (Thermo-Finnegan Neptune, Durham University) equipped with an Aridus II desolvating nebuliser. Samples were aspirated at ~35 µl min-1 using a Cetac nebuliser and the maximum sensitivity was ~400 v ppm^{-1}. Measurements were made in low resolution static mode with 1 block of 50 cycles. Total procedural blanks for aqueous samples were < 1 ng Mo and data reduction was carried out offline using a deconvolution routine (Pearce et al., 2009) based on the Newton-Raphson method outlined by Albarède & Beard (2004).

All Mo isotope compositions are reported in delta notation in parts-per-thousand relative to a reference solution (equation 1) with errors of 2 standard deviations from the mean. Given the inconsistent reporting of Mo isotope data in the literature it is important to note that in this paper all data are reported referenced to SRM NIST 3134 = 0‰ (Greber et al., 2012; Goldberg et al., 2013) and literature data has been recalculated (Table ES1) to be comparable.

$$\delta^{98/95}Mo_{NIST} = \left[\left(\frac{\frac{^{98}Mo}{^{95}Mo_{SAMPLE}}}{\frac{^{98}Mo}{^{95}Mo_{NIST\ 3134}}} \right) - 1 \right] \cdot 1000 \qquad (1)$$

The reproducibility was determined by measurement of an in-house Romil standard, which gave δ^{98}Mo +0.05±0.05‰, n=183. Additionally, IAPSO seawater was run as an "unknown standard" yielding δ^{98}Mo +2.09±0.08‰ (n=43, nchem=17), which is comparable with the mean of published values of +2.08±0.10‰ (compiled in Goldberg et al., 2013). Taken together, these data suggest a long term external reproducibility of ± 0.08‰ or better for the δ^{98}Mo measurements. However, it is worth noting that the errors on the condensed vapour phase are somewhat larger (on average they are twice that of the long term reproducibility of the IAPSO standard). We attribute this to relatively low Mo concentrations requiring large sample aliquots and subsequent incomplete removal of an unusual matrix. All vapour samples were passed through chemistry and analysis in duplicate in an attempt to better constrain these values.

There is diversity in data reporting methods across all of the Mo literature and it is especially noticeable in high temperature systems. As such, all Mo isotope compositions in this study are referred relative to NIST = 0 as suggested for the international standard by

Greber et al (2012) and Goldberg et al. (2013). When necessary, literature data has been recalculated and details of this can be seen in the electronic supplements table ES1.

5.2.3 Component calculations – WATCH

Calculation of component concentrations and aqueous species distribution in the deep aquifer fluid was carried out by WATCH chemical speciation program (Arnórsson et al., 1982) version 2.4 (Bjarnason 2010). The deep fluid composition is calculated at a reference temperature determined for each well (Óskarsson et al., 2015; Óskarsson 2015). In brief, this reference temperature is determined by comparison between the measured temperature within the well at the depth of producing aquifers and the calculated quartz temperature of the deep liquid. Both the reference temperature and the calculated quartz temperature are shown in table 2.

The saturation state of the reservoir fluid with respect to certain minerals has been assessed using the results from the WATCH and PHREEQC calculations. The minerals presented here are those containing significant sulphur that have previously been identified in geothermal fields around Iceland: Anhydrite ($CaSO_4$); Pyrite (FeS_2); and Molybdenite (MoS_2) and Basalt (Table ES1).

The saturation index (SI) is defined as

$$SI = \log(Q/K) \quad (2)$$

Where Q is the reaction quotient of a mineral dissolution reaction and K is the equilibrium constant.

Anhydrite example:

$$CaSO_4^0 \rightleftharpoons Ca^{2+} + SO_4^{2-}$$

$$Q = \alpha_{Ca^{2+}} \cdot \alpha_{SO_4^{2-}}$$

$$\alpha_{Ca^{2+}} = \gamma_{Ca^{2+}} \cdot [Ca^{2+}]$$

$$\therefore$$

$$Q = (\gamma_{Ca^{2+}} \cdot [Ca^{2+}]) \cdot (\gamma_{SO_4^{2-}} \cdot [SO_4^{2-}])$$

Where α is the activity and γ the activity coefficient and calculated concentrations are in mol kg^{-1}. Both the chemical species concentration and the activity coefficient are given by WATCH, allowing calculation of saturation indices for important mineral phases within the systems.

Another important parameter calculated in WATCH is the vapour fraction at the time and pressure of sampling. Assuming a closed system, this allows calculation of the deep fluid concentration and isotopic composition for elements such as Mo, measured in the liquid and vapour phase but not included in the program.

$$[Mo]_{DF} = F_V \cdot [Mo]_V + (1\text{-}F_v) \cdot [Mo]_L \quad (3)$$

$$\delta^{98}Mo_{DF} = F_v \cdot \delta^{98}Mo_v \cdot \frac{[Mo]_V}{[Mo]_{DF}} + (1\text{-}F_v) \cdot \delta^{98}Mo_L \cdot \frac{[Mo]_L}{[Mo]_{DF}} \quad (4)$$

The calculated deep fluid isotopic composition is not sensitive to the proportion of the vapour phase, F_V, (Fig. ES1); at vapour fraction values less than 0.5 at the time of sampling, the calculated range of deep fluid isotopic composition is, for example in Reykjanes, from +1.68‰ to +1.48‰, indistinguishable within long-term sample reproducibility (2σ = 0.1‰). Therefore, the WATCH generated F_V values are used in the calculation of the deep fluid calculation. These calculations depend upon the assumption that this is a closed system and that all relevant Mo reservoirs have been sampled.

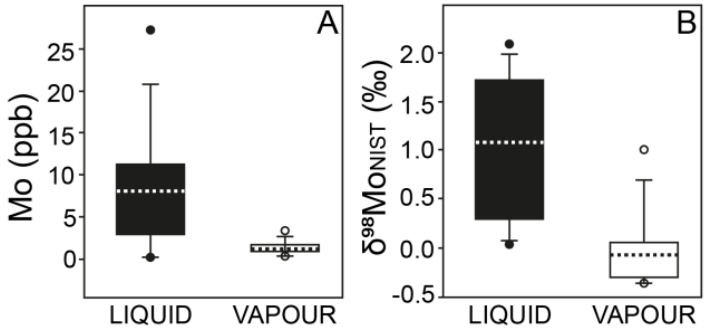

Figure 3: Box plot to show the variation in Mo concentration (A) and isotope composition (B) of the liquid and condensed vapour phases. The averages, in this case the mean, of the sample groups are shown by the dashed lines.

5.3 Results

All of the vapour phase samples contain measurable Mo. Concentrations in the condensed vapour range from 0.30 to 3.27 ppb with a mean of 1.25 ppb. In all cases the vapour phases contain less Mo than their corresponding liquid samples. The liquid phase samples have between 0.90 and 17.1 ppb Mo with the higher Mo concentrations generally associated with those reservoirs affected by a seawater component (Reykjanes and Svartsengi).

As shown in figures 3 and 4, the liquid samples show greater variation in both concentration and Mo isotope composition than the vapour phase samples. The liquid phase samples show a large range of Mo isotope compositions from δ^{98}Mo +0.06 to +2.87‰ with a mean of δ^{98}Mo +1.15‰. Again, those reservoirs dominated by seawater (Reykjanes and Svartsengi) tend to reflect that in their chemistry with more enriched compositions, closer to that of seawater (δ^{98}Mo +2.08‰), than the samples from Krafla and Námafjall. The vapour phase samples are, with the exception of K21, all isotopically lighter than their corresponding liquid samples (Fig. 3). The vapour phase samples range from δ^{98}Mo -0.35 to +0.74‰ with a mean of δ^{98}Mo -0.05‰.

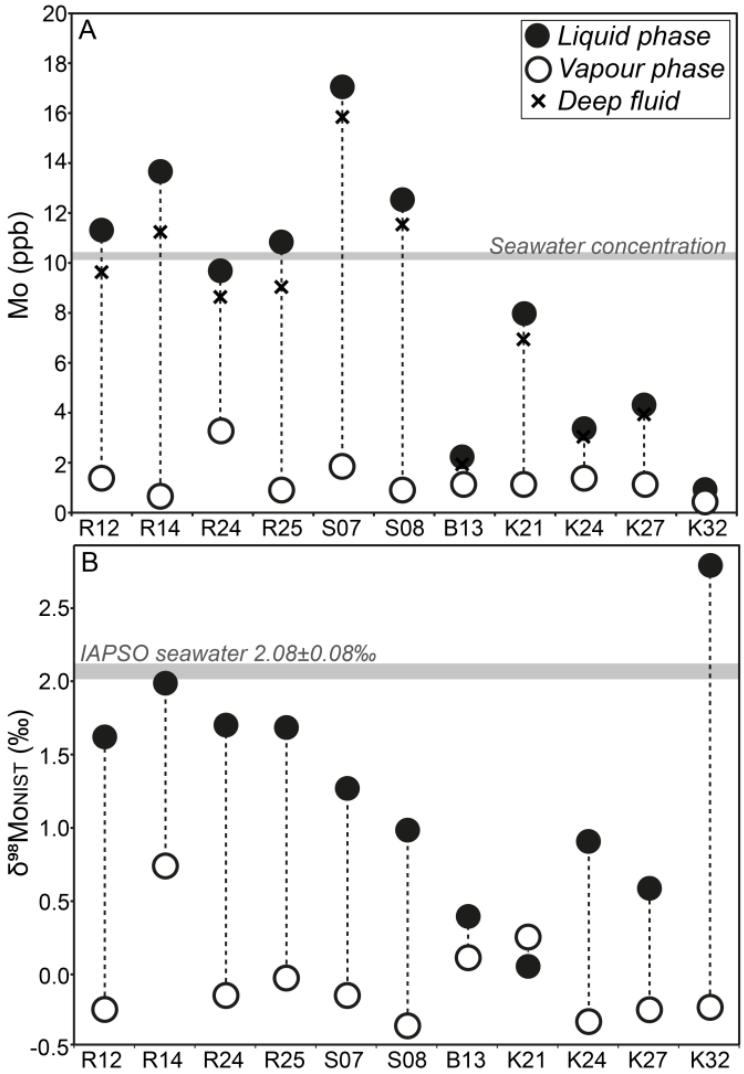

Figure 4: Comparison between the Mo chemistry (A: concentration, B: isotopes) in the sampled liquid and condensed vapour phase for specific wells in the geothermal fields. The calculated reservoir deep fluid composition is plotted as the cross but is so dominated by the liquid phase that it is indistinguishable from that phase in the Mo isotope composition plot. The Mo concentration and isotope composition for seawater (grey bar) has been added for comparison.

Table 1: Chemical composition of the liquid and vapour phases as sampled at the wellhead under the given sampling pressure and temperature conditions.

			Reykjanes				Svartsengi		Náma	Krafla			
		Wellhead	**R12**	**R14**	**R24**	**R25**	**S07**	**S08**	**B13**	**K21**	**K24**	**K27**	**K32**
	P	bar-abs	29.7	29.0	24.8	27.0	16.0	14.7	13.1	11.5	3.0	11.7	10.9
	T	°C	232.6	225.4	223.4	220.0	197.7	194.0	193.6	185.6	132.4	186.5	185.0
Liquid phase	**pH**		5.6	5.4	5.8	5.5	6.3	6.8	8.6	8.7	9.4	8.8	8.8
		°C	23.6	23.2	23.9	23.6	24.6	25.0	33.5	33.9	24.0	29.9	26.2
	CO_2	ppm	57.4	37.2	34.6	20.1	19.5	14.6	0.5	34.4	30.7	33.2	34.6
	H_2S	ppm	2.43	1.44	0.96	1.35	0.82	0.17	66.09	32.87	29.26	40.05	106.85
	B	ppm	8.81	9.45	8.67	9.67	6.94	7.45	2.1	0.81	0.62	0.56	0.58
	SiO_2	ppm	842	772	733	794	451	505	846	585	351	516	
	Na	ppm	11130	880	11100	12890	9820	7070	120	200	224	219	265
	K	ppm	1580	1740	1570	1830	996	1040	23	27	18	29	40
	Mg	ppm	0.94	1.72	0.66	2.2	0.33	0.54	0.07	0.07	0.07	0.07	0.06
	Ca	ppm	1920	1930	1830	2210	1050	1110	0.72	1.64	3.72	3.7	3.7
	F	ppm	0.24	0.22	0.23	0.23	0.21	0.19	0.987	1.047	0.813	1.051	1.154
	Cl	ppm	22170	23460	22030	25760	13510	14040	63.24	167.9	44.13	36.56	34.77
	Br	ppm	78.8	82.6	77.6	90.7	46.5	49					
	SO_4	ppm	15.3	26.2	18	21.8	28.7	26.1	7.56	36.1	110	125	255
	Al	ppm	0.11	0.15	0.11	0.14	0.17	0.16	0.79	1.41	0.78	1.3	1.5
	Fe	ppm	0.139	0.342	0.0857	1.26	0.056	0.044	0.014	0.032	0.012		0.032
	Mo	ppb	11.3	13.7	9.64	10.8	17.1	12.6	2.2	8	3.3	4.3	0.9
	$\delta^{98}Mo$	‰	1.68	2.05	1.74	1.74	1.3	1.02	0.42	0.06	0.94	0.61	2.87
	2SD		0.05	0.10	0.05	0.03	0.26	0.05	0.08	0.06	0.03	0.03	0.04
	n		5 (2)	5 (2)	5 (2)	5 (2)	5 (2)	5 (2)	4 (2)	4 (2)	3 (2)	4 (2)	3
Vapour phase	**CO_2**	ppm	12450	7810	7920	1860	6970	3860	292	1882	823	1932	2333
	H_2S	ppm	330	420	180	160	160	19	683	288	150	269	859
	H_2	%	0.57	4.13	0.47	1.49	2.89	0.51	97.27	53.15	10.88	59.21	96.06
	N_2	%	79.8	58	77.1	56.2	70.3	54.5	2.07	26.34	69.37	29.37	2.7
	Ar	%	2.34	1.61	2.21	0.49	1.95	1.63	0	1.01	0	1.82	0
	O_2	%	0	0	3.79	1.2	3.68	7.92	0	0.1	0.6	0.44	0.18
	CH_4	%	1.2	0.53	0.86	0.43	0.57	0.36	0.03	19.4	18.97	9.16	1.06
	NH_3	ppm	3.83	3.22	4	3.3	3.14	3.4					
	B	ppm	0.36	0.67	0.33	0.34	0.17	0.18					
	Na	ppm	0.34	1.3	6.16	3.41	0.33	0.21	0.17	0.08	0.14	0.33	0.09
	Mo	ppb	1.32	0.55	3.27	0.96	1.91	0.79	1.05	1.18	1.34	1.21	0.3
	$\delta^{98}Mo$	‰	-0.23	0.74	-0.15	-0.02	-0.14	-0.35	0.11	0.26	-0.32	-0.24	-0.22
	2SD		0.15	0.47	0.31	0.15	0.10	0.06	0.16	0.07	0.03	0.16	0.11
	n		4 (2)	3 (2)	3 (2)	3 (2)	4 (2)	4 (2)	3 (2)	3 (2)	3 (2)	3 (2)	3 (2)

5.4 Discussion

Table 2: Calculated reservoir conditions and fluid composition made using WATCH and mass balance calculations.

			Reykjanes				Svartsengi		Náma		Krafla			IAPSO
	Wellhead		**R12**	**R14**	**R24**	**R25**	**S07**	**S08**	**B13**	**K21**	**K24**	**K27**	**K32**	
	P	bar-a	83.2	88.0	71.2	80.8	33.6	33.1	75.0	43.5	18.6	36.7	40.3	
	$T_{(ref)}$		295	300	285	295	238.0	238.0		245	200	250		
	$T_{(qtz)}$	°C	306.5	287.1	284.1	293.2	239.8	247.9	290.0	254.6	208.2	244.6	249.7	
	Enthalpy	kJ kg	1317	1345	1263	1317	1028	1028	1291	1739	938	1716	1084	
	F_{VAP}		0.17	0.19	0.16	0.18	0.09	0.10	0.24	0.16	0.15	0.10	0.20	
	pH		4.82	4.79	4.92	4.92	4.95	5.19	7.27	7.03	7.12	7.02	6.92	
Reservoir fluid	**Eh_{H2S}**		-0.41	-0.41	-0.40	-0.41	-0.35	-0.37	-0.73	-0.63	-0.55	-0.60	-0.60	
	CO_2	ppm	2205	1527	1333	544	628	385	70.7	330	151	288	386	
	H_2S	ppm	59.2	81.6	30.4	30.6	14.8	1.98	215	73.7	47.7	70.7	222	
	B	ppm	7.28	7.64	7.24	7.89	6.33	6.76	1.59	0.68	0.53	0.49	0.49	
	SiO_2	ppm	696	624	612	647	421	456	642	491	298	447	469	
	Na	ppm	9200	9604	9272	10511	6223	6390	91.1	168	190	190	225	
	K	ppm	1306	1407	1311	1492	909	940	17.5	22.7	15.3	25.1	33.9	
	Mg	ppm	0.78	1.39	0.55	1.79	0.3	0.49	0.05	0.06	0.06	0.06	0.05	
	Ca	ppm	1587	1560	1529	1802	958	1003	0.55	1.38	3.15	3.2	3.14	
	F	ppm	0.2	0.18	0.19	0.19	0.19	0.17	0.75	0.88	0.69	0.91	0.98	
	Cl	ppm	18326	18965	18402	21006	12327	12689	48	141	37	32	29	
	SO_4	ppm	12.65	21.18	15.04	17.37	26.19	23.59	5.74	30.63	93.42	108.26	216.1	
	Al	ppm	0.091	0.122	0.088	0.11	0.159	0.14	0.6	1.185	0.661	1.126	1.271	
	Fe	ppm	0.115	0.277	0.072	1.028	0.051	0.04	0.011	0.027	0.01		0.027	
	Mo	ppb	9.6	11.2	8.6	9	15.8	11.5	1.9	6.9	3	3.9	0.8	10.8
	$\delta^{98}Mo$	‰	1.6	2.0	1.6	1.7	1.3	1.0	0.4	0.1	0.9	0.6	2.7	2.08
	α_{V-L}		0.9981	0.9987	0.9982	0.9983	0.9986	0.9986	1.000	1.000	0.9988	0.9992	0.997	
	ε_{V-L}		-1.87	-1.29	-1.77	-1.72	-1.42	-1.36	-0.27	0.20	-1.17	-0.81	-2.92	

$\alpha<1$ and $\varepsilon<0$ means vapour phase lighter than liquid

5.4.1 Reservoir/deep fluid composition

The WATCH calculations show that, at the time and pressure of sampling, the vapour phase fraction (F_V) was never more than 0.24. Assuming that this is a closed system with respect to Mo - that Mo is neither gained nor lost from the system - then the reservoir fluid composition can be calculated using equations 3 and 4. As the liquid phase samples can contain an order of magnitude more Mo than the vapour phase samples, the deep reservoir fluid compositions are dominated by the liquid phase values (Table 2 and Fig. 4).

The Mo composition of the Reykjanes reservoir is relatively uniform with a mean reservoir composition of 9.0 ppb and δ^{98}Mo = +1.7‰. Only R14 shows slightly elevated concentrations and an isotopic composition that differs from the remaining samples. This compares well with the known seawater source of these geothermal fluids (Marks et al., 2010) with seawater having a homogeneous composition of 10.8 ppb Mo and δ^{98}Mo +2.08‰ (Table 2). As such, this may suggest that during the circulation of these fluids through the geothermal system there is some loss of isotopically heavy Mo. Although within the uncertainties associated with these calculated reservoir fluid compositions it is possible that little to no chemical exchange has taken place.

Alternatively, the compositional similarity between the seawater endmember and the calculated reservoir fluid could be due to basalt-seawater interaction, contributing isotopically light Mo to the system which is then precipitated as Mo-sulphides. As shown in table ES1, basalts are always undersaturated in these systems and as such, tend towards dissolution. If 0.1 mol of basalt congruently dissolves for every 1 kg of seawater then the combined Mo concentration would be some 23 ppb with a Mo isotope composition of 2.0‰ (with basaltic glass 123 g per mole and taking a basaltic composition of 1 ppmMo and δ^{98}Mo -0.1‰). This would imply that basalt dissolution accounts for some 50% of the Mo in the reservoir. As this is not what is measured in the well-head samples it is reasonable to assume that precipitation of sulphides has occurred during fluid boiling (e.g. Arnórsson & Ívarsson 1985). These sulphides, whilst ranging in isotopic composition can be as light as -1.6‰ (Breillat et al., 2016), precipitate, removing Mo and leaving the fluid enriched in the heavier isotopes once more, coincidentally similar in composition to seawater. However, initial calculations made in PHREEQC (Parkhurst & Appelo 2013) with minteq.v4 database additions for Mo indicate that molybdenite (MoS_2) is actually undersaturated in the Reykjanes system (Table ES1) and therefore unlikely to be precipitating.

Svartsengi is a mixed seawater-meteoric reservoir. Simple two component mixing of seawater (10.8 ppb Mo and δ^{98}Mo +2.1‰) and meteoric water (7 ppt Mo and δ^{98}Mo +1.1‰; King et al., 2016) results in a theoretical reservoir of 7.2 ppb Mo with as isotope composition of +2.1‰. However the reservoir calculated from the measured components in this study is far from this predicted composition with Mo concentrations up to 15.8 ppb and a Mo isotope composition of +1.1‰ (Table 2). So, whilst the Reykjanes system suggests some overall loss of Mo, the reservoir fluid at Svartsengi has elevated Mo concentrations relative to seawater. Rather than being simply diluted by the contribution of meteoric water this reservoir has an additional source of Mo beyond that of seawater and meteoric water. This additional source of Mo is most likely from the basalt host of this reservoir. As seen in Table 3, the basalts of the Reykjanes peninsula are all isotopically light, from δ^{98}Mo -0.37‰ to -0.09‰ which is comparable to the Hawaiian bedrock basalts measured in King et al. (2016) -- δ^{98}Mo -0.26‰ to -0.11‰ -- and contain between 0.2 ppm and 4.7 ppm Mo (compared with between 0.24 ppm and 0.67 ppm in King et al. (2016)). Due to the relatively high Mo concentration within the basalt even a small contribution will result in significant modification of the Mo chemistry in these waters.

It is noted that, as is typical of mid ocean ridges, anhydrite is calculated (Table ES1) to be oversaturated in these samples: both at Reykjanes and Svartsengi, affected by seawater recharge.

Table 2: Selected data for complimentary basalt samples

	Mo ppm	δ^{98}Mo ‰	2 SD	n
ICELANDIC BASALT*				
RN09-642	1.007	-0.31	± 0.06	4 (2)
RN09-900	0.242	-0.37	± 0.08	2
RN09-1102	0.135	-0.25	± 0.08	2
RN09-1200 (Hyaloclastite)	4.665	-0.09	± 0.03	3 (2)

Bulk rock measurements from Neely et al., 2017

The Krafla and Námafjall reservoirs are known to be more heterogeneous and this is borne out in the Mo isotope compositions. Being of meteoric origin, these fluids are mostly isotopically lighter than both Reykjanes and Svartsengi but show far greater variation ranging from δ^{98}Mo +0.1‰ to +2.7‰. Again, with Mo concentrations greater than those of meteoric water, the host basalts are likely contributors of additional Mo and therefore the balance between basalt dissolution and sulfide precipitation is a likely controlling factor on the reservoir composition. However, the cause of this isotopic variation is difficult to constrain due to the limited sample number and the variation in conditions ranging from reservoir temperature and pressure, to chemical composition, all of which have the potential to influence the isotope composition.

In general, the Mo isotope and elemental chemistry of these reservoirs demonstrate that they are significantly influenced by the endmember fluids, whether seawater or meteoric. However, as suggested for Reykjanes contributions from chemical reactions within the reservoir rocks are capable of significantly altering the Mo chemistry of the fluids. In general, the host basalts are undersaturated and as such are likely to be dissolving, contributing Mo to the system. The major sulphide minerals of interest (e.g. molybdenite and pyrite) are undersaturated in all reservoirs suggesting that they are not precipitating at depth. However, boiling is known to facilitate the formation of these mineral phases (Arnórrsson & Ívarsson 1985) and indeed, scaling of the wells with these sulphides is a well-documented occurrence (e.g. Hjardardóttir et al., 2010).

5.4.2 Vapour phase fractionation

The condensed vapour phase Mo concentrations are relatively uniform, between 0.30 ppb and 3.27 ppb, especially when compared with the variations in their initial reservoir compositions and sampled liquids (Fig. 3 & 4). Whilst these concentrations are significant they are at the lowest end of those found in experimental studies of the solubility of Mo in the vapour phase and in field investigations. Mo vapour concentrations from high-temperature fumaroles range from 2 ppb to 2.8 ppm (e.g. in Williams-Jones & Heinrich 2005 and Hurtig & Williams-Jones 2014) with sublimates around these fumaroles often containing ilsemanite -- otherwise known as Molybdenum Blue, $Mo_3O_8.nH_2O$ (Williams-Jones & Heinrich 2005) -- and in experimental studies Mo concentrations can reach as much as 2500 ppm (at 350°C, 138 bars, and in a HCl-rich vapour; Rempel et al., 2008). However, it is understood that Mo in the vapour phase increases with increasing pressure

and temperature (e.g. Hurtig & Williams-Jones 2014) and as such, at the sampled reservoir conditions in this study, of less than 300°C and a maximum pressure of some 80 bars, Mo concentrations would not be expected to reach those of the high- temperature and pressure experiments.

With the exception of sample K21, all of the vapour phase samples are isotopically lighter than their corresponding liquid samples and calculated reservoir fluids. The segregation of the liquid brine and vapour phases is clearly accompanied by the preferential incorporation of isotopically light Mo into the vapour phase whilst the residual brine/liquid phase becomes increasingly heavy. This finding is at odds with the work of Yao et al. (2016) who invoke the preferential incorporation of heavy Mo into the vapour phase in order to explain their data. However, it is consistent with the observation of Shafiei et al. (2015) who find the high temperature (>400°C) brine phase to deposit isotopically heavier Mo (δ^{98}Mo +0.42%) in the early stages of crystallisation whilst the vapour crystallised isotopically lighter molybdenite (δ^{98}Mo -0.15‰) in the hydrothermal fracture system. The incorporation of isotopically light Mo into the vapour phase is further supported by molecular vibration theory which predicts that the lighter isotope tends to be incorporated into the vapour (e.g. McSween et al., 2003).

5.4.3 Fractionation factors

Given the ability to measure the coexisting liquid and vapour phases it is possible to calculate the fractionation factors associated with fluid boiling and phase segregation. This is of particular significance given the current lack of theoretical or experimental data on the potential magnitude of fractionation associated with phase separation (c.f. Shafiei et al., 2015). The fractionation factor, α, is calculated using equation 5 in which the subscripts *V* and *L* denote vapour and liquid respectively.

$$\alpha_{V\text{-}L} = (10^3 + \delta_V) / (10^3 + \delta_L) \quad (5)$$

When $\alpha<1$ then the vapour phase is isotopically lighter than the corresponding liquid phase. Consequently, when $\alpha>1$ the liquid phase is lighter than the vapour. Due to the small extent of these fractionations, it is easier to express as ε, the enrichment factor. This is related to the fractionation factor by equation 6.

$$\varepsilon_{V\text{-}L} = (\alpha_{V\text{-}L} - 1)\ 10^3 \quad (6)$$

In this case, when $\varepsilon<0$ the vapour phase is isotopically lighter than the liquid and vice versa when $\varepsilon>0$.

As already stated, all save one of the vapour phase samples are isotopically lighter than the liquid brine resulting in negative enrichment factors, that range from +0.2 to -1.9 (Table 2; Fig. 5). As might be expected, given the relatively homogenous nature of the Reykjanes and Svartsengi reservoirs these systems demonstrate consistent enrichment factors of -1.7 for Reykjanes and -1.4 for Svartsengi, whilst Krafla and Námafjall show much greater variation. The magnitude of fractionation between liquid and vapour is independent of both reservoir and sampling pressure and temperature. The observed correlation with the calculated redox state of the reservoir fluid as seen in figure 5 is noted.

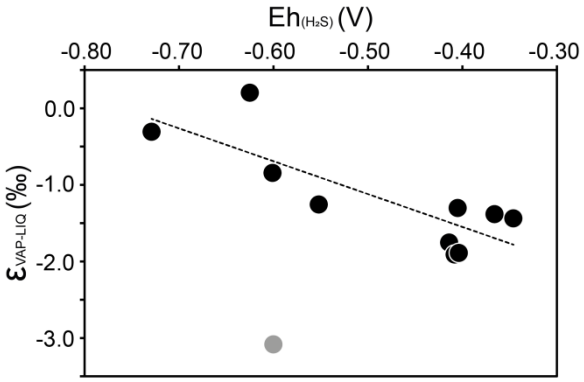

Figure 5: Fractionation factors between vapour and residual liquid phases from all of the four geothermal systems. They show a good correlation with Eh (R^2=0.67) if excluding K32 (in grey). In general the more reducing systems show greater fractionation than the more oxidising systems.

5.4.4 Rayleigh fractionation and molybdenite crystallisation

To explore the potential evolution of the reservoir fluids a simple Rayleigh fractionation model is implemented. Whilst physiochemical changes such as changes in pH, redox, and other reactions are recognised as being capable of generating considerable variation the use of Rayleigh fractionation alone allows the estimation of the isotope variations from this simple mechanism alone. As the reservoir fluid boils, the vapour portion increases and is removed from the decreasing (yet replenished) fluid and as such a Rayleigh model is appropriate as defined by equations 7 and 8

$$\delta_L = (\delta_L^{\circ} + 10^3) \cdot f^{\alpha-1} - 10^3 \quad (7)$$

$$\delta_V = (\delta_L + 10^3) \cdot \alpha - 10^3 \quad (8)$$

in which the subscripts *L* and *V* denote liquid and vapour, respectively and the evolving composition is a function of the original composition of the reservoir fluid ($\delta_L°$).

Figure 6 shows the isotopic evolution of the fluids from a homogenous Reykjanes reservoir via Rayleigh fractionation. In this example, the deep reservoir fluid has an initial Mo isotope composition of δ^{98}Mo (δ_L°) of +1.7‰ and the fractionation factor between liquid and vapour is 0.998 (ε = -1.7), based on the observed fractionation (Table 2). As the light Mo isotopes are preferentially partitioned into the vapour phase the residual liquid becomes increasingly heavy. As such, the first vapour formed is isotopically the lightest fluid formed and the very last liquid is the heaviest. In Reykjanes, the potential range of vapour Mo isotope values varies from -0.1‰ to nearly 10% (at the theoretical point for 100% vapour).

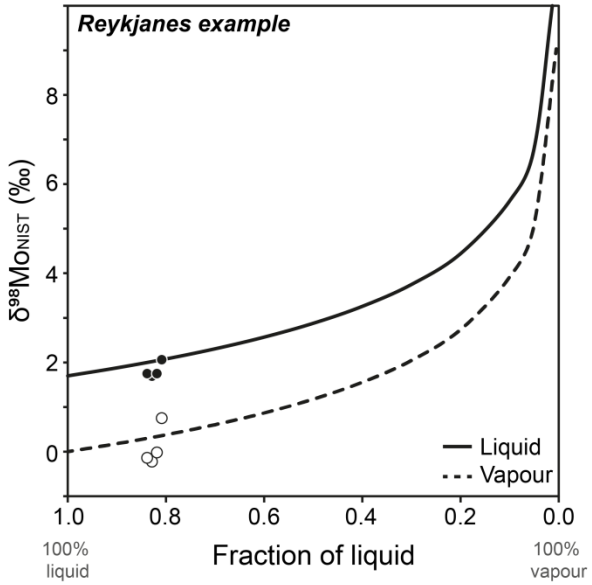

Figure 6: An example of fluid (both liquid and vapour) evolution for the Reykjanes system. Fluid boiling and phase segregation occurs via Rayleigh fractionation, during which lighter isotopes are preferentially incorporated into the vapour phase. The reservoir fluid starts with a δ^{98}Mo composition of +1.7‰ and a fractionation factor of $\alpha_{V\text{-}L}$ of 0.998 is used throughout. Measured liquid (filled circle) and vapour (open circle) Mo compositions are plotted at calculated vapour fractions.

The consensus from previous work is that even in the vapour phase Mo is most commonly transported as oxidised species such as $MoO_3.nH_2O$ (e.g. Rempel et al., 2006; Hannah et al., 2007). Consequently, that the precipitation of molybdenite (MoS_2) is a strong reduction reaction whether precipitating from the vapour or the residual brine. As such, stable isotope theory would predict that the lighter isotopes would be preferentially incorporated into the reduced crystalline phase and this is supported by the theoretical work of Tossell (2005) who calculate a fractionation factor of -1.8‰ amu^{-1} between MoO_4^{-2} and MoS_4^{-2}. Similar to Hannah et al. (2007) we can therefore apply a conservative estimate of fractionation between $MoO_3.nH_2O$ (vapour) and MoS_2 (crystalline) (ε = -3.0) to calculate the theoretical molybdenite composition precipitating from the evolving vapour (and liquid) phases (Fig. 7 for Reykjanes and Krafla examples). In Reykjanes this results in highly variable molybdenite compositions from δ^{98}Mo -1.3‰ to +8.0‰ for molybdenites

precipitating from the liquid phase (mean +0.6‰) and from δ^{98}Mo -3.1‰ to +6.4‰ for those precipitating from the vapour phase (mean -1.4‰). Whilst greater than the total range observed in naturally occurring molybdenites this is not unexpected as these calculations are taken to extreme conditions, such as 100% vapour, probably not reached in the natural environment.

Due to the heterogeneity of the Krafla system, such generalised modelling is harder to constrain. However, in Figure 7, taking the isotopically lighter starting composition of +0.75‰ and lower fractionation factor of 0.999 (ε = -1.1) it is possible to generate molybdenites from -3.3‰ to +3.3‰ (Fig. 7). At the lighter end, these are well outside of the observed molybdenite range (δ^{98}Mo -1.6‰ to +2.3‰; Breillat et al., 2016) and would require more than 50% vapour to be formed before precipitating molybdenites within the observed range (the green bands on Fig. 7). Even within the Reykjanes system, whilst isotopically reasonable molybdenites are initially able to be formed from the liquid phase it takes until the vapour phase is more than 50% for the theoretical molybdenites precipitating to correspond to values actually measured in deposits (Fig. 7).

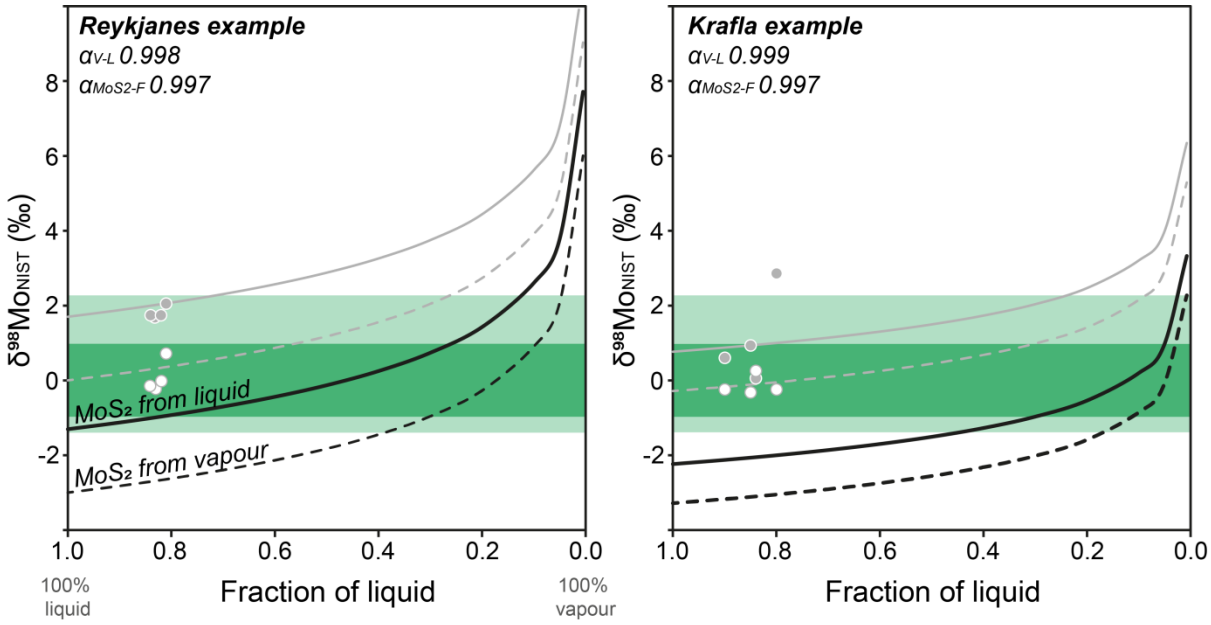

Figure 7: Rayleigh fractionation models for the compositions of molybdenites (MoS2), shown by the black lines, precipitating from the evolving liquid and vapour phases (in grey). The differences between the Reykjanes and Krafla examples are the starting reservoir compositions (1.7‰ and 0.8‰ respectively) and the liquid-vapour fractionation factor (αV-L 0.998 and 0.999 respectively) whilst the fractionation factor between the fluids and precipitating molybdenite (αMoS-F) is modelled as 0.997 in all cases as assumed in Hannah et al. (2007) based upon calculated fractionation factors in Tossell (2005). The total range of Mo isotope compositions for molybdenites (Breillat et al., 2016) is shaded in green with porphyry deposits specifically depicted in the darker green. Superimposed on these models are the liquid and vapour sample compositions at the sampling vapour fractions for the different reservoirs.

5.4.5 Molybdenite deposits

As supported by all of the vapour analyses and fractionation factors (save K21) in this study, Shafei et al. (2015) previously suggested -- via indirect measurements of molybdenite deposits -- that the vapour phase preferentially incorporated light Mo. In a Cu-porphyry deposit in Iran deposits from the high temperature brine phase (δ^{98}Mo +0.42‰) were found to be to be isotopically heavier than those from a transitional vapour phase (δ^{98}Mo -0.15‰). However, whilst recognising the significance of vapour transport, Yao et al. (2016) invoke the preferential enrichment of heavy Mo in the vapour phase to explain the isotope data from the cogenetic chalcopyrite and molybdenite deposit of the Dahutang W-Cu-Mo ore field, China, contrary to both the findings of Shafiei et al. (2015) and, now, the direct observations of vapour behaviour made in this study.

Hannah et al. (2007) assumed an initial Mo vapour composition of 0‰ to model the precipitation of MoS_2 from vapour. The results from this study suggest 0‰ to be a reasonable, if a little high, assumption with the mean vapour composition in this study some -0.1‰. Whilst the vapour phase is recognised as an ore-forming fluid in its own right (e.g. Pokrovski et al., 2008; Henley and McNabb 1978; Kouzmanov & Pokrovski 2012; Heinrich et al., 1999) and has been shown to be capable of generating large Mo isotope variations via Rayleigh fractionation (Fig. 6 &7; Hannah et al., 2007; Shafei et al., 2015) a number of other processes capable of contributing to the observed Mo isotopic complexity have been suggested:

Temperature variation: Deposits formed at higher crystallisation temperatures (represented by porphyries and granites) have, on average, lower δ^{98}Mo values of approximately -0.2‰ (e.g. Mathur et al., 2010; Shafiei et al., 2015; Breillat et al., 2016) than those observed for lower temperature deposits such as greisen (δ^{98}Mo +1.00‰) and iron oxide Cu-Au (δ^{98}Mo +0.80‰) (e.g. Mathur et al., 2010; Breillat et al., 2016). However, it should be noted that there is considerable overlap in compositions between deposit types and the sampling bias in the literature favours high temperature samples (as clearly shown in Breillat et al. (2016), fig. 4). Other than the suggested temperature control, there appears to be little systematic change in the isotopic signatures between deposit type, whether porphyry, skarns, or granites.

Fractional crystallisation: Hannah et al. (2007) demonstrated that fractional crystallisation of an isotopically light molybdenite from a theoretical vapour phase is capable of generating variations exceeding those observed in crustal rocks. As the residual vapour continues to move through the system it has an ever evolving Mo isotope composition, and calculations predict a systematic increase in the Mo isotope composition of molybdenites. Indeed, spatially and temporally increasing Mo isotope compositions within a deposit were demonstrated by Greber et al. (2014) in the porphyry-type Questa deposit, USA. Molybdenites from the early magmatic phase were isotopically light (δ^{98}Mo -0.54‰) but increased to -0.30‰ for later hydrothermal deposits and to almost 0.0‰ for the late stage stockwork veining. This progression is attributed to the preferential incorporation of light isotopes into the mineral structure and associated fractional crystallisation (Greber et al., 2014).

Source magma and redox: Greber et al. (2014) also attributed some of this variation to the preferential incorporation of heavy Mo into the magmatic-hydrothermal fluids upon exsolution. This is supported by the bi-modal distribution of Mo isotopes, with peaks at

δ^{98}Mo +0.82‰ and -0.08‰, in the quartz-molybdenite veins of the Aar Massif, Switzerland that Greber et al. (2011) use as evidence against single-stage Rayleigh fractionation. Instead, multi-phased magma exsolution from an evolving magma source and dominant redox conditions were thought to control Mo isotope composition (Greber et al., 2011, see also Mathur et al., 2010). Further investigating the role played by the source magma, Wang et al. (2016) used Nd isotopes and Re concentrations in conjunction with Mo isotopes on five porphyry molybdenum deposits from the Tibetan Plateau. Those deposits with a crustal dominated source, as demonstrated by low εNd and low Re, are isotopically heavier (Chagele: δ^{98}Mo +1.03‰) than those with a mantle derived magma (Jigongeun: δ^{98}Mo -1.07‰) or mixed source (Sharang: δ^{98}Mo -0.23‰). However, large variations are also seen within single deposits in which the magma source cannot be the dominant control.

It is clear from just these few examples that molybdenite deposits and geothermal systems are complex systems when examined individually, let alone on a global scale. The degree of variation in Mo isotopes in molybdenites is perhaps not. surprising when all of these processes are interacting to different extents, at different times and scales. It is interesting that, with many assumptions made, it is possible to generate considerable isotope variation with phase separation and mineral precipitation alone (Figs. 6 & 7). The observations of vapour fractionation in Icelandic geothermal systems made in this study support the idea of the preferential incorporation of light Mo into the vapour phase (Shafiei et al., 2015).

5.5 Summary & conclusions

This direct study of the Mo isotope composition of modern geothermal liquids and vapours -- analogous to exhumed ore deposits -- has demonstrated that the vapour phase is isotopically lighter than its corresponding liquid in all but one case. The observed fractionation between the vapour and liquid ($\varepsilon_{V\text{-}L}$ 0.2 to -2.9; Table 2) is of the same magnitude as that calculated for the fractionation driven by the precipitation of molybdenite (MoS_2) and as such is capable of generating the variation in Mo isotopes measured in Mo ore deposits via simple Rayleigh fractionation and precipitation. Via this mechanism, the formation of MoS_2 within the measured isotopic range appears easier from high salinity seawater fluids with a heavier Mo isotope reservoir composition than from more dilute systems (Fig. 7). Whilst these data are interpreted in a simple framework in which we must assume to have sampled the relevant Mo reservoirs to calculate fractionation factors, they do, for the first time, allow direct observations of the liquid and vapour phases and the corresponding Mo isotope systematics.

References

ALBARÈDE, F. & BEARD, B. 2004. Analytical methods for non-traditional isotopes. Reviews in mineralogy and geochemistry, 55, 113-152.

ARNÓRSSON, S., SIGURDSSON, S. & SVAVARSSON, H. 1982. The chemistry of geothermal waters in Iceland. I. Calculation of aqueous speciation from 0° to 370°C. Geochimica et Cosmochimica Acta, 46, 1513-1532.

ARNÓRSSON, S. & ÍVARSSON, G. 1985. Molybdenum in Icelandic geothermal waters. Contributions to Mineralogy and Petrology, 90, 179-189.

ARNÓRSSON, S. 1995. Geothermal systems in Iceland: Structure and conceptual models—I. High-temperature areas. Geothermics, 24, 561-602.

BARLING, J., ARNOLD, G. L. & ANBAR, A. D. 2001. Natural mass-dependent variations in the isotopic composition of molybdenum. Earth and Planetary Science Letters, 193, 447-457.

BARNES, H. L. 2015. Hydrothermal processes: The development of geochemical concepts in the latter half of the twentieth century. GEOCHEMICAL PERSPECTIVES, 4, 1-87.

BJARNASON, J. Ö. (2010). Manual for the chemical speciation program WATCH v. 2.4. http://www.geothermal.is/sites/geothermal.is/files/download/watch_readme.pdf

BJORNSSON, S., ARNORSSON, S. & TOMASSON, J. 1972. Economic evaluation of Reykjanes thermal brine area, Iceland. AAPG Bulletin, 56, 2380-2391.

BREILLAT, N., GUERROT, C., MARCOUX, E. & NÉGREL, P. 2016. A new global database of δ98Mo in molybdenites: A literature review and new data. Journal of Geochemical Exploration, 161, 1-15.

FRIDRIKSSON, T., KRISTJÁNSSON, B. R., ÁRMANNSSON, H., MARGRÉTARDÓTTIR, E., ÓLAFSDÓTTIR, S. & CHIODINI, G. 2006. CO2 emissions and heat flow through soil, fumaroles, and steam heated mud pools at the Reykjanes geothermal area, SW Iceland. Applied Geochemistry, 21, 1551-1569.

GIGGENBACH, W. F. 1975. A simple method for the collection and analysis of volcanic gas samples. Bulletin Volcanologique, 39, 132-145.

GOLDBERG, T., GORDON, G., IZON, G., ARCHER, C., PEARCE, C. R., MCMANUS, J., ANBAR, A. D. & REHKÄMPER, M. 2013. Resolution of inter-laboratory discrepancies in Mo isotope data: an intercalibration. Journal of Analytical Atomic Spectrometry, 28, 724-735.

GREBER, N. D., HOFMANN, B. A., VOEGELIN, A. R., VILLA, I. M. & NÄGLER, T. F. 2011. Mo isotope composition in Mo-rich high- and low-T hydrothermal systems from the Swiss Alps. Geochimica et Cosmochimica Acta, 75, 6600-6609.

GREBER, N. D., SIEBERT, C., NÄGLER, T. F. & PETTKE, T. 2012. δ98/95Mo values and Molybdenum Concentration Data for NIST SRM 610, 612 and 3134: Towards a

Common Protocol for Reporting Mo Data. Geostandards and Geoanalytical Research, 36, 291-300.

GREBER, N. D., PETTKE, T. & NÄGLER, T. F. 2014. Magmatic–hydrothermal molybdenum isotope fractionation and its relevance to the igneous crustal signature. Lithos, 190–191, 104-110.

GUDMUNDSSON, J. & THORHALLSSON, S. 1986. The Svartsengi reservoir in Iceland. Geothermics, 15, 3-15.

GUDMUNDSSON, A. 1995. Infrastructure and mechanics of volcanic systems in Iceland. Journal of Volcanology and Geothermal Research, 64, 1-22.

HANNAH, J., STEIN, H., WIESER, M., DE LAETER, J. & VARNER, M. 2007. Molybdenum isotope variations in molybdenite: Vapor transport and Rayleigh fractionation of Mo. Geology, 35, 703-706.

HEINRICH, C. A., RYAN, C. G., MERNAGH, T. P. & EADINGTON, P. J. 1992. Segregation of ore metals between magmatic brine and vapor; a fluid inclusion study using PIXE microanalysis. Economic Geology, 87, 1566-1583.

HEINRICH, C., GÜNTHER, D., AUDÉTAT, A., ULRICH, T. & FRISCHKNECHT, R. 1999. Metal fractionation between magmatic brine and vapor, determined by microanalysis of fluid inclusions. Geology, 27, 755-758.

HENLEY, R. & MCNABB, A. 1978. Magmatic vapor plumes and ground-water interaction in porphyry copper emplacement. Economic Geology, 73, 1-20.

HENLEY, R. W. & ELLIS, A. J. 1983. Geothermal systems ancient and modern: a geochemical review. Earth-science reviews, 19, 1-50.

HARDARDÓTTIR, V., HANNINGTON, M., HEDENQUIST, J., KJARSGAARD, I. & HOAL, K. 2010. Cu-rich scales in the Reykjanes geothermal system, Iceland. Economic Geology, 105, 1143-1155.

HURTIG, N. C. & WILLIAMS-JONES, A. E. 2014. An experimental study of the solubility of MoO 3 in aqueous vapour and low to intermediate density supercritical fluids. Geochimica et Cosmochimica Acta, 136, 169-193.

HURTIG, N. C. & WILLIAMS-JONES, A. E. 2015. Porphyry-epithermal Au-Ag-Mo ore formation by vapor-like fluids: New insights from geochemical modeling. Geology, G36685. 1.

JAKOBSSON, S. P., JÓNSSON, J. & SHIDO, F. 1978. Petrology of the western Reykjanes peninsula, Iceland. Journal of Petrology, 19, 669-705.

KARINGITHI, C. W., ARNÓRSSON, S. & GRÖNVOLD, K. 2010. Processes controlling aquifer fluid compositions in the Olkaria geothermal system, Kenya. Journal of Volcanology and Geothermal Research, 196, 57-76.

KENDALL, B., DAHL, T., ANABAR, A. 2016. Good Golly, Why Moly? The Stable Isotope Geochemistry of Molybdenum, Reviews in Mineralogy and Geochemistry, 82, 683-732.

KING, E. K., THOMPSON, A., CHADWICK, O. A. & PETT-RIDGE, J. C. Molybdenum sources and isotopic composition during early stages of pedogenesis along a basaltic climate transect. Chemical Geology.

KOUZMANOV, K. & POKROVSKI, G. S. 2012. Hydrothermal controls on metal distribution in porphyry Cu (-Mo-Au) systems. Special Publication of the Society of Economic Geologists, 16, 573–618.

MARKS, N., SCHIFFMAN, P., ZIERENBERG, R. A., FRANZSON, H. & FRIDLEIFSSON, G. Ó. 2010. Hydrothermal alteration in the Reykjanes geothermal system: Insights from Iceland deep drilling program well RN-17. Journal of Volcanology and Geothermal Research, 189, 172-190.

MATHUR, R., BRANTLEY, S., ANBAR, A., MUNIZAGA, F., MAKSAEV, V., NEWBERRY, R., VERVOORT, J. & HART, G. 2010. Variation of Mo isotopes from molybdenite in high-temperature hydrothermal ore deposits. Mineralium Deposita, 45, 43-50.

McSween HY, Richardson SM, Uhle ME (2003) Geochemistry; pathways and processes, 2nd edn. Columbia University Press, New York, 359 p

OLAFSSON, M. & ARMANNSSON, H. 2013. The Namafjall high temperature system, NE Iceland; chemical characteristics of the fluid for a power plant. Proceedings of the Fourteenth International Symposium on Water-Rock Interaction, Wri 14, 7, 640-643.

ÓSKARSSON, F. 2015. Svartsengi production field: Geochemical monitoring in 2014. Iceland Geosurvey prepared for HS Orka Ltd. ÍSOR-2015/009. Project no.: 14-0002.

ÓSKARSSON, F., WEISENBERGER, T. B. & ÞORBJÖRNSSON, D. 2015. Reykjanes production field: Geochemical monitoring in 2014. Iceland Geosurvey prepared for HS Orka Ltd. ÍSOR-2015/010. Project no.: 14-0006.

PARKHURST, D.L., & APPELO, C.A.J., 2013, Description of input and examples for PHREEQC version 3—A computer program for speciation, batch-reaction, one-dimensional transport, and inverse geochemical calculations: U.S. Geological Survey Techniques and Methods, book 6, chap. A43, 497 p., available only at https://pubs.usgs.gov/tm/06/a43/.

PEARCE, C. R., COHEN, A. S. & PARKINSON, I. J. 2009. Quantitative Separation of Molybdenum and Rhenium from Geological Materials for Isotopic Determination by MC-ICP-MS. Geostandards and Geoanalytical Research, 33, 219-229.

RAGNARSDÓTTIR, K. V., WALTHER, J. V. & ARNÓRSSON, S. 1984. Description and interpretation of the composition of fluid and alteration mineralogy in the geothermal system, at Svartsengi, Iceland. Geochimica et Cosmochimica Acta, 48, 1535-1553.

REMPEL, K. U., MIGDISOV, A. A. & WILLIAMS-JONES, A. E. 2006. The solubility and speciation of molybdenum in water vapour at elevated temperatures and pressures: Implications for ore genesis. Geochimica et Cosmochimica Acta, 70, 687-696.

REMPEL, K., WILLIAMS-JONES, A. & MIGDISOV, A. 2008. The solubility of molybdenum dioxide and trioxide in HCl-bearing water vapour at 350 C and pressures up to 160 bars. Geochimica et Cosmochimica Acta, 72, 3074-3083.

RUDGE, J. F., REYNOLDS, B. C. & BOURDON, B. 2009. The double spike toolbox. Chemical Geology, 265, 420-431.

SHAFIEI, B., SHAMANIAN, G., MATHUR, R. & MIRNEJAD, H. 2015. Mo isotope fractionation during hydrothermal evolution of porphyry Cu systems. Mineralium Deposita, 50, 281-291.

SIEBERT, C., NÄGLER, T. F., VON BLANCKENBURG, F. & KRAMERS, J. D. 2003. Molybdenum isotope records as a potential new proxy for paleoceanography. Earth and Planetary Science Letters, 211, 159-171.

THORDARSON, T. & LARSEN, G. 2007. Volcanism in Iceland in historical time: Volcano types, eruption styles and eruptive history. Journal of Geodynamics, 43, 118-152.

TOSSELL, J. A. 2005. Calculating the partitioning of the isotopes of Mo between oxidic and sulfidic species in aqueous solution. Geochimica et Cosmochimica Acta, 69, 2981-2993.

WANG, Y., ZHOU, L., GAO, S., LI, J.-W., HU, Z.-F., YANG, L. & HU, Z.-C. 2016. Variation of molybdenum isotopes in molybdenite from porphyry and vein Mo deposits in the Gangdese metallogenic belt, Tibetan plateau and its implications. Mineralium Deposita, 51, 201-210.

WIESER, M. E. & DE LAETER, J. R. 2003. A preliminary study of isotope fractionation in molybdenites. International Journal of Mass Spectrometry, 225, 177-183.

WILLIAMS-JONES, A. E. & HEINRICH, C. A. 2005. 100th Anniversary special paper: vapor transport of metals and the formation of magmatic-hydrothermal ore deposits. Economic Geology, 100, 1287-1312.

YAO, J., MATHUR, R., SUN, W., SONG, W., CHEN, H., MUTTI, L., XIANG, X. & LUO, X. 2016. Fractionation of Cu and Mo isotopes caused by vapor-liquid partitioning, evidence from the Dahutang W-Cu-Mo ore field. Geochemistry, Geophysics, Geosystems.

Acknowledgements

We greatly appreciate both HS Orka and Landsvirkjun for permission to sample and publish data whilst the geochemists of ÍSOR are thanked for assistance in sampling Reykjanes and Svartsengi and Helgi Arnar Alfreðsson for Krafla and Námafjall. Geoff Nowell is thanked for his generous help in the preparation and isotopic analysis of the samples and Chris Ottley for assistance with ICP-MS analysis. We acknowledge financial support from Initial Training Network, MetTrans, grant number 290336 from the European Research Council.

Author contributions

R.A.N. conceived the project and sampling was coordinated and carried out by R.A.N. with assistance from ÍSOR. Mo isotopes were analysed by R.A.N. with some assistance from C.R.P. Data interpretation and writing was led by R.A.N. with contributions from all authors.

Table ES1: Literature data renormalised to NIST = 0‰

Reference	Sample	Reference Standard	Ref. STND & NIST offset	$\delta^{97/95}Mo$	$\delta^{98/95}Mo$	$\delta^{98/95}Mo_{NIST=+0.25}$	$\delta^{98/95}Mo_{NIST=0}$
			‰	‰	‰	‰	‰
Wang et al., 2016	Chagele molybdenite	JMC	-0.28	0.88	1.32	1.29	**1.04**
		JMC	-0.28	0.85	1.28	1.25	**1.00**
	Jigongeun molybdeite	JMC	-0.28	-0.48	-0.72	-0.75	**-1.00**
		JMC	-0.28	-0.58	-0.87	-0.90	**-1.15**
	Sharang molybenite	JMC	-0.28	0.05	0.08	0.05	**-0.21**
		JMC	-0.28	0.05	0.08	0.05	**-0.21**
		JMC	-0.28	-0.01	-0.02	-0.05	**-0.30**
	SDO-1 STND	JMC	-0.28	0.73	1.10	1.07	**0.82**
Greber et al., 2014	Early Magmatic	NIST = 0.25				-0.29	**-0.54**
	Hydrothermal	NIST = 0.25				-0.05	**-0.30**
	late Stockwork	NIST = 0.25				0.22	**-0.03**
	Rhyolite	NIST = 0.25				-0.57	**-0.82**
Mathur et al., 2010	Porphyry	JMC	-0.28	0.07	0.11	0.08	**-0.18**
	Skarn	JMC	-0.28	0.42	0.63	0.60	**0.35**
	Fe oxide Cu-Au	JMC	-0.28	0.64	0.96	0.93	**0.68**
Greber et al., 2011	Seawater	JMC	-0.28		2.3	2.27	**2.02**
	bi-modal distribution	JMC	-0.28		1.1	1.07	**0.82**
	bi-modal distribution	JMC	-0.28		0.2	0.17	**-0.08**

Value given in literaute

Table ES2: Mineral saturation states for reservoir fluids

	Plagioclase feldspar		Pyroxene			Olivine		Basaltic Glass	Basalt		
Sample	Albite	Anorthite	CPX	Diopside	Enstatite	Fayalite	Forsterite		Stapafell*		
	$NaAlSi_3O_8$	$CaAl_2Si_2O_8$	$Ca_{0.7}Mg_{0.84}$	$MgCa(SiO_3)_2$	$MgSiO_3$	Fe_2SiO_4	Mg_2SiO4	$SiAl_{0.36}O_2(OH)$			
R12	-12.2	1.31	17.53	8.23	-2.09	-2.49	-44.4	-2.00	-4.65	-5.36	-4.01
R14	-9.73	5.49	17.47	8.56	-2.05	-2.18	-44.91	-1.00	-3.85	-4.56	-3.24
R24	-7.72	8.95	17.09	8.62	-2.28	-3.02	-42.64	-0.25	-3.22	-3.93	-2.64
R25	-8.93	7.17	18.54	9.47	-1.67	-0.57	-42.18	-0.78	-3.63	-4.34	-3
S07	-3.38	15.64	15.07	7.49	-3.1	-4.1	-40.9	1.74	-1.76	-2.48	-1.29
S08	-3.57	15.93	16.66	8.95	-2.24	-3.12	-40.06	1.48	-1.88	-2.61	-1.38
B13	-2.35	19.53	20.66	12.11	1.17	-0.97	-36.39	1.41	-1.45	-2.24	-0.87
K21	-1.13	20.21	19.89	11.91	0.58	0.23	-34.39	2.20	-1.16	-1.91	-0.65
K24	-1.19	18.73	18.63	12.22	-0.08	-1.52	-31.89	2.64	-1.34	-2.03	-0.93
K27	-1.25	20.46	19.8	12.13	0.43	-0.69	-34.66	2.15	-1.22	-1.97	-0.71
K32	-1.22	20.24	19.29	11.57	0.11	-1.02	-35.32	2.17	-1.19	-1.94	-0.69

Saturation index calcualtions made in PHREEQC using the S(-2)/S(+6) redox pair and WATCH calcualted reservoir conditions for temperature and pH

Molybdenite additons from minteq.v4 database

	Sulphides				Iron (oxyhydr)oxides		Carbonates			Anhydrite
Sample	Molybdenite	Pyrite	Pyrrhotite	Mackinawite	Ferrihydrite	Goethite	Dolomite	Calcite	Aragonite	
	MoS_2	FeS_2	FeS	FeS	Fe(OH)3	FeOOH	CaMg(CO3	CaCO3	CaCO3	CaSO4
R12	-1.88	-3.12	-3.83		-2.47	-0.31	-15.55	-2.36	-2.4	0.91
R14	-3.77	-1.49	-2.98		-2.33	-0.11	-13.49	-1.84	-1.88	1.31
R24	-4	-2.18	-3.56		-2.76	-0.52	-12.64	-1.46	-1.5	1.11
R25	-1.91	-1.52	-2.61		-1.53	0.69	-14.17	-2.1	-2.14	1.46
S07	-0.81	-0.83	-3.24		-3.28	-0.92	-10.68	-1.27	-6.09	0.77
S08	-4.05	-2.6	-3.93		-2.72	-0.4	-10.49	-1.14	-1.19	0.93
B13	-6.03	-1.49	-2.08		-2.23	-0.02	-11.46	-2.27	-2.31	-2.72
K21	-3.07	0.88	-0.84		-1.51	0.81	-7.41	-0.94	-0.99	-1.49
K24	-0.84	1.87	-0.88		-2.38	0.07	-4.97	0.03	-0.03	-0.5
K27	-3.48	0.55	-1.3		-1.88	0.44	-7.24	-0.59	-0.64	-0.52
K32	-2.96	1.39	-0.96		-2.07	0.25	-7.56	-0.71	-0.76	-0.34

A. The fate of dissolved molybdenum in the estuarine low salinity mixing zone: a study of three contrasting arctic estuaries

Rebecca A. Neely, Sigurdur R. Gislason, Alex Dickinson, Hanne Wouters, Don Porcelli, Kevin W. Burton

1. Introduction

The use of molybdenum as a proxy for the global extent of ocean anoxia in the geological past has been a common practice for well over a decade (e.g. Emerson and Huested, 1991, Siebert et al., 2003, Arnold et al., 2004, Anbar and Rouxel, 2007, Lyons et al., 2009, Dickson and Cohen, 2012). The first observations pertained to Mo concentrations alone (e.g. Emerson & Huested, 1991) whilst, as analytical techniques improved, isotope analysis has since played a significant role in quantifying the extent of ocean anoxia (e.g. Pearce et al., 2008; Dickinson et al., 2012; Wang 2016, Goldberg et al., 2016). In order for an accurate and quantitative interpretation of the Mo isotope record both sources and sinks of Mo in the oceans need to be accurately characterised and understood.

Despite low crustal concentrations (~1-2 ppm; Taylor and McLennan, 1985), Mo is the most abundant transition metal in the modern oceans at ~10 ppb (e.g. Nakagawa et al., 2012). This relatively high concentration results from the efficient transport of Mo from the continents to the oceans due to the solubility of Mo phases transported via oxidative weathering, and its subsequent slow removal from the oceans in the presence of dissolved O^{2-}. The resulting residence time of Mo in the oceans of 440 ka (Miller et al., 2011), is more than two orders of magnitude greater than the ocean mixing time of approximately 1.5 ka (in Kendall et al., 2016). Consequently the oceans are well mixed, with uniform Mo for both elemental abundance and isotopic composition (Nakagawa et al., 2012). Under oxidising conditions Mo is present as a stable molybdate ion, MoO_4^{2-}, which is relatively unreactive. In this form Mo is slowly removed from the water column through uptake into ferromanganese phases, which preferentially incorporate isotopically light Mo (e.g. Barling et al., 2001; Barling & Andbar 2004; Goldberg et al., 2009; Miller et al., 2011; Wasylenki et al., 2011) resulting in the modern oceans being the heaviest Mo reservoir on Earth (Kendall et al., 2016). In contrast, in anoxic-sulfidic waters Mo is readily removed from solution, sequestered into organic-rich sediments such as shales, with very little isotopic fractionation. In the presence of reduced sulfur, Mo forms oxothiomolybdate ions, $MoO_{4-x}S_x^{2-}$, which are highly particle-reactive and thus rapidly removed from solution (e.g. Barling et al., 2001). This behaviour underpins the application of Mo isotopes and abundances as a proxy for past ocean anoxia (e.g. Pearce et al., 2008, Dickinson et al.,

2012, Goldberg et al., 2016). Rivers are the major source of Mo to the oceans, contributing some 90% whilst the remaining 10% comprises hydrothermal sources (Poulson Brucker et al., 2009). However, the composition of Mo delivered to the global oceans via the world's rivers is far from simple.

Initially it was thought that the composition of the continental input could be characterised from crustal rocks (e.g. Barling et al., 2001; Arnold et al., 2004; Siebert et al., 2006; Anbar & Rouxel 2007). However, increasingly abundant data demonstrate that continental rocks have greater intrinsic isotopic variability than previously thought. It is also clear that as well as source rock variation, Mo crustal signatures are modified during weathering and transport with the dissolved load preferentially enriched in the heavier isotopes both globally (e.g. $\delta^{98}Mo_{GLOBAL\ RIVERS}$ = +0.35‰ to +2.05‰; Archer & Vance 2008) and locally (e.g. $\delta^{98}Mo_{ICELAND\ RIVERS}$ = 0‰ to +1‰ in a basaltic (<0‰) catchment; Pearce et al., 2010). This enrichment in the dissolved phase is attributed to a number of processes including: incongruent dissolution during weathering (e.g. Neubert et al., 2011; Voegelin et al., 2012); adsorption of isotopically light Mo to organic phases in soils (e.g. Siebert et al., 2015; King et al., 2016); and, although considered small in terms of mass balance, adsorption of light Mo to riverine particles (e.g. Archer & Vance 2008; Pearce et al., 2010). Less often considered have been the effects of groundwaters both as contributors to river signatures and direct discharges to the oceans (e.g. Neely et al., 2017). And, although suggested by Pearce et al. (2010) to be contributing to the enrichment of heavy Mo in an Icelandic catchment both Neely et al. (2017) and King et al. (2016) show that groundwaters from basaltic terrains ($\delta^{98}Mo_{BASALT}$ <0‰) show limited fractionation away from the host rocks and as such are isotopically light ($\delta^{98}Mo_{GROUNDWATER}$ ~-0.1‰).

Whilst there is increasingly abundant data on the riverine composition of (dissolved) Mo delivered to the oceans, for this to reach the open ocean it must first transit through coastal, estuarine environments. In general, in the application of Mo as a paleoredox proxy, it has been assumed to transit through these coastal environments without modification by estuarine processes. However, whilst the chemical composition of seawater is largely controlled by land to ocean transfer, the global terrigenous flux exceeds that of the dissolved flux by some factor of 17 to 30 (Jeandal 2016) and it is in these estuarine environments, with increasing pH and ionic strength, that significant interactions between solute and particles occur. Important, recent examples for such interactions between the particulate and dissolved phases in estuarine environments are the release of Nd and Sr from the particulate phase to the dissolved phase, despite preference for the solid phase (Nd: Pearce et al., 2013; Sr: Jones et al., 2014).

For Mo chemistry, a number of studies, in a variety of geological and geographical locations, have attempted to constrain the potential for estuarine modification on the Mo input to the oceans. The fact that many of the published studies (e.g. Head & Burton 1970; Dellwig et al., 2007; Rahaman et al., 2014) demonstrate both conservative and non-conservative behaviour maybe highlights some of the complexity in understanding this system. Possible mechanisms for estuarine modification are: biological uptake (Head & Burton 1970; Dellwig et al., 2007; Gurumurthy et al., 2017; Wang, D et al., 2016); adsorption or desorption from suspended particles and Fe-Mn (oxhydr)oxides (Rahaman et al., 2014, Dalai et al., 2005; Gurumurthy et al., 2017, Wang, D et al., 2016); sequestering in, or release from, bottom sediments (Dalai et al., 2005; Gurumurthy et al., 2017); and anthropogenic effects (Rahaman et al., 2014).

Studies including Mo isotope analysis also demonstrate both conservative and non-conservative behaviour. The earliest study on the effect of estuarine transport on Mo isotope transfer to the oceans found that the Mo isotope compositions of the Itchen Estuary, United Kingdom could be explained by simple mixing between the dissolved riverine and seawater endmembers (Archer & Vance 2008). To some extent this is corroborated by Pearce et al. (2010) who found that the Borgarfjörður Estuary, Iceland was similarly dominated by simple mixing but with some potential for some addition of isotopically light Mo form the particulate or colloidal phases in the low salinity mixing zone. However, estuaries dominated by non-conservative mixing have been described by both Scheiderich et al. (2010) and Rahaman et al. (2014). In Chesapeake Bay, USA, DMo is lost to the sediments but with little effect on the Mo isotope composition of the bay (Scheiderich et al., 2010) and in the Narmada Estuary, India, DMo is similarly lost by adsorption onto Fe-Mn (oxyhydr)oxides (Rahaman et al., 2014) whilst the increase in DMo in the Tapi Estuary, India, is attributed to the substantial anthropogenic input of Mo from the steel industry (Rahaman et al., 2014). In both of these Indian estuaries, the modifications to DMo are associated with isotope fractionations.

2. Geological setting & methods

2.1. Geological setting

The two regions sampled in this study offer contrasting estuarine environments. Borgarfjörður, Iceland is an enclosed, shallow, and well mixed fjord whilst the Kalix and Råne estuaries, Sweden drain into the Bothnian Bay, a stably stratified bay devoid of a strong tidal influence. Both of the regions have been extensively studied and are well characterised elsewhere in the literature but new sampling expeditions to the two regions were carried out in 2014 and are detailed below.

Borgarfjörður Estuary, Hvítá River

Descriptions of the Borgarfjörður estuary and Hvítá River catchment can be found in Pearce et al. (2010); Pogge von Strandmann et al. (2006); and Jones et al. (2014). The catchment is underlain by relatively homogenous tertiary basalts (~3.1 Ma) with poorly developed soils and sparse vegetation. The estuary is dominated by the Hvítá River, which is at least partially sourced from Langjökull glacier, but includes several non-glacial tributaries. The estuary itself is some 25 km long and 5 km wide; with water depths of 1 to 2 m in the inner 5 km, the estuary is tidally dominated and well mixed both horizontally and vertically. High physical erosions rates (1090 t km-2 yr-1) result in the delivery of readily weathered material with a high surface area and the shallow estuary means a high particulate-water ratio, maximising the likelihood of continued particulate weathering in the estuary itself (Jones et al., 2014).

The estuary itself has previously been studied for Mo isotopes (Pearce et al., 2010) however, this study focussed on the entire salinity range: from fresh water to the open

ocean (~35 PSU and Cl concentration of 19200 ppm). However, Pearce et al. (2010) noted the potential for the release of isotopically light Mo in the low salinity zone (LSZ) and Jones et al. (2014) suggest a similar release of Sr from riverine particles in the LSZ. As such, the aim of this new Mo isotope study is to specifically sample the low salinity zone with greater resolution than previously achieved in Pearce et al. (2010).

Low salinity zone (LSZ) samples were collected in October 2014 with similar sampling methods employed as in previous studies (Pogge von Strandmann et al., 2008; Pearce et al., 2010; Jones et al., 2014) and briefly described here. As a shallow, less than 2 m deep, estuary, sampling took place on a high and turning tide from a rigid, flat bottomed zodiac boat crewed by the Borganes rescue team. The first, river end-member, sample was taken from just east of the Hvitávellir bridge. Subsequent sampling locations were determined by direct conductivity measurements. At each location, surface samples (~30 cm depth) were taken into pre-cleaned, pre-contaminated, 10 L high density polyethylene containers.

Bothnian Bay, Kalix and Råne rivers

The Bothnian Bay is the northern-most part of the Baltic Sea with a catchment of some 260,700 km^2 fed by several rivers including the Kalix and Råne. The Kalix River catchment is described in Wortberg et al. (2017). It originates on the slopes of the Kebnekaise Mountain before flowing through lowland wetlands and into the Bothnian Bay (Fig. 2). The total drainage area covers 23,102 km^2 and is dominated by woodland (55-65%). The characteristic rock types for the mountain headwaters are mica schist, quartzite, and amphibolite whilst granites dominate the lowlands. Soil coverage is till with well-developed podsols. The catchment is ice-covered for up to six months every year and was indeed ice-covered at the time of this sampling campaign (April 2014). The Råne River is sourced in the lake Råne träsk and is a smaller catchment at 4,207 km^2. With woodland coverage up to 72%, it too is dominated by forests with minor contributions from wetlands and lakes. In both cases, less than 1% of the catchment is affected by farmland or human population.

Samples were collected during the ice-covered winter period (April 2014), where the ice thickness averaged one metre. At three stations in each estuary a vertical profile (including temperature, conductivity, salinity, and total dissolved solids (TDS)) was collected in addition to 20 L samples from three discrete depths; 0.5, 5.0, and 10.0 m below the ice.

In both cases (Iceland and Sweden), bulk samples were filtered through acid cleaned 0.2 µm nitrocellulose filters within 24 hours. Sub-samples were taken, distributed, and treated as required for various analytical procedures. Typically, liquid samples for isotope analysis were sub-sampled into acid washed nalgene bottles and acidified with suprapure HCl to a pH of less than 1. Borgarfjörður filters were rinsed with at least 2 L of milli-Q water to remove salts before being dried and stored.

2.2. Molybdenum isotope analysis

The Borgarfjörður samples, both dissolved and particulate phases, were prepared and analysed at the Department of Earth Sciences, Durham University whilst the Kalix and Råne samples were prepared and analysed at the Department of Earth Sciences at the University of Oxford. Whilst the same Mo purification chemistry was used in all cases, the Mo isotope analyses were made on a Neptune (Thermo-Finnigan) multi collector inductive coupled plasma mass spectrometer (MC ICP-MS) at Durham University and a Nu Plasma (Nu Instruments) MC ICP-MS at the University of Oxford.

For analysis of dissolved Mo, a working Mo concentration was measured via ICP-MS and enough sampled weighed to generate some 100 ng of natural Mo. This was then spiked with a ^{97}Mo-^{100}Mo double-spike to yield a ~1:1 ratio of spike to natural Mo (Rudge et al., 2009) and allowed to equilibrate before being evaporated to dryness. Chemical separation of Mo was achieved using a single pass anion exchange procedure detailed in Pearce et al. (2009), with an additional 12 ml 0.5 M HF matrix elution step to ensure complete removal of Zn before final Mo elution in 3 M HNO_3. For analysis of the Borgarfjörður particulates, the filters were washed with 18.2 MΩ milli-Q water and placed in beakers which were shaken in an ultrasonic bath to remove the remaining suspended material. This material was then put through total dissolution via concentrated HF HNO_3 (1:2) digestion before a working concentration check via ICP-MS. From this point these particulate samples were treated in the same way as the dissolved phase (although due to sample limitation total natural Mo was closer to 50 ng).

Total procedural blanks were <1 ng per sample and analyses were carried out via MC ICP-MS with appropriate desolvating nebulisers fitted as the sample introduction system (Aridus on the Neptune and DSN for the Nu). All seven naturally occurring Mo isotopes were monitored along with ^{91}Zr and ^{99}Ru to check for isobaric interferences. Data deconvolution was carried out offline using a deconvolution routine (Pearce et al., 2009) based on the Newton-Raphson method (Albarède & Beard 2004).

All Mo isotope compositions are reported in conventional delta notation in parts-per-thousand relative to a reference solution (Eq. 1) with errors given as 2 standard deviations from the mean when n (number of analyses) is greater than 2. When n<2, the long term reproducibility of seawater is used to estimate the uncertainty. Given the inconsistent reporting of Mo isotope data in the literature it is important to note that in this paper all data, including literature data, are reported referenced to SRM NIST 3134 = 0‰ (Goldberg et al., 2013).

$$\delta^{98/95}Mo_{NIST} = \left[\left(\frac{\frac{^{98}Mo}{^{95}Mo}_{SAMPLE}}{\frac{^{98}Mo}{^{95}Mo}_{NIST\ 3134}}\right) - 1\right] \cdot 1000 \quad (1)$$

Long-term machine reproducibility for Durham University was determined by measurement of an in-house Romil standard, which gave δ^{98}Mo = +0.05 ± 0.05‰ (n = 183). The IAPSO seawater standard gave a δ^{98}Mo composition of +2.09 ± 0.08‰ (n = 43),

which is indistinguishable from the mean of published values of +2.08 ± 0.10‰ (given in Goldberg et al., 2013). Comparison between analyses at Durham University and the University of Oxford was made by analysing the same aliquot of IAPSO seawater which at the University of Oxford gave a δ^{98}Mo composition of +2.07 ± 0.15‰ (n = 4), indistinguishable from the Durham University value and literature data.

3. Results

3.1. Borgarfjörður, Iceland

In the dissolved (<0.2 µm) phase, the chlorine (Cl) concentration in the Borgarfjörður samples ranged from 5.35 ppm in the river endmember to 5852 ppm in the most saline of the estuary samples (Table 1; Fig. 3 & 4). However, most of the sampling focussed on the low salinity samples. Molybdenum concentration, along with SO42- and conductivity, increased with increasing salinity (Cl concentration), with Mo ranging from 0.27 ppb to 4.04 ppb (Fig. 3). Similarly, the Mo isotope composition increased from a minimum in the river mouth of δ^{98}Mo +0.16‰ to a maximum of +2.06‰ in the most saline sample, BF10, (Fig. 4). In the corresponding suspended sediment (>0.2 µm) samples, Mo concentration ranged from 0.54 ppm to 2.2 ppm (Fig. 3) and all are isotopically light with Mo isotope compositions from δ^{98}Mo 0.24‰ to 0.47‰ (Fig. 4).

Table 1: Selected data for the dissolved and suspended phases for Borgarfjördur estuary

					Dissolved (<0.2 µm) phase						Suspended (>0.2 µm)			
	Temp. °C	Cond. µS	pH	/°C	Cl ppm	SO_4 ppm	[Mo] ppb	δ^{98}Mo ‰	2sd	n	[Mo] ppm	δ^{98}Mo ‰	2sd	n
Borgarfjörður, Iceland														
14BF01	0.9	102	7.88	/21.4	5.35	2.29	0.27	0.24	0.08	2	2.22	-0.30	0.08	2
14BF02	0.8	97	7.96	/21.6	4.48	2.17	0.29	0.16	0.08	2	0.61	*-0.56**	0.08	2
14BF03	0.4	90	7.87	/21.6	5.36	2.27	0.25	0.25	0.08	2	1.07	-0.41	0.08	2
14BF04	0.2	112	7.86	/21.3	5.61	2.34	0.26	0.22	0.08	2	0.79	-0.47	0.08	2
14BF05	0.1	131	7.88	/21.4	19.8	4.65	0.27	0.30	0.08	2	0.54	-0.33	0.08	2
14BF06	0.3	516	7.85	/21.4	73.3	13.50	0.31	0.51	0.08	2	0.67	-0.31	0.08	2
14BF07	0.1	737	7.79	/21.4	204	35.24	0.32	0.80	0.08	2	0.58	-0.26	0.08	2
14BF08	0.2	2300	7.85	/21.2	737	126.3	0.68	1.41	0.08	2	0.59	*-0.63**	0.08	2
14BF09	0.7	5670	7.87	/21.4	1959		1.37	1.83	0.08	2	1.79	-0.24	0.08	2
14BF10	2.5	16809	7.96	/21.2	5851		4.04	2.06	0.08	2	0.78	*-0.62**	0.08	2

*Ru interference – excluded from discussion

3.2. Bothnian Bay, Sweden

Due to sample limitations and low Mo concentrations in the suspended (>0.2 µm) phase only the dissolved (<0.2 µm) phase was able to be analysed in this study.

Kalix river

The surface waters are more dilute than at depth with Mo concentrations in the surface waters relatively uniform at 0.36 ppb (Figure 5A). In all locations, at both 5 m and 10 m

depth Mo concentrations increase to between 0.9 ppb and 1.0 ppb but with little difference between the sampling stations. More variation is observed within the Mo isotope compositions of these waters with the surface sample increasing from δ^{98}Mo +1.07‰ to +1.16‰ with increasing distance from the river mouth (Table 1; Fig. 6). Waters also get increasingly heavy with depth, from δ^{98}Mo +1.16‰ in the surface waters at station 3 to +1.97‰ at 10 m depth (Fig. 6).

Råne river

The Mo concentration in the surface waters (0.5 m) increases with distance from the river mouth: from 0.41 ppb at station 1 to 0.98 ppb at station 3 (Fig. 5). Only at station 1 is there a distinctive difference between the surface waters (Mo: 0.41 ppb) and those at depth (Mo: 0.80 ppb). In all other stations the waters differ in Mo concentration by little more than 0.1 ppb, ranging from a minimum of 0.85 ppb at 10 m (station 2) to a maximum of 0.98 ppb at the surface (station 3). However, at both station 2 and 3, these small concentration variations are characterised by decreasing Mo with depth. Contrary to Mo concentrations, Mo isotope composition increases with depth in all 3 stations. The greatest isotopic range is at station 2 with surface waters of δ^{98}Mo +1.54‰ and at 10 m depth, +2.16‰ (Fig. 6).

Table 2: Selected data for the dissolved phases from Kalix and Råne estuaries

Kalix							
	Temp (°C)	Cond (µS)	pH	Cl uM	Cl ppm	Mo (ppb)	δ^{98}Mo
Station 1							
0.5 m		181		99	3.51	0.36	1.07
5 m		3956		9249	327.90	0.90	1.59
Station 2							
0.5 m	0.41	89.5		58	2.06	0.35	1.17
5 m	0.16	3776		9167	325.00	1.05	1.28
10 m	0.4	4884		12522	443.94	0.94	2.11
Station 3							
0.5 m	0.04	164		219	7.76	0.36	1.16
5 m	0.04	4071		9384	332.69	0.99	1.43
10 m	0.01	4851		11630	412.32	0.96	1.97
Råne							
	Temp (°C)	Cond (µS)	pH			Mo (ppb)	δ^{98}Mo
Station 1							
0.5 m	0.11	104	6.91	3218	114.09	0.41	1.89
5 m	0.90	4496	7.44	10549	373.99	0.80	1.97
Station 2							
0.5 m	0.30	259	6.58	7509	266.22	0.93	1.54
5 m	0.19	4507	7.63	10277	364.35	0.88	1.92
10 m	0.68	4655	7.60	10540	373.67	0.85	2.16
Station 3							
0.5 m		1784		9169	325.07	0.98	1.61
5 m		4525		9428	334.25	0.92	1.71
10 m		4829		10441	370.16	0.89	2.00

4. Discussion

4.1. Borgarfjörður, Iceland

Isotopically heavy dissolved phase

As is recognised in all Mo isotope studies of rivers, the dissolved phase is isotopically heavier than the particulate phase and catchment source rocks (in this case, basalt). This is indeed true for Borgarfjörður with a riverine endmember of δ^{98}Mo +0.2‰ (Table 1, Fig. 4) in a basalt catchment when the mean global basalt composition is δ^{98}Mo -0.1‰ (Yang et al., 2017), and ranges between -0.4‰ and -0.1‰ for Icelandic basalts specifically (Neely et al., 2017; Yang et al., 2015). The corresponding particulate (>0.2 µm) load for the riverine endmember (BF01) has an isotopically light signature of δ^{98}Mo -0.3‰: lighter than the mean global basaltic average but within the range of values measured for Icelandic basalts. Whilst these data offer no new insight into the possible cause of this fractionation during riverine transport previous studies have attributed this to: preferential weathering of isotopically light lithologies and/or phases (e.g. Neubert et al., 2011; Voegelin et al.,

2012); retention of isotopically light Mo associated with organic phases in soils (e.g. Siebert et al., 2015; King et al., 2016); adsorption of light Mo onto Fe-Mn (oxhydr)oxides (e.g. Archer & Vance 2008; Pearce et al., 2010); and, although more recent groundwater studies have found them to be isotopically light (King et al., 2016; Neely et al., 2017), the addition of isotopically heavy groundwaters was also suggested to contribute to the increasingly heavy composition of rivers in this Borgarfjörður catchment (e.g. Pearce et al., 2010).

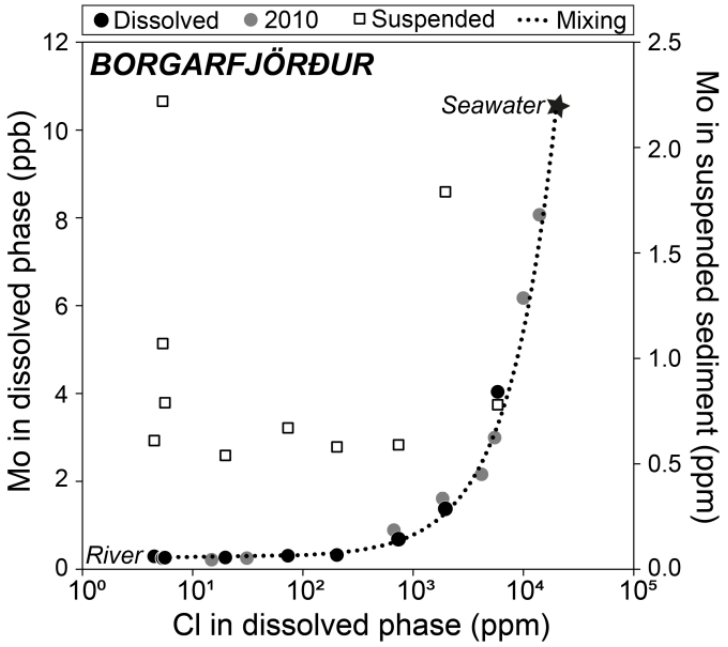

Figure 3: Molybdenum concentrations in both the dissolved (<0.2 µm) and suspended phases for the Borgarfjörður estuary. Ideal mixing between the river and seawater endmember (star) is shown by the dotted line. 2010 data are taken from Pearce et al., 2010.

Mo isotope composition in the Borgarfjörður Estuary transect

Dissolved phase: Along the estuarine transect, with increasing salinity the Mo concentration of the dissolved phase (DMo) increases (Fig. 3). Indeed, there is a direct, linear correlation between dissolved Cl and Mo concentrations with an R^2 of 1.0. These data fit to a theoretical mixing line between the dilute river water and a saline seawater endmember (Fig. 4) suggesting that there is no significant modification of the DMo as it transits through this estuary. This is further corroborated by comparison with a similar September 2003 sampling campaign (Pearce et al., 2010). Despite the coarser, higher salinity sampling strategy these earlier data fit to the same simple mixing curve as that defined for the current study (Fig. 4) with a combined R^2 of 1.0.

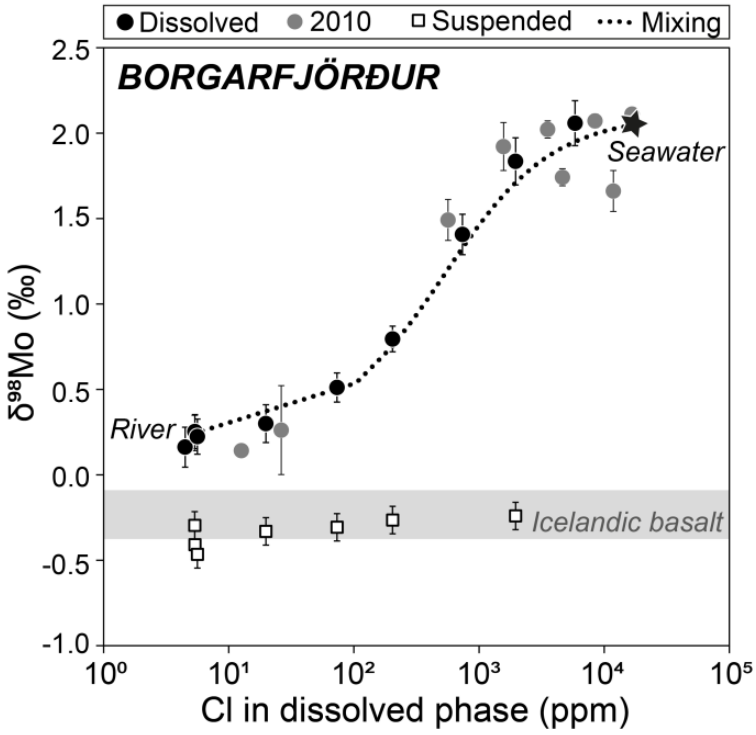

Figure 4: Molybdenum isotope composition of both the dissolved (<0.2 µm) and suspended phases for the Borgarfjörður estuary. Ideal mixing between the river and seawater endmember (star) is shown by the dotted line. Typical Icelandic basalt Mo isotope compositions are shown by the grey bar for comparison with the sediment data.

Particulate phase: The particulate load often dominates the flux of metals to the oceans for all save sodium (Oelkers et al., 2011), and the truly dissolved Mo load only accounts for some 40% of the Mo reaching the oceans with the majority residing in the suspended fraction (Pearce et al., 2010). As such, in this study a complimentary set of samples were taken and analysed for the corresponding suspended particulate phase. The particulate load (PMo) in these estuarine samples shows a range of Mo concentrations. It appears that the highest Mo content, 2.22 ppm, is found in the suspended fraction of the low salinity riverine endmember (BF01). This then decreases rapidly in the low salinity zone to some 0.6 ppm by ~10 ppm Cl with the exception of sample BF09 which has a similar PMo concentration to the riverine endmember (Fig. 3). As is clearly demonstrated in Fig. 4, the Mo isotope compositions of the suspended fraction fit within the range defined for Icelandic basalts, albeit at the lighter end. Whilst caution must be applied due to the small variation and analytical uncertainty, the suspended fraction data hint at an initial decrease in Mo isotope composition (concomitant with the decreasing PMo concentration) from δ^{98}Mo -0.30‰ to -0.47‰ in the low salinity zone before a gradual increase to δ^{98}Mo -0.24‰ in the high salinity samples (Fig. 4).

These particulate data are from total dissolutions of all material greater than 0.2 µm. Although no quantitative analysis of grain size or lithology was made, from visual observation alone it was clear that the low salinity samples (BF01 to BF03) contained a significant proportion of black sand: interpreted as physically weathered basalt carried in the relatively high energy river environment before being deposited as the energy in the

estuary decreases. This black sand was absent from the higher salinity samples where only very fine-grained, brown silt and/or clay was observed. As indicated by Pearce et al. (2010) Fe precipitates contain less Mo (0.01 to 0.06 ppm) and are isotopically lighter (δ^{98}Mo -0.3‰ to -1.02‰) than basalt. As such, the initial decrease in both the concentration and isotopic composition of the particulate phase could be explained by the decreasing influence of basaltic sand. The subsequent isotope composition increase in the particulate phase (Fig. 4), although small, is somewhat similar to that observed in the Narmada Estuary, India during the monsoon season in which the PMo and Mo isotope composition both increased with salinity (Rahaman et al., 2014). In the Narmada Estuary this is interpreted as the adsorption of DMo onto the particulates with a loss of some 8% of dissolved Mo (Rahaman et al., 2014). However, in Borgarfjörður, there is no corresponding change in the dissolved phase and as such, if there is Mo-interaction between the suspended fraction and the dissolved phase it is deemed insignificant.

4.2. Bothnian Bay, Sweden

Despite the clearly stated significance of the particulate phase in the transport of metals to the oceans, due to sample limitations, only the dissolved phase of these estuaries, the Kalix and Råne, were able to be analysed for Mo isotopes.

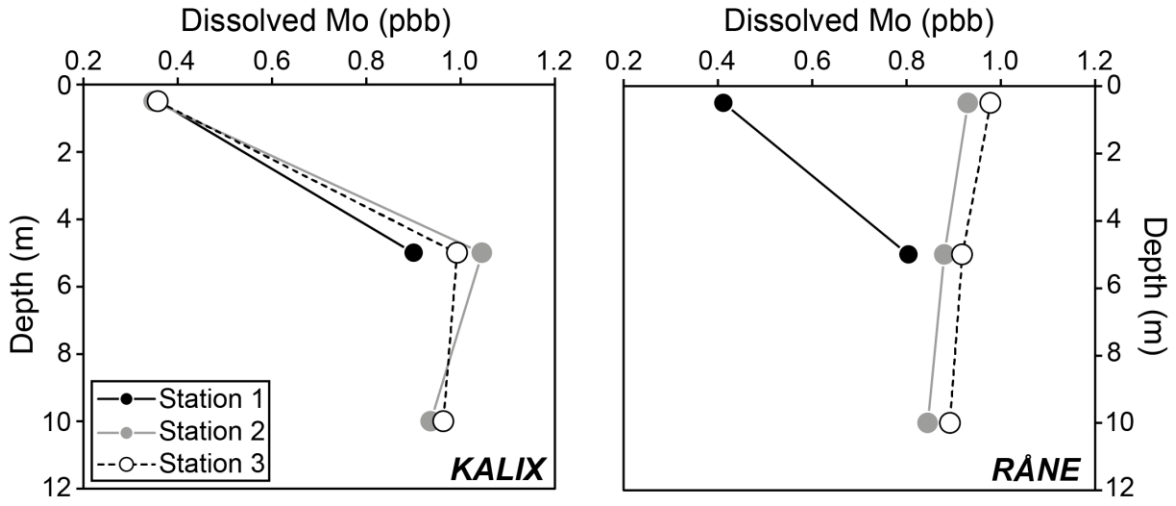

Figure 5: Dissolved Mo concentrations in the Kalix and Råne estuaries, Sweden shown with depth and where station 1 is the most proximal to the river mouth and station 3 the most distal.

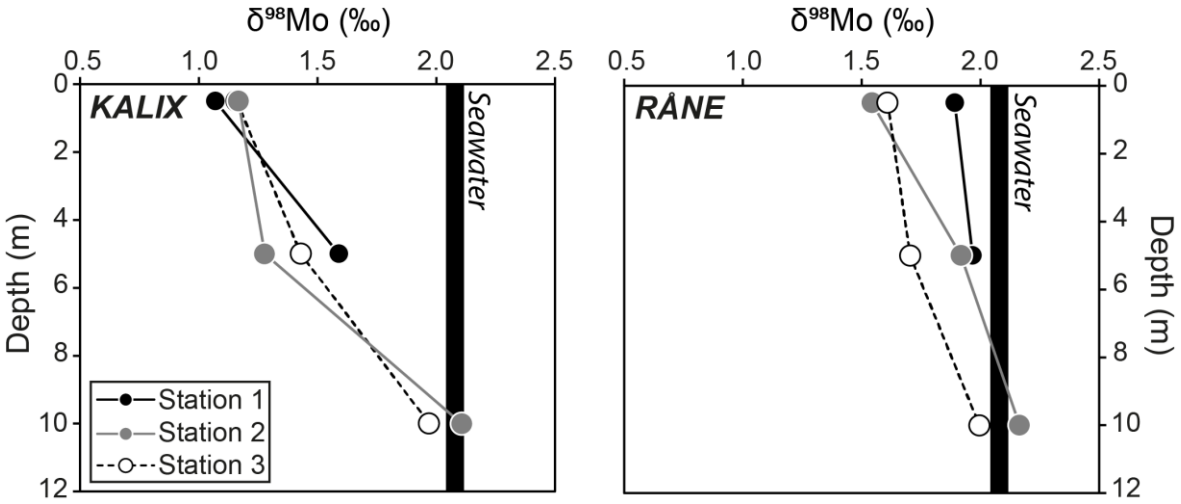

Figure 6: Molybdenum isotope compositions in the dissolved phases of the Kalix and Råne estuaries, Sweden shown with depth and where station 1 is the most proximal to the river mouth and station 3 the most distal. The isotopic composition of seawater is shown for comparison.

B. Speciation calculation and Eh-pH diagram

S-O-H aqueous system with available Mo data from *minteq.v4* database

25°C and 1 atm pressure

	Log K
(1) $H^+ + SO_4^{2-} \leftrightarrow HSO_4^-$	1.99
(2) $SO_4^{2-} + 9H^+ + 8e^- \leftrightarrow HS^- + 4H_2O$	33.66
(3) $HS^- \leftrightarrow S^{2-} + H^+$	-17.3
(4) $H^+ + HS^- \leftrightarrow H_2S$	7.02
$SO_4^{2-} + 10H^+ + 8e^- \leftrightarrow H_2S + 4H_2O$	40.68
(5) $MoO_4^{2-} + H^+ \leftrightarrow HMoO_4^-$	4.2988
(6) $MoO_4^{2-} + 2H^+ \leftrightarrow H_2MoO_4$	8.1636

$pH = -\log[H^+]$
$pe = 16.9\ Eh$

$H^+ + SO_4^{2-} \leftrightarrow HSO_4^-$ **1.99**

$$K_1 = \frac{[HSO_4^-]}{[H^+][SO_4^{2-}]}$$

$$\log K_1 = \log[HSO_4^-] - \log[SO_4^{2-}] - \log[H^+]$$

$$\mathbf{pH = 1.99}$$

$SO_4^{2-} + 9H^+ + 8e^- \leftrightarrow HS^- + 4H_2O$ **33.66**

$$K_2 = \frac{[HS^-][H_2O]^4}{[SO_4^{2-}][H^+]^9[e^-]^8}$$

$$\log K_2 = \log[HS^-] - \log[SO_4^{2-}] - 9\log[H^+] - 8\log[e^-]$$

$$\log K_2 = 9pH + 8pe$$

$$pe = 4.2075 - 1.125pH$$

Eh = 0.249 – 0.0665pH

$\mathbf{HS^- \leftrightarrow S^{2-} + H^+}$ **-17.3**

$$K_3 = \frac{[S^{2-}][H^+]}{[HS^-]}$$

$$\log K_3 = \log[S^{2-}] + \log[H^+] - \log[HS^-]$$

pH = 17.3

$\mathbf{H^+ + HS^- \leftrightarrow H_2S}$ **7.02**

$$K_4 = \frac{[H_2S]}{[H^+][HS^-]}$$

$$\log K_4 = \log[H_2S] - \log[H^+] - \log[HS^-]$$

pH = 7.02

$\mathbf{SO_4^{2-} + 10H^+ + 8e^- \leftrightarrow H_2S + 4H_2O}$ **(2) + (4) 40.68**

$$K_{2+4} = \frac{[H_2S][H_2O]^4}{[SO_4^{2-}][H^+]^{10}[e^-]^8}$$

$$\log K_{2+4} = \log[H_2S] - \log[SO_4^{2-}] - 10H^+ - 8e^-$$

$$\log K_{2+4} = 10pH + 8pe$$

$$pe = 5.085 - 1.25pH$$

Eh = 0.301 – 0.0740pH

$\mathbf{MoO_4^{2-} + H^+ \leftrightarrow HMoO_4^-}$ **4.2988**

$$K_5 = \frac{[HMoO_4^-]}{[MoO_4^{2-}][H^+]}$$

$$\log K_5 = \log[HMoO_4^-] - \log[MoO_4^{2-}] - \log[H^+]$$

pH = 4.2988

$\mathbf{MoO_4^{2-} + 2H^+ \leftrightarrow H_2MoO_4}$ **8.1636**

$$K_6 = \frac{[H_2MoO_4]}{[MoO_4^{2-}][H^+]^2}$$

$$\log K_6 = \log[H_2MoO_4] - \log[MoO_4^{2-}] - 2\log[H^+]$$

pH = 4.0818

C. Mývatn snowmelt calculation

Mývatn
Area: 37 km^2
Depth: 2.5 m

➔ Volume: 9.25×10^7 m^3

Molybdenum
Average: 0.8 ppm
April: 0.6 ppm

$V_2 = C_1 \times V_1 / C_2$
$V_2 = 1.2 \times 10^9$

Additional volume: 30×10^6 m^3

Sodium
Average: 22 ppm
April: 17.5 ppm

$V_2 = C_1 \times V_1 / C_2$
$V_2 = 1.2 \times 10^9$

Additional volume: 24×10^6 m^3

Average additional volume: 27×10^6 m^3
Ice thickness: 27×10^6 m^3 / 37×10^6 m^2
→ 70 cm